AXIAL LOAD CAPACITY OF CIRCULAR STEEL TUBE COLUMNS FILLED WITH HIGH STRENGTH CONCRETE

by

W.S. CLARK, B.Eng. (Building)

Supervised by
A. Hira and I. Campbell

A thesis submitted in fulfilment of the requirements for the degree of Master of Engineering at the Victoria University of Technology.

Department of Civil and Building Engineering
Victoria University of Technology
Victoria
Australia

June 1994.

FOREWORD

This thesis contains no material which has previously been submitted for an award or degree at any University. To my knowledge the work reported in this thesis is original and contains no material published by other investigations, except where appropriate reference has been given to the source of the material.

[redacted]

W.S. CLARK

SYNOPSIS

This study examines the axial load capacity of circular Concrete Filled Steel Tube columns using High Strength Concrete (CFST-HSC). Emphasis is drawn to the enhanced axial capacity of short columns attributed to the lateral confinement of the concrete infill provided by the steel encasement. The degree of confinement has been found to be dependent on several geometric and mechanical parameters. At present, significant discrepancies exist with respect to quantifying the effective strength of the confined concrete. Existing design models and codes are predominantly derived from the characteristics of normal strength concrete and therefore may be inappropriate for concrete filled steel columns utilising High Strength Concrete (HSC).

An extensive experimental program was initiated to examine the axial capacity of CFST-HSC columns. The results of 62 concentrically loaded scale model columns filled with High Strength Concrete (46-100 MPa) are presented. The principal experimental parameters were concrete and steel strengths, tube diameter to wall thickness ratio, and column slenderness ratio. The columns tested were classified as short thin walled sections and were tested as isolated column elements under short term loading. The results are compared with the predictions of several existing design procedures and recommendations are proposed.

ACKNOWLEDGMENTS

The research work described in this thesis was performed at the Department of Civil and Building Engineering, Victoria University of Technology, under the supervision of Mr. A. Hira and Mr. I. Campbell. The author wishes to thank both supervisors for their assistance, guidance and patience, as well as Mr. J. Webb from Connell Wagner Pty Ltd who acted as co-supervisor in the initial stages of the project.

The author also wishes to express his appreciation to :

- The Victoria University of Technology for financial support given in the form of an Industrial Postgraduate Scholarship.
- The Department of Civil and Building Engineering (VUT) for providing resources and equipment for the experimental program.
- Mr. R. Flentje, Concrete Laboratory Technician (VUT) for his invaluable assistance with the experimental work and for making the time spent in the Laboratory less tedious and enjoyable.
- Dr. Ian Bennetts and BHP Research Laboratories - Clayton for allowing use of their excellent Structural Laboratory facilities. Also to Mr. M. Skarajew and the other technical staff for their assistance.
- BTM Tube makers of Australia Ltd., through the agency of Mr. A. Summit for supplying the steel tube used for the test program ;
- Final year Building Engineering Degree students Messrs A. Bortoli, M. Havryluk, B. Richardson and D. Tarola (1991) for their participation in the research program.
- Mr. B. Lucy for assisting with the machining of the tubular test specimens.
- Mr. G. Bain from Boral Concrete for his assistance with the concrete mix design, and for organising supply of selected concrete additives.

Finally, I would like to thank my mother for her assistance in typing the manuscript and the rest of my family and friends for their encouragement and support throughout the course of my studies.

CONTENTS

	Page
FOREWORD	ii
SYNOPSIS	iii
ACKNOWLEDGEMENTS	iv
CONTENTS	v
LIST OF FIGURE	ix
LIST OF TABLES	xii
LIST OF PLATES	xiv
LIST OF ABBREVIATIONS	xv
NOTATIONS	xvi
1.0 INTRODUCTION	
1.1 Introduction	1.1
1.2 Aims and Scope of Investigation	1.3
1.3 Outline of Thesis	1.3
2.0 BACKGROUND AND LITERATURE REVIEW	
2.1 Overview	2.1
2.1.1 Application of CFST Columns in Australia	2.1
2.1.2 Brief Research Background	2.2
2.2 Behaviour of CFST Columns	2.3
2.2.1 Structural Action of a CFST Section	2.4
2.2.2 Strength of Axially Loaded CFST Columns	2.5
2.2.2.1 Further Factors Effecting Column Strength	2.7
2.2.3 Stress - Strain Relationship	2.8
2.3 Characteristics of High Strength Concrete	2.11
2.3.1 Development of High Strength Concrete	2.11
2.3.2 Uniaxial Compression	2.12
2.3.3 Triaxial Compression	2.15
2.3.3.1 Failure Criteria for Laterally Confined HSC	2.17
2.3.3.1.1 Linear Failure Criteria	2.18
2.3.3.1.2 Mander et al. (1988).	2.18
2.3.3.1.3 Fafitis and Shah (1986).	2.19
2.3.3.1.4 Setunge et al. (1992).	2.19
2.3.3.2 Empirical Stress-Strain Models for Laterally Confined HSC.	2.20
2.3.3.2.1 Fafitis and Shah (1986).	2.20
2.3.3.2.2 Mander et al. (1988).	2.22
2.3.3.2.3 Setunge et al. (1992)	2.23
2.3.4 Poisson's Ratio	2.24
2.3.5 Elastic Modulus	2.25
2.3.6 Application of HSC on CFST Behaviour	2.26
2.4 Determination of CFST Column Strength	2.26

		2.4.1 Types of Analysis	2.26
		2.4.2 Historical Background of Triaxial Analysis	2.27
		2.4.3 Implementation of Design Code Provisions	2.28
		2.4.4 Effective Steel tube Stresses - Plasticity Function	2.31
		2.4.4.1 Derivation of Plasticity Function - Tomii et al. (1977)	2.32
		2.4.4.2 Empirical Models for Determining dυ	2.33
		2.4.5 Application of Concrete Failure Criteria	2.35
	2.5	Concluding Comments	2.35
3.0	EXPERIMENTAL PROGRAM		
	3.1	General Scope	3.1
	3.2	Material Properties	3.2
		3.2.1 Steel Tube	3.2
		3.2.1.1 Tensile Testing of Steel Tube Properties	3.3
		3.2.2 Concrete Properties	3.5
		3.2.2.1 Casting and Curing of HSC Cylinders	3.6
		3.2.2.2 Preparation of End Capping	3.7
		3.2.2.3 Compressive Strengths	3.8
		3.2.2.4 Discussion of Concrete Properties	3.9
	3.3	Test Procedures	3.10
		3.3.1 Testing of CFST Columns	3.10
		3.3.1.1 Loading Arrangement and Instrumentation : Series I (VUT)	3.11
		3.3.1.2 Loading Arrangement and Instrumentation : Series II (BHP)	3.12
		3.3.2 Hollow Steel Tube Tests	3.13
		3.3.3 Concrete Core Tests	3.13
		3.3.3.1 Type A Core Tests	3.14
		3.3.3.2 Type B Core Tests	3.14
	3.4	Geometric Properties of Test Specimens	3.14
	3.5	Verification of Experimental Procedures	3.16
		3.5.1 Effects of Curing Condition on Concrete Strengths	3.17
		3.5.2 Effects of Specimen Size and Load Rate	3.18
4.0	TEST RESULTS AND OBSERVATIONS		
	4.1	Overview	4.1
	4.2	Experimental Results - Unconfined HSC	4.1
		4.2.1 Behaviour of Unconfined HSC	4.1
		4.2.1.1 Strain at Peak Stress	4.3
		4.2.1.2 Elastic Modulus E_c	4.4
		4.2.1.3 Modified Stress-Strain Model for HSC - Uniaxial Conditions	4.5
	4.3	Experimental Results - Hollow Steel Tubes	4.6
		4.3.1 Ultimate Squash Load Capacity - Hollow Steel Tubes	4.6
		4.3.2 Load - Strain Relationships	4.7
		4.3.3 Modes of Failure	4.10
	4.4	Experimental Results - CFST Columns	4.12

4.4.1 General Behaviour 4.12
4.4.2 Failure Loads 4.13
4.4.2.1 Effects of Steel Contribution Ratio 4.17
4.4.2.2 Effects of Concrete Compressive Strength 4.19
4.4.2.3 Effects of Column Slenderness 4.20
4.4.3 Load - Displacement Relationship 4.21
4.4.3.1 Strains at Ultimate Conditions 4.24
4.4.3.2 Discussion - Compressibility of Sulphur Capping 4.25
4.4.3.3 Column Ductility 4.26
4.4.4 Modes of Failure 4.28
4.4.4.1 Concrete Shear Failure 4.28
4.4.4.2 Column Buckling 4.31
4.4.5 Load-Strain Relationships - SERIES II Tests 4.32
4.4.6 Relationship between Transverse and Longitudinal Strains 4.35
4.5 General Discussion 4.38

5.0 THEORETICAL INTERPRETATION OF RESULTS
5.1 Ultimate Axial Capacity 5.1
5.1.1 General Assumptions 5.1
5.1.2 Plasticity Function - Steel Tube Stresses 5.2
5.1.2.1 $d\upsilon$-δ_s Relationships 5.2
5.1.3 Failure Criteria for Laterally Confined HSC 5.3
5.1.4 Analysis of Test Results 5.5
5.1.4.1 Empirical Model for $d\upsilon$ 5.6
5.2 Stress-Strain Relationship of CFST-HSC Sections 5.7
5.2.1 Load-Strain Relationship for the Steel Tube 5.7
5.2.1 Load-Strain Relationship for the Concrete Core 5.10

6.0 DESIGN CODES AND COMPARISONS
6.1 Introduction 6.1
6.2 Overview of Code Procedures 6.1
6.2.1 BS5400 Part 5 (1979) 6.1
6.2.1.1 Section Capacity 6.2
6.2.1.2 Member Capacity 6.2
6.2.2 CAN3-S16.1-M84 6.3
6.2.2.1 Member Capacity 6.3
6.2.2.2 Concrete Component 6.3
6.2.2.3 Steel Component 6.4
6.2.2.4 Confinement Co-efficients 6.4
6.2.3 Eurocode 4 (EC4) (1990) 6.5
6.2.3.1 Section Capacity 6.5
6.2.3.2 Member Capacity 6.6
6.2.4 Discussion on Confinement Co-efficients 6.7
6.2.5 Discussion on Design Procedures 6.8
6.3 Comparison with Experimental Results 6.8
6.3.1 Mild Steel Columns 6.10
6.3.2 High Strength Steel CFST Columns 6.11

6.3.3 Statistical Summary of Comparisons 6.12
6.3.3.1 BS5400 6.13
6.3.3.2 CAN3-S16.1-M84 6.13
6.3.3.3 Eurocode 4 6.14
6.4 Parametric Study 6.15
6.4.1 Effects of D/t Ratio 6.16
6.4.2 Effects of Concrete Compressive Strength 6.17
6.4.3 Effects of Steel Strength 6.19
6.4.3.1 Discussion on Eurocode 4 Confinement Co-efficients 6.20
6.4.4 Effects of Elastic Modulus of Concrete 6.21
6.5 Conclusions and Recommendations 6.21

7.0 CONCLUSIONS AND RECOMMENDATIONS
7.1 General Conclusions Experimental Program 7.1
7.2 Design Recommendations 7.2
7.2.1 Semi Empirical Model 7.2
7.2.2 Existing Design Codes 7.2
7.3 Recommendations for Further Research 7.3

REFERENCES R.1

APPENDIX A: MATERIAL PROPERTIES TEST RESULTS A.1

APPENDIX B: LOAD-DISPLACEMENT CURVES B.1
B.1 CFST Columns B.1
B.2 Steel Columns B.5

APPENDIX C: ADDITIONAL CFST TEST RESULTS - VUT 1990 C.1

APPENDIX D: DESIGN CODE PROVISIONS D.1
D.1 BS5400 Part 5 D.1
D.2 CAN3-S16.1-M84 D.2
D.3 Eurocode 4 D.5

LIST OF FIGURES

Figure	Title	Pages
2.1	Schematic stress diagram for concrete core and steel tube, where σ_{sl} and σ_{cl} are the longitudinal stresses in the steel and concrete respectively, σ_{st} the hoop stress in the tube and σ_{cr} the lateral confining stress in the core.	2.4
2.2	Equilibrium conditions of a CFST cross section.	2.6
2.3	Generalised stress-strain relationships for CFST columns.	2.9
2.4	Proposed influences of steel ratios and column slenderness on the stress-strain relationship for CFST columns by Pan and Zhong.	2.10
2.5	Typical stress-strain curves for variations in concrete strength as reported by Fafitis and Shah (1986).	2.12
2.6	Comparison of predicted stress-strain relationships for concrete based on Desayi and Krishnan (1964) and Fafitis and Shah (1986).	2.14
2.7	Shear crack patterns in normal strength and high strength concretes.	2.16
2.8	Stress-strain relationship of laterally confined HSC as proposed by Fafitis and Shah (1986).	2.22
2.9	Stress-strain relationship for laterally confined HSC as proposed by yong et al. 1988 and Setunge et al. 1992.	2.23
2.10	Predicted relationships of elastic modulus of concrete.	2.25
2.11	Column buckling curves for composite columns.	2.31
2.12	Empirical models for determining the $d\upsilon$-δ_s relationship as proposed by Tomii et al. (1977), and $d\upsilon$-Φ relationship as proposed by Zhong and Maio (1987).	2.34
2.13	Definition of column strength by Tomii et al. (1977) and Zhong and Maio (1987).	2.35
3.1	Longitudinal steel tensile coupons cut from circular tube. Where 'b' and 't' are the respective width and thickness of the specimen, 'L_o' gauge length, 'L_c' minimum parallel distance, 'A_{coup}' cross sectional area and 'r' the transition radius.	3.4
3.2	Generalised stress-strain relationships observed from tensile tests.	3.5
3.3	Strain gauge arrangement for concrete cylinders.	3.8
3.4	Capping Techniques for CFST specimens.	3.11

3.5	Composite test specimen set-up: 1. Loading platens 2. Displacement gauges 3. Composite specimens 4. Spherical bearing seat, 5. Capping compound.	3.12
3.6	Strain gauge arrangement for BHP test specimens from castings CA11 and CA13.	3.13
4.1	Experimental stress-strain relationship for HSC cylinders - castings CA11 (Mix B) and CA12 (Mix A).	4.2
4.2	Experimental stress-strain curves for HSC (Uniaxial conditions) as compared with predictions by Fafitis and Shah. (1986).	4.5
4.3	Load-strain relationships for Hollow Steel Tube Sections.	4.8
4.4	Stress-strain relationship for steel stub columns (L/D) = 3.	4.10
4.5	Normalised stress-strain relationship steel stub columns (L/D = 3).	4.10
4.6	Generalised load displacement relationship for CFST-HSC Columns.	4.12
4.7	Stub column load versus steel contribution ratio relationship.	4.17
4.8	Load-relative slenderness relationship.	4.21
4.9	Load-displacement relationships - short columns length = 230 mm.	4.22
4.10.	Dimensionless load-displacement relationships - short columns length = 230 mm.	4.22
4.11	Peak strain-steel contribution ratio relationship.	4.24
4.12	Comparative load-displacement curves for different capping techniques.	4.25
4.13	Definition of ductility index.	4.26
4.14	Ductility index of CFST Columns.	4.27
4.15	Shear failure angles of CFST specimens.	4.29
4.16	Load-strain relationships : CA11-47.6-MB-1 (length = 230 mm).	4.33
4.17	Load-strain relationships : CA11-47.6-MB-4 (length = 460 mm).	4.33
4.18	Load-strain relationships : CA13-38-MB-1 (length = 230 mm).	4.34
4.19	Load-strain relationships : CA13-38-MB-4 (length = 460 mm).	4.34
4.20	Measured Poisson's Ratio υ- Series II tests.	4.36
4.21	Measured Incremental Poisson's Ratio $d\upsilon$ - Series II tests.	4.37

5.1	Experimental results for dυ.	5.3
5.2	Predicted values of dυ.	5.5
5.3	Stress-strain relationships of composite materials.	5.7
5.4	Incremental Poisson's Ratio (dυ) and longitudinal strain (ε) relationship.	5.8
5.5	Comparison of experimental stress-strain curves for hollow steel tube specimens and predictions based on modified Ramberg-Osgood functions	5.9
5.6	Load-strain curve for steel tube component in a CFST section.	5.9
5.7	Derivation of composite load-strain relationships and experimental comparison	5.11
6.1	Design load curves based on Eurocode 4 predictions.	6.6
6.2	Failure load comparison with predicted curves for mild steel tube columns D/t ratio = 47.6.	6.9
6.3	Failure load comparison with predicted curves for mild steel tube columns D/t ratio = 60.3.	6.9
6.4	Failure load comparison with predicted curves for mild steel tube columns D/t ratio = 87.8.	6.10
6.5	Failure load comparison with predicted curves for high strength steel tube columns D/t ratio = 38.05.	6.12
6.6	Statistical summary of experimental comparisons with British Standard - BS5400 Part 5.	6.13
6.7	Statistical summary of experimental comparisons with Canadian Standard - CAN3-S16.1-M84.	6.14
6.8	Statistical summary of experimental comparisons with European Standard - Eurocode 4.	6.15
6.9	Effects of D/t ratio on predicted capacities.	6.17
6.10	Effects of f'_c on predicted capacities.	6.18
6.11	Effects of f_y on predicted capacities.	6.19
6.12	Effects of E_c on predicted capacities.	6.21

LIST OF TABLES

Table	Title	Pages
3.1	Strength Properties of Steel Tubes.	3.4
3.2	Concrete Mix Design.	3.6
3.3	Characteristic Strength of Concrete for Castings.	3.8
3.4	Geometric Properties of CFST Specimens.	3.15
3.5	Geometric Properties of Hollow Steel Tube.	3.16
3.6	Geometric Properties of Concrete Core Tests.	3.16
3.7	Effects of Curing Conditions on the Compressive Strength of Concrete.	3.18
4.1	Stress-Strain Test Results of Unconfined Concrete.	4.2
4.2	Elastic Modulus of HSC Cylinders.	4.4
4.3	Hollow Steel Column - Squash Load Capacities.	4.7
4.4	Experimental Failure Loads and Peak Strains CFST Specimens - Mild Steel Tube.	4.14
4.5	Experimental Failure Loads and Peak Strains CFST Specimens - High Strength Steel Tube.	4.15
4.6	Statistical Assessment of Experimental Results.	4.16
4.7	Summary of Series II CFST Results.	4.35
5.1	Comparison of Experimental Failure Loads with Predicted capacities based on Various Failure Criteria for Laterally confined HSC.	5.4
6.1	BS5400 Confinement Co-efficients.	6.2
6.2	Summary of Design Confinement Co-efficients.	6.7
6.3	Input Data for Parametric Study.	6.16

A.1	Results of Steel Tensile Coupon Tests.	A-1
A.2	Average Compressive Strength of Concrete Cylinder Tests and Statistical Assessment.	A-2
A.3	Results of Concrete Core Tests - Type A.	A-3
A.4	Results of Concrete Core Tests - Type B.	A-4
C.1	CFST Test Results 1990.	C-1

LIST OF PLATES

Plate	Title	Pages
4.1	Failure modes of hollow steel columns: a) Mild Steel Tube D/t = 47.6 b) High Strength Steel Tube D/t = 38.05.	4.11
4.2	Typical shear failure CFST Stub column - steel removed.	4.30
4.3	Shear plane of concrete core passing through both mortar and aggregate.	4.30
4.4	Variation in shear failure angles for all D/t ratios (L/D = 460 mm).	4.30
4.5	Shear failure observed for very thinwalled (D/t = 87.8) CFST Specimens.	4.30
4.6	Column failure for various slenderness ratios and column buckling.	4.31

LIST OF ABBREVIATIONS

BHP	Broken Hill Proprietary Co Ltd.
CFST	Concrete Filled Steel Tube
CHS	Circular Hollow Section
HSC	High Strength Concrete
HSS	High Strength Steel
HST	Hollow Steel Tube
LVDT	Linear Variable Displacement Transducer
MS	Mild Steel
NSC	Normal Strength Concrete
SD	Standard Deviation
SRC	Spirally Reinforced Concrete
VUT	Victoria University of Technology

NOTATION

A_c	Cross sectional area of concrete
A_{coup}	Cross sectional area of tensile section
A_e	Effective area of steel section (determined in accordance with AS4100)
A_g	Gross area of composite section
A_r	Cross sectional area of longitudinal reinforcement
A_s	Cross sectional area of structural steel section
b	Width of steel coupon specimens used for tensile tests
D	External diameter of steel tube
D_e	Effective diameter of circular section (determined in accordance to AS4100)
d_c	Diameter of concrete
E_c	Elastic modulus of concrete
E_s	Elastic modulus of steel
$(EI)_e$	Effective stiffness of composite section
e	Eccentricity of applied load
e_f	% elongation at fracture of steel tensile coupons
f_c	Compressive strength of unconfined concrete
f'_c	Characteristic strength of concrete cylinders
f'_{cc}	Compressive strength of laterally confined concrete
f'_{cm}	Mean strength of concrete
f_{cu}	Cube strength of concrete
f_r	Lateral confining stress (also defined by σ_{cr})
f_{yr}	Yield strength of reinforcement
f_u	Ultimate strength of steel
f_y	Yield strength of steel
I_c	Second moment of area concrete section
I_s	Second moment of area steel section
K	Coefficient of lateral confinement
K_1	Slenderness reduction factor BS5400
k	Effective length factor
L	Length of member
L_e	Effective length of compression member
L_e/r	Geometrical Slenderness ratio
N	Axial compressive force
N_c	Axial compressive load of concrete component
N_{calc}	Calculated load capacity
N_{cr}	Critical buckling load

N_d	Design axial capacity
N_{exp}	Experiment load capacity
N_o	Nominal squash load capacity of section assuming uniaxial conditions ($N_o = f_yA_s + f'_cA_c$)
N_{pl}	Squash load capacity considering confinement enhancement
N_s	Axial compressive load of steel component
n	Modular ratio (E_s / E_c)
r	Radius of gyration : or Geometric radius of circular section
r_c	Radius of gyration concrete section
r_s	Radius of gyration steel section
sd	Standard deviation
t	Thickness

Greek Symbols

α	Steel ratio (A_s / A_c) : or Concrete design strength reduction factor
α_c	Concrete contribution factor (f'_cA_c/N_o)
χ	European buckling curve reduction factor (Eurocode 4)
Δ	Longitudinal deformation (shortening)
δ_s	Steel contribution factor
ε	Strain
ε_{cl}	Longitudinal concrete strain
ε_{cr}	Radial concrete strain
ε_{sl}	Longitudinal steel strain
ε_{st}	Transverse steel strain (circumferential)
ε_u	Strain at ultimate stress
ε_y	Yield strain
Φ	Confinement Index of composite section ($\Phi = A_s f_y / A_c f'_c$)
γ_c	Material partial safety for concrete
γ_r	Material partial safety for reinforcement
γ_s	Material partial safety for structural steel
η_1 η_2	Confinement factors for concrete enhancement and steel reduction (Eurocode 4)
λ	Column slenderness (L/r)
$\bar{\lambda}$	Non dimensional relative slenderness
π	PI (3.141593)
θ	Shear failure angle

ρ	Density
σ	Stress
σ_{cl}	Longitudinal stress in concrete
σ_{cr}	Radial stress in concrete or confining pressure
σ_{sl}	Longitudinal stress in steel tube
σ_{st}	Transverse stress in steel tube
σ_u	Ultimate stress
σ_y	Yield stress of material (or 0.2% Proof stress for tensile tests.)
υ	Poisson's ratio
υ_c	Poisson's ratio for concrete
υ_s	Poisson's ratio for steel
$d\upsilon$	Incremental Poisson's Ratio

Units: Unless specified otherwise, all dimensional units in expressions for length, force and stress, shall be taken as Millimetres (mm), Newtons (N) and Megapascals (MPa) respectively.

Note: The symbols listed above are the principle symbols used throughout this document. In selected circumstances, the symbols may be used to define more than one term. In these cases, due reference shall be given to the particular definition within the body of text, otherwise the default definitions listed shall be adopted.

CHAPTER 1: INTRODUCTION

1.1 INTRODUCTION

Concrete Filled Steel Tube (CFST) columns have been used widely in the construction industry over the past thirty years in parts of Europe, Asia and North America, primarily for low to medium rise buildings. It has been well documented that for short, circular CFST columns, there exists an enhancement in strength of the composite section relative to its uniaxial capacity. This effect is attributed to the lateral confinement of the concrete infill provided by the steel encasement. Despite the advantages and benefits of this form of construction, its application in the Australian building industry has been slow, possibly due to the lack of a suitable design code and local technical data.

During the late 1980's, Australia experienced a boom in the building industry including the construction of many highrise buildings over 40 stories in the major capital cities. Coinciding with the building boom, the financial sector was experiencing high interest rates. These factors forced designers to develop innovative solutions for construction systems resulting in economical structures in terms of both material and labour costs, and speed of construction. Webb and Peyton (1990) identified the use of CFST columns with High Strength Concrete (HSC) as a viable and cost effective alternative for the column elements. This technique has been utilised successfully in several landmark highrise buildings.

To some extent the practical application of CFST-HSC columns has preceded conclusive substantiation of design code provisions and experimental validation. Although the behaviour and ultimate axial capacity of CFST columns have been the topic of numerous research investigations, most interest has focused on Normal Strength Concrete (NSC) with compressive strengths less than 50 MPa. The majority of theoretical models and current design code provisions have emanated from such research origins.

Recent developments in concrete technology have seen designers specifying concrete strengths in the order of 100 MPa for column elements in multi-storey buildings. It has been identified by many previous research investigations that the properties and behaviour of HSC under uniaxial and triaxial compression, are distinctly different to that of NSC. In particular, the influences of lateral confinement on HSC have shown to be less effective than in the lower strength material (Ahmad and Shah, 1982; Yong et al., 1988; Setunge et al., 1992). Therefore determining HSC characteristics by extrapolation of existing relationships for NSC may be inappropriate. Consequently, there is a necessity to review current CFST design methods to verify their suitability to high strength materials.

In order to assess the behaviour of CFST-HSC columns under complex loadings and actual frame conditions, it is necessary to establish the behaviour of the column as an isolated element under idealised concentric loading. A review of available literature has indicated the lack of experimental data for such columns. Hence, to substantiate design procedures, an experimental investigation was performed as part of this study.

The experimental program consisted of tests performed on 62 concentrically loaded scale model columns filled with HSC up to 100 MPa. Several experimental parameters were varied to examine their effects on the concrete confinement and properties of the composite section. Column specimens were classified as short thin walled sections and were tested under short term load conditions. Experimental parameters investigated included:

- Tube diameter to wall thickness ratio (D/t) $(38 < D/t < 87.8)$
- Length to diameter ratio (L/D) $(3 < L/D < 9.7)$

- Concrete Compressive Strength (f'_c) $(46.3 < f'_c < 100.6$ MPa)
- Steel Tube Grade (f_y) $(239 < f_y < 495$ MPa)

The results of the experimental investigation and the appraisal of numerous design models form the basis of this thesis.

1.2 AIMS AND SCOPE OF INVESTIGATION

The principal objective of this study is to recommend design procedures for determining the ultimate axial capacity of CFST columns filled with HSC, verified by experimental data. In order to fulfil this objective several specific aims were established:

- To produce scale model specimens apportioned to replicate geometric and strength parameters found in typical highrise construction in Australia.
- To examine the true nature of the composite action between the steel tube and concrete filling
- To determine the effect of steel tube confinement on the concrete in terms of the enhanced ultimate capacity of the composite section for a range of column size and strength parameters.
- To review and recommend design procedures for predicting the axial load capacity of short circular CFST columns, filled with HSC.

1.3 OUTLINE OF THESIS

In Chapter 2, the structural action and stress states of the composite section under axial load are described. A review of literature relating to the behaviour of CFST columns and the application of HSC is then presented. This includes an overview of analytical procedures for the enhanced strength of short CFST columns and the derivation of design procedures in several international codes.

Details and results of experimental work performed as part of this study are presented in Chapters 3 and 4 respectively. The influence of geometric and mechanical parameters on the ultimate load capacity and load-displacement relationships for the CFST specimens are the principal factors examined. A theoretical interpretation of results is then performed in light of various failure criteria for the laterally confined HSC and using plasticity theory to determine the effective steel tube stresses in Chapter 5.

Chapter 6 includes a comparative study of the experimental failure loads with predicted capacities of several existing design code provisions. A parametric study of the predicted capacities is also presented. Recommendations are then made for an appropriate design method for the HSC composite columns.

The experimental results are reviewed and recommendations for design and further research are detailed in Chapter 7. Additional experimental data not contained in Chapter 4 are included in Appendices.

CHAPTER 2: BACKGROUND AND LITERATURE REVIEW

2.1 OVERVIEW

2.1.1 Application of CFST Columns in Australia

It is only in recent years that CFST columns have been incorporated into the design of Australian multi-storey buildings (Watson and O'Brien, 1990; Webb and Peyton, 1990). In addition to the enhanced strength due to confinement in short circular columns, this form of construction has shown to provide many constructional and economic advantages. The tubular columns have been used with either unreinforced or reinforced concrete cores. In the latter, internal reinforcement is generally used to satisfy fire rating requirements. This quantity is relatively small in comparison to reinforced concrete columns. With the absence of formwork and a reduction in reinforcement requirements, there is a subsequent reduction in the on-site labour costs and material handling. These benefits are further extended by the ability to automate prefabrication of steel columns and connection details off-site.

Once erected, the hollow steel columns are capable of supporting several levels of structural framework prior to the concrete filling operation. This enables construction activities to progress simultaneously on multiple levels with the concrete filling process not a critical activity. Subsequent to these factors, the floor to floor level construction duration is reduced as is the amount of labour required. Webb and Peyton performed an economic comparison on six column alternatives for a highrise building case study. They found that unreinforced CFST-HSC columns compared favourably with the cheapest form of column construction. Combining the economic and constructional advantages of these columns, they have proved to be a practical option for a range of structural applications.

In the absence of a relevant Australian standard, design of CFST columns has been based on a combination of International design codes such as Eurocode 4 - *The Design of Composite Steel and Concrete Structures* (1990), and selected practices of Australian Concrete and Steel Design Codes AS3600 (1988) and AS4100 (1990). The Eurocode 4 and AS3600 standards, both limit the design strength of concrete (f'_c) to 50 MPa.

2.1.2 Brief Research Background

The behaviour of CFST columns has been the subject of numerous experimental and theoretical studies since Kloppel and Godar (1957). Tests have been performed on short and slender columns under a variety of axial and eccentric load conditions. Detailed experimental studies into the enhanced strength and ductility of short columns have been published by Sen (1969), Tomii et al. (1977), Cai (1987) and Zhong and Maio (1987). Accompanying such investigations a multitude of design models have been derived empirically or theoretically. Such research has lead to the implementation of CFST design provisions in several International design standards. Due to variations in analytical procedures, design philosophy or empirical data-bases used, significant discrepancies exist with respect to quantifying the ultimate capacity of the composite section. This non-uniformity and the onset of HSC has emphasised the importance of further research required into the behaviour of CFST columns.

Since the early 1980's, significant headway has been made in the development of HSC's. In recent years, experimental programs such as reported by Mak and Sanjayan (1990), have developed concrete mix designs which achieve compressive strengths exceeding 130 MPa. Concurrent with its evolution, much research has examined HSC's unique properties and application in many structural elements. However, only a meagre amount of activity has considered its function in CFST columns. At present, the majority of work examining the effects of lateral confinement on HSC has focused upon:

- Spirally Reinforced Concrete (SRC) columns or
- Concrete subjected to Hydrostatic Fluid Pressure.

Recently in Australia CFST-HSC research has commenced with results published by the Centre for Advanced Structural Engineering - University of Sydney (1990), Campbell et al. (1991), Rangan and Joyce (1992) and O'Brien and Rangan (1993). Research programs as reported by the University of Sydney and Campbell et al. included experiments on short thinwalled columns under concentric axial load. However, these tests were limited in terms of both number and parameters examined. The latter investigations dealt with eccentrically loaded slender columns which fall outside the scope of this thesis.

In the absence of sufficient literature for CFST-HSC columns, it is essential to examine:

- The structural interactive processes between the steel tube and concrete infill within a CFST cross section under applied load.
- The characteristics of HSC and the ensuing effects on the composite action.

2.2 BEHAVIOUR OF CFST COLUMNS

The ultimate load capacity and stress-strain relationship of a CFST column is influenced by complex interactions between the steel tube and concrete core components. In short columns such actions are governed by the strength and characteristics of the materials, while for slender columns mechanical instability is a consideration. As the focus of this thesis is on the confinement effects in short columns, the structural mechanism by which confinement conditions develop and identification of effective parameters, shall be addressed.

2.2.1 Structural Action of a CFST Section

The structural action of a CFST section throughout the loading sequence may be described in terms of concrete microcracking theories and the Poisson's effects of the constituent materials (Guiaux and Janss, 1970; Cai, 1987). In the initial stages of loading prior to the development of microcracking, the Poisson's ratio of the steel (υ_s) is greater than that of the concrete (υ_c). This implies that there would be a tendency for separation to occur between the two materials due to the greater lateral expansion of the steel tube. If bond stresses at the concrete-steel interface were sufficient to restrict this separation, lateral tension would develop in the outer surface of the concrete core. This type of interaction is generally neglected as bond stresses are small between 1.0 and 1.8 MPa (Virdi and Dowling, 1975; Tomii, 1984). The two materials are therefore assumed to act under uniaxial stress states.

Under the application of further load, longitudinal strains increase to a point at which microcracking within the concrete propagates, producing a lateral dilation of the core. As the concrete bears outward against the tube wall, an opposing restraining pressure is applied by the steel. Consequentially the steel tube develops a biaxial stress state sustaining longitudinal compression (σ_{sl}) and transverse hoop tension (σ_{st}). The concrete core is then subjected to a triaxial stress state induced by radial confining pressure (σ_{cr}) and axial compression (σ_{cl}). These stresses are represented in Figure 2.1.

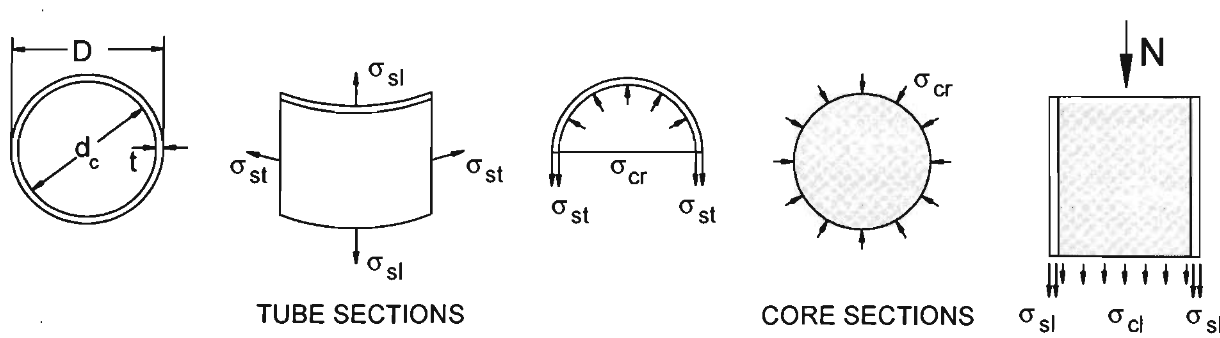

Figure 2.1 *Schematic stress diagram for concrete core and steel tube, where σ_{sl} and σ_{cl} are the longitudinal stresses in the steel and concrete respectively, σ_{st} the hoop stress in the tube and σ_{cr} the lateral confining stress in the core.*

As the confinement pressure develops, there is an augmentation in the axial capacity and ductility of the concrete. It has been recognised since early this century (Richart et al., 1929) that for laterally confined concrete, the propagation of microcracking is impeded by the confining stress σ_{cr}. Therefore, the concrete core is able to sustain stress and strain intensities in excess of those characteristics under uniaxial conditions, prior to failure. At the same time, there occurs a reduction in the longitudinal steel tube capacity owing to the biaxial stress condition. The net effect is an enhancement in the strength of the composite section relative to its nominal uniaxial capacity (N_o) determined from material strengths.

Tomii (1991) described that due to the limited bond in the CFST cross section, the composite action can not be classified as either non composite or fully composite. In a non composite action no bond or interaction would exist and uniaxial conditions remain. For a fully composite action to occur, bond would need to be sufficient to prevent any differential movement between the steel and concrete. Therefore the materials would essentially act as a uniform material. In fact, the true action of a circular CFST column may be described as 'partially composite' falling between the two extremities.

2.2.2 Strength of Axially Loaded CFST Columns

The ultimate capacity of a composite section is generally represented as a summation of the strength components of the constituent materials. For uniaxial conditions, neglecting composite interactions, the nominal capacity is determined based on the characteristic strengths of the steel (f_y) and the concrete (f'_c) as given by Eqn. 2.1. For columns in which the confinement actions are eminent, the material strengths are replaced with the effective longitudinal stresses σ_{sl} and σ_{cl} to give Eqn. 2.2.

$$N = f_y A_s + f'_c A_c \tag{2.1}$$

$$N = \sigma_{sl} A_s + \sigma_{cl} A_c \tag{2.2}$$

It has been well established that the strength of concrete subject to triaxial compression (σ_{cl}), is a function of the concrete's uniaxial compressive strength (f'_c) and the lateral confining pressure (σ_{cr}). (Note: σ_{cl} and σ_{cr} terms may be represented elsewhere in the text by f'_{cc} and f_r respectively). For the steel tube, the effective longitudinal stress (σ_{sl}), is related to the transverse stress (σ_{st}) and the material yield strength (f_y), pertaining to the development of a biaxial stress state. Therefore to determine the capacity of a CFST section, the principal variables which require quantification are the lateral stresses σ_{cr} and σ_{st}. By solving the equilibrium conditions of a cross section shown in Figure 2.2, the following relationship between the two stresses can be derived:

$$\sigma_{cr} = \frac{2t}{d_c} . \sigma_{st} \tag{2.3}$$

where t is the thickness of the steel tube.

d_c is the diameter of the concrete core.

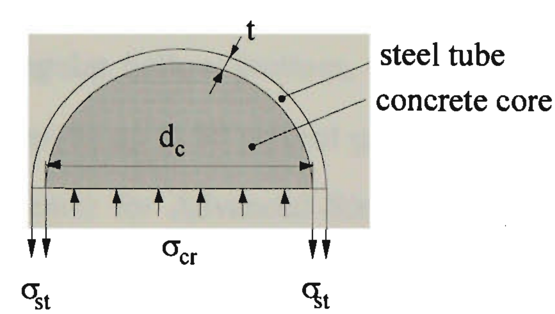

Figure 2.2: *Equilibrium conditions of a CFST cross section.*

The confinement stresses (σ_{cr} σ_{st}) at ultimate conditions vary according to many factors, in particular the quantity of the steel tube, and the dilation characteristics and failure criteria of the confined concrete. (Tomii et al., 1977). Confinement actions are greatest in short thick walled columns, under concentric loading. As slenderness ratios of the column increase, the peak strain at ultimate load (ε_o) decreases to below the strain required to initiate dilation of the concrete core. Therefore, the confinement stress on the concrete diminishes to zero (uniaxial conditions) at limits of column slenderness. This is also true of columns under an increasing eccentricity of applied load.

2.2.2.1 Further Factors Effecting Column Strength

In addition to the actions of confinement, several other factors have been suggested as having potential effects on the capacity of CFST sections. They are briefly:

- Local buckling of the steel tube.
- Strain hardening of the steel and the effects of manufacturing residual stresses
- Application of load (monotonic - cyclic) and load rates.

Local Buckling

In very thin walled sections, local buckling failure of the steel tube wall can occur prematurely, inhibiting the development of confinement conditions on the concrete infill, and lowering the capacity of the tube itself. It has been widely observed that the presence of concrete in a CFST column provides additional stability of the tube wall to such local buckling mechanisms. It was reported by Matsui (1985) that in CFST columns made from rectangular hollow sections, the local buckling resistance of the steel tube concrete filled, can be up to 50 percent greater than in similar hollow section. Tests performed by the Centre for Advanced Structural Engineering - University of Sydney (1990) on specimens having tube D/t ratios of 120, observed local buckling in the tube wall to form prior to the specimens reaching their ultimate load. To account for this effect, many design procedures apply limitations on the plate slenderness ratio (D/t) of the tube (Elnashi et al., 1991). For mild steel sections having nominal yield strengths of 250 MPa, design is generally restricted to D/t $\approx$ 90.

Strain Hardening

It has been proposed by previous experimental studies, that the enhancement in strength of a CFST column can be partially attributed to the effects of strain hardening characteristics of the steel tube (Tomii et al., 1977; Zhong and Maio, 1987; Sakino and Hayashi, 1991). Tomii et al. suggested that to quantify such effects it becomes a complex situation and is quite often omitted from consideration. One reason for this is the practical difficulties in isolating the effects of strain hardening of the tube, to that of the enhanced strength due to concrete confinement. The authors identified that the extents of strain hardening are difficult to ascertain as the tube is subjected to a biaxial stress state at ultimate conditions. Furthermore, hardening effects are dependent on the strain intensity in the steel tube, and subsequently diminish with decreases in tube wall thickness and increases in column slenderness. Rather than attempt to quantify the effects of strain hardening, Tomii et al. adopted to define the strength of a CFST column at stages of loading (strain intensities) where hardening is not expected. This approach was latter applied by Zhong and Maio (1987). As a result of the uncertainty towards such behaviour, design models which incorporate hardening rules based on the characteristics of steel tube under uniaxial conditions, such as Tsuji et al. (1991) and Sakino and Hayashi (1991), may be treated with some scepticism. As the attention of this thesis is predominantly concerned with thinwalled sections (D/t > 38), strain hardening effects have not been examined in detail.

2.2.3 Stress Strain Relationship

The relationship between axial compressive stress and longitudinal strain for CFST columns utilising normal grade concretes has been observed from vast experimental studies. Zhong et al. (1991) stated that the stress-strain curve of a CFST section can exhibit very ductile responses more characteristic of structural steel behaviour than that of unrestrained concrete. The observed shape of the σ-ε curve has been shown to be dependent on numerous strength and geometric parameters, primarily the quantity of the steel tube in the cross section. Test results show that for a particular concrete, increases in size of the steel tube represents a greater confining pressure on the concrete core (σ_{cr}). This has a marked effect on the behaviour of the composite column whereby:

- The capacity of the section is enhanced under increased confinement pressures.
- The ductility of the column is increased with greater peak strains at ultimate conditions, and elongated unloading characteristics in the post ultimate range.

Tomii et al. (1977) and several proceeding investigations chose to classify the stress-strain relationship of CFST columns in three generalised forms represented in Figure 2.3. These observations were established from experimental programs utilising normal strength concrete's.

1) Strengthening or strain hardening (Type A)
2) Elasto - Plastic (Type B)
3) Load degradation (Type C)

It has generally been observed that 'Type A' relationships are observed for thick walled stub columns while 'Type C' behaviour is more apparent in thinwalled or slender columns. For tests reported by Zhong and Maio (1987), specimens with very low D/t and L/D ratios exhibited no ultimate load up to strains exceeding 100,000 με. Similar results were also observed by Cai (1987).

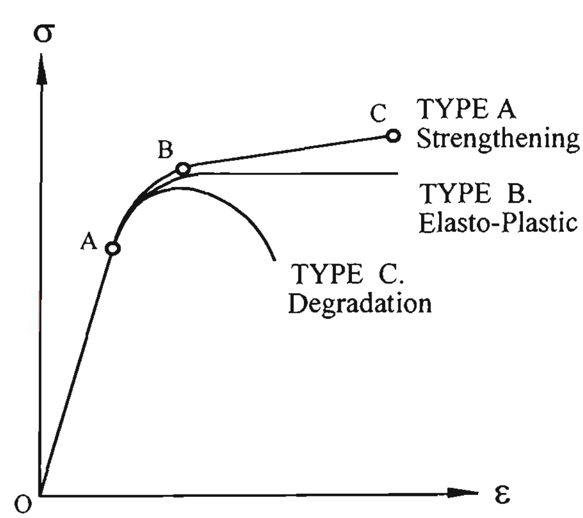

Figure 2.3: *Generalised stress-strain relationships for CFST columns*

Zhong et al. (1991) categorised the stress-strain relationship of short columns (3≤L/D≤ 3.5) into three consecutive stages illustrated in Figure 2.3. In the initial stages of loading, the CFST section is said to behave in a linear elastic manner as shown by the line segment 'OA'. The authors propose that at point 'A' the stresses in the tube reach their proportional limits. Prior to this point, initial microcracking of the concrete occurs. In the elasto-plastic stage 'AB', the biaxial and triaxial stress states develop in the steel tube and concrete core respectively. In the strengthening stage 'BC', the load resistance of the column continues to increase due to the enhanced strength of the confined concrete (and possible strain hardening of the steel tube) until failure processes occur. For short columns, the literature reviewed indicates failure is typically caused by crushing or shearing of the concrete infill, or by local buckling of the steel tube.

Pan and Zhong (1991), attempted to classify the influence of column geometric proportions on the characteristic stress-strain relationship as illustrated in Figure 2.4 a) and b). In Figure a), the quantity of steel in the cross section is represented in terms of a proportional ratio between the cross sectional areas of the steel tube and concrete infill 'α' (A_s/A_c). In the latter diagram the effects of column slenderness L/D are shown. Although representative of observations made during previous experimental studies performed by the authors, the effects of material strengths have not been incorporated. Therefore, such relationships are only validated for the limited range of material strengths examined.

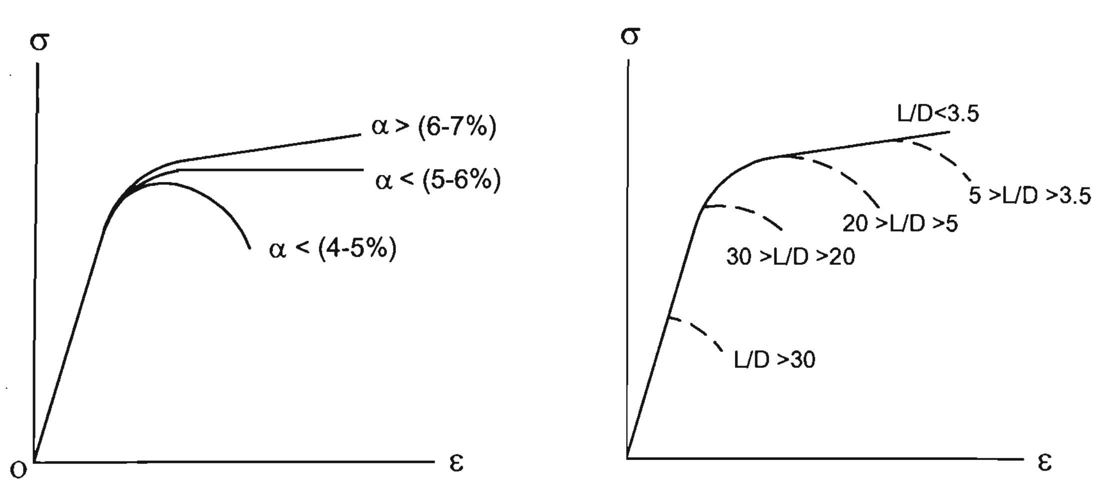

a) Effects of steel ratio *b) Slenderness Effects*

Figure 2.4: *Proposed influences of steel ratios and column slenderness on the stress-strain relationship for CFST columns by Pan & Zhong.*

2.3 CHARACTERISTICS OF HIGH STRENGTH CONCRETE

The term 'High Strength Concrete' is time related and is constantly redefined coinciding with developments in concrete technology. Since the mid 1980's HSC has generally referred to concretes having compressive strengths exceeding 50 MPa (ACI Committee 363, 1984). This definition applies to HSC as referred to in this thesis. As concrete strengths increase, there is a progressive change in the properties and behaviour of the material resulting in notable differences between the characteristics of low to high strength concrete, which has instigated significant research activity into HSC behaviour. In 1984, the American Concrete Institute (ACI) Committee 363 published a "*State of the Art Report on High Strength Concrete*" which provided a compendium of HSC research up to that time. More recently in Australia, a similar publication was jointly composed by the National Readymix Concrete Association of Australia (NRMCA) and the Cement and Concrete Association of Australia (C&CAA), titled "*High Strength Concrete*" (1992). These reports provide valuable background knowledge into various aspects of HSC behaviour and its application.

2.3.1 Development of High Strength Concrete

HSC is generally achieved by using low water/cement ratios in conjunction with relatively high cement contents and high performance materials. In years gone by, the limits of water/cement ratio have been restricted by workability requirements of the concrete. The advent of chemical admixtures such as water reducing agents and superplasticisers has permitted the use of very low water contents. More recently, the incorporation of finely ground pozzolanic materials such as 'silica fume', has lead to strengthening of both the mortar matrix and the adhesive properties of the aggregate / mortar interface. Mak and Sanjayan (1990) found that for an identical concrete mix, replacing 8 % of the cement content with silica fume increased the concrete compressive strength from 112 to 140 MPa. The use of chemical additives and pozzolanic materials has distinct effects on the properties of the concrete. Due to the variation in mix compositions and type of aggregates used, two concretes of similar compressive strength can exhibit unique characteristics. Setunge et al. (1992) found this to be particularly true when comparing concretes obtained with and without silica fume.

2.3.2 Uniaxial Compression

The stress-strain relationship of HSC under uniaxial compression has been the subject of many research investigations (Carrasquillo et al., 1981; Ahmad and Shah, 1982-85; Fafitis and Shah, 1986; Setunge et al., 1992). The general features recognised for HSC in comparison to NSC are:

- As compressive strength increases, the stress-strain relationship exhibits steeper gradients in both the ascending and descending branches.
- The peak strain at ultimate conditions is slightly increased with compressive strength.
- Linearity of the ascending branch is observed for a greater proportion of the ultimate stress.

These characteristics are illustrated in Figure 2.5 which shows the stress-strain relationship of various strength concrete as proposed by Fafitis and Shah (1986).

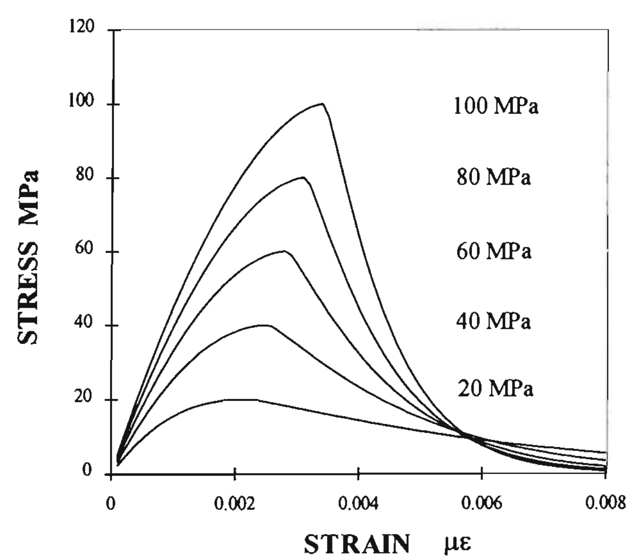

Figure 2.5 *Typical stress-strain curves for variations in concrete strengths as reported by Fafitis and Shah (1986).*

The shape of the stress-strain relationship for HSC has been explained by microcracking studies such as Carrasquillo et al. (1981) and Smadi and Slate (1989). Carrasquillo et al. used X-ray techniques to monitor the propagation of cracking within the concrete microstructure throughout the entire loading sequence for concrete strengths between 21 to 76 MPa. The authors proposed that the stress-strain relationship of concrete be divided into three successive stages. In the initial stages of loading, existing bond cracks at the mortar aggregate interface increase in length. This generally occurs at proportional loads of 40 % peak stress in NSC, and up to 70 % in HSC. In the second stage, microcracks increase in terms of number, width and length, and branch out into the mortar and form combined cracks. This propagation is representative of the divergence of the stress-strain relationship from its initial linearity, and also signifies lateral dilation of the concrete. In NSC this stage was found to be in the order of 70 % peak stress while for HSC the corresponding limit reached above 90 %. It is evident that in HSC the degree of microcracking is reduced due to the strengthened mortar matrix. This leads to a reduction in the volumetric expansion of the higher strength material. In the final stage, combined cracks propagate causing failure of the concrete. In HSC the reduced amount of microcracking leads to a more brittle unloading behaviour as the higher strength material is unable to redistribute stress as effectively as in normal grade concretes (NRMCA & CCA, 1992).

Due to the brittle failure of HSC, researchers have encountered some practical difficulties in obtaining the unloading characteristics of the concrete. Many experimental programs observed explosive failure of the concrete to occur simultaneously with peak strength. In order to obtain the unloading relationship for unconfined HSC, specialised experimental apparatus and procedures have been detailed by Ahmad and Shah (1985) and Setunge et al., (1992).

To demonstrate the differences between predicted stress-strain relationships derived from normal strength to high strength concrete studies, models proposed by Desayi and

Krishnan (1964) and Ahmad and Shah (1985) are shown in Figure 2.6. The model proposed by Desayi and Krishnan represents the σ-ε curve as a parabolic curve function defined by Eqn 2.4 which has been widely accepted for normal strength concretes. Ahmad and Shah's model is based on empirical results for concrete strengths up to 83 MPa. The HSC model defines the relationship by two functions for the ascending and descending stages given by Eqn's. 2.5 to 2.10.

Desayi and Krishnan (1964) $\sigma = {E_c . \varepsilon}\Big/{(1 + (\varepsilon/\varepsilon_{co})^2)}$ **(2.4)**

Ahmad and Shah (1985) $\sigma = f'_c[1-(1-\varepsilon/\varepsilon_{co})^A]$ $\quad \varepsilon < \varepsilon_{co}$ **(2.5)**

$$\sigma = f'_c \exp[-k(\varepsilon - \varepsilon_{co})^{1.15}] \quad \varepsilon > \varepsilon_{co} \qquad \textbf{(2.6)}$$

where σ is the stress at strain ε

f'_c & ε_{co} are the peak stress and corresponding strain

$$A = E_c(\varepsilon_{co}/f'_c) \qquad \textbf{(2.7)}$$

$$k = 24.7f'_c \qquad \textbf{(2.8)}$$

$$\varepsilon_{co} = 0.001648 + 1.65x10^{-5}f'_c \qquad \textbf{(2.9)}$$

$$E_c = 0.0356\rho^{1.5}\sqrt{f'_c} \qquad \textbf{(2.10)}$$

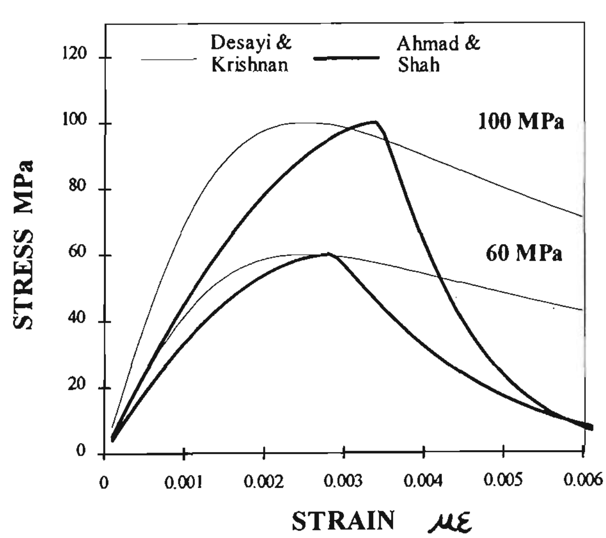

Figure 2.6: *Comparison of predicted stress-strain relationships for concrete based on Desayi and Krishnan (1964) and Fafitis and Shah (1986).*

It is clearly demonstrated from this comparison, that the stress-strain relationships based on the behaviour of NSC, are inappropriate for HSC as they overestimate the ductility to a large degree and show less linearity.

2.3.3 Triaxial Compression

The enhanced strength of laterally confined concrete (f'_{cc}) is generally represented as a function of lateral confining pressure (f_r) and concrete strength (f'_c). In a majority of the literature reviewed the relationship is represented in the simplified form of Eqn. 2.11.

$$f'_{cc} = f'_c + K.f_r \qquad \textbf{(2.11)}$$

where K is a co-efficient of lateral restraint given as a numerical constant or derived from empirical equations.

Richart et al. (1929) proposed the relationship between f'_{cc}, f'_c and f_r to be linear with the co-efficient of lateral restraint 'K' given as a constant equal to 4.1. Hence, the enhancement in strength of the concrete over its uniaxial capacity is only variable with respect to the confining pressure f_r. Contrary to this, recent HSC studies such as Setunge et al. (1992) have found that the failure criteria for confined concrete is variable with respect to the compressive strength and mechanical characteristics of the concrete. Reviewing available literature, it is apparent that there is significant diversity between existing empirical formula for predicting $f'_{cc.}$

Experimental studies on laterally confined HSC have generally been in the form of Spirally Reinforced Concrete (SRC) columns such as Ahmad and Shah (1982-85), Fafitis and Shah (1986), and Yong et al. (1988). More recently some investigations have been performed under hydrostatic fluid pressure (Setunge et al., 1992). The difference between the two cases is that in SRC columns, confinement pressures on the concrete core are 'passive', only developing as the concrete core dilates and the lateral steel restrains this action. In the latter, confinement pressures are 'active' being constantly applied from the onset of loading. In a CFST column, confinement pressures are 'passive' as in the SRC application, however the pressures are uniformly distributed similar to under hydrostatic pressure. SRC applications require the determination of an effective confinement pressure.

In SRC columns the enhanced strength component of the concrete (f'_{cc} / f'_c), has shown to be considerably less in HSC than in NSC columns having identical configurations of lateral reinforcement (Ahmad and Shah, 1982). This may be partially attributed to the reduced volumetric dilation of concrete observed for increases in compressive strength. As a result, stresses developed in the lateral steel would be greater in the NSC to HSC. Experimental studies reported by Ahmad and Shah (1982) showed that for identical configurations of lateral reinforcement, the stresses measured on the confining steel reduced from 317 to 138 MPa as the compressive strength of the concrete increased from 21 to 65 MPa. Furthermore, as failure in confined concrete is predominantly under the actions of shear (Setunge et al., 1992), the inherent shear strength of the confined concrete governs its effective axial strength f'_{cc}.

In NSC, microcracks develop at the mortar / aggregate interface. As they propagate they are forced to diverge around the stronger elements in the material. Therefore the shear resistance of NSC is improved by the interlocking mechanisms of the aggregate. In HSC the increased strength of the mortar matrix becomes closer to that of the aggregate. Consequently, the failure surface of HSC is smoother and passes through an increasing fraction of the aggregate. This effectively reduces the interlocking mechanisms leading to lower relative shear stresses than in NSC. The failure surfaces of NSC and HSC as described, are illustrated in Figure 2.7.

The clearer shear plane in HSC can be attributed to the steeper unloading characteristics observed after ultimate load. Once a shear or failure plane is formed, unloading occurs as the concrete sections bisected by the plane slide against each other. Therefore, the quantity of confining steel and the frictional resistance of the concrete to the differential movement contribute to the concrete's resistance to destructive processes. In HSC, the smoother failure surface offers little resistance in comparison to the irregular plane in NSC resulting in a less ductile behaviour.

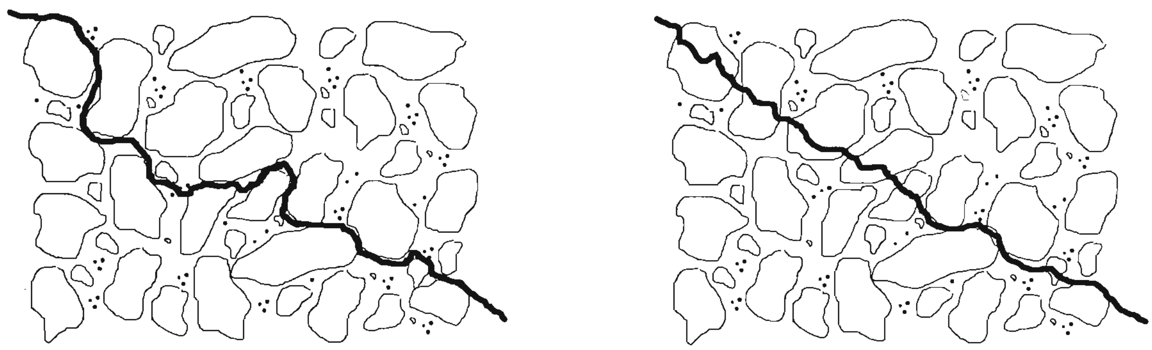

a) NSC *b) HSC*

Figure 2.7: *Shear crack patterns in normal strength and high strength concretes.*

2.3.3.1 Failure Criteria for Laterally Confined HSC

The failure criteria for laterally confined concrete has been evaluated using various analytical theories. Maio (1991) proposed failure criteria for concrete confined within a CFST column using Mohrs Criteria, Octahedral Shear Stress, Generalised Mises Criteria and the Griffith's micro-failure theory. However, these methods can be complex and require detailed knowledge of constitutive material characteristics. More frequently models are derived empirically from experimental results and the effective strength f'_{cc} represented as simplified functions of f'_c and f_r. Many of these empirical failure criteria are derived from experimental studies on spirally reinforced columns. One problem associated with SRC models is that in some circumstances the researcher's base their analysis on the assumption that the steel reinforcement is yielding at ultimate conditions. It has been proven for HSC in particular that this is not necessarily the case and some models possibly incorporate this error (Ahmad and Shah 1982). Therefore it is sometimes preferable to apply failure criteria based on uniform hydrostatic fluid pressure testing where the confinement pressure is known. Recently empirical models for triaxially stressed HSC have been proposed from both SRC and hydrostatic applications.

2.3.3.1.1 Linear Failure Criteria

A review of literature showed that early empirically based failure criteria for confined concrete proposed the effective strength f'_{cc} to be linearly related to the confinement pressure f_r as given by Eqn. 2.11. As proposed by Richart et al. (1929), Salani and Sims (1964) and many others, the co-efficient of lateral restraint 'K' was assumed to equal approximately 4 for NSC. In recent discussion by Setunge et al. (1992) it is suggested that for HSC applications the numerical constant may be as low as 3 to account for the reduced effectiveness of confinement in HSC.

2.3.3.1.2 Mander et al. (1988).

Mander et al. proposed a failure criteria for SRC based on the constitutive 'five parameter' failure surface for concrete as proposed by William and Warnke (1976). The William and Warnke model incorporates material factors such as hardening and flow rules, dilatancy factors and linear softening. Experimental resulted for concrete strengths up to 55 MPa were used to derive an empirical relationship for concrete subjected to triaxial compression. Setunge et al. (1992) later confirmed that the equation exhibited reasonable agreement with their experimental results for NSC as well as HSC using silica fume between 90 to 130 MPa.

$$f'_{cc} = f'_c(-1.254 + 2.254\sqrt{1 + 7.94\frac{f_r}{f'_c}} - 2\frac{f_r}{f'_c}) \qquad \textbf{(2.12)}$$

2.3.3.1.3 Fafitis and Shah (1986).

Fafitis and Shah proposed an empirical model for determining f'_{cc} based on SRC experiments with concrete strengths up to 83 MPa. The effective strength is defined by the following equation:

$$f'_{cc} = \lambda_2[f'_c + (1.15 + 21/f'_c).f_r] \tag{2.13}$$

$$\text{where} \qquad \lambda_2 = 1 + 15(f_r / f'_c)^3 \tag{2.14}$$

This failure criteria was later shown to considerably underestimate results reported elsewhere by Setunge et al. (1992).

2.3.3.1.4 Setunge et al. (1992).

Setunge et al. published results of an extensive experimental program on laterally confined HSC under hydrostatic fluid pressure. An important aspect of this investigation was that it incorporated a range of concrete strengths as well as investigated the effects of various aggregate types. Three different types of concrete were examined:

- High Strength Concrete (90-130 MPa) with Silica Fume
- High Strength Concrete (90-120 MPa) without Silica Fume
- Medium Strength Concrete (58 MPa)

The authors identified substantial differences in HSC obtained with and without silica fume. Subsequently separate failure criteria were proposed for each mix. Empirical equations were derived in the form of the two parameter failure envelop for geomaterials as proposed by Johnston defined by Eqn. 2.15. Johnston's model incorporated parameters 'B' and 'M' which were proposed as factors relating to compressive strength and material properties respectively.

$$f'_{cc} = f'_c(\frac{M}{B}\frac{f_r}{f'_c} + 1)^B \tag{2.15}$$

By performing least squares best fit to the experimental data, Setunge et al. observed that within the strength ranges for the HSC (90 to 130 MPa), values of 'B' remained reasonably constant. A value of 0.45 was applied and 'M' was taken as the only variable. For the medium strength concrete it was found that 'B' was equal to 0.63. The following equations were then derived:

HSC - Silica Fume
$$f'_{cc} = f'_c(18.67\frac{f_r}{f'_c} + 1)^{0.45} \tag{2.16}$$

HSC - No Silica Fume
$$f'_{cc} = f'_c(14.67\frac{f_r}{f'_c} + 1)^{0.45} \tag{2.17}$$

NSC up to 58 MPa
$$f'_{cc} = f'_c(13.07\frac{f_r}{f'_c} + 1)^{0.63} \tag{2.18}$$

2.3.3.2 Empirical Stress-Strain Models for Laterally Confined HSC.

Coinciding with many investigations into the failure criteria of HSC, a number of empirical models have been proposed to predict the stress-strain relationship of HSC under lateral confinement. Similar to the effective strength of confined concrete f'_{cc}, there is substantial discrepancy between models with respect to determining curve shape, peak strain (ε_o), and unloading characteristics. In the proceeding section three empirical models are detailed. In previous investigations (Fafitis and Shah, 1986; Mander et al., 1988; Setunge et al., 1992) the correlation between predicted and experimental σ-ε relationships has shown to be dependent on:

- Empirical databases used to derive models.
- Properties of the particular HSC.
- The range of confining pressures applied.

2.3.3.2.1 Fafitis and Shah (1986).

Fafitis and Shah proposed an empirical model for the stress-strain relationship of concrete under both uniaxial and triaxial stress states where the curve is defined by two functions for the ascending and descending stages. Equations 2.19 to 2.26 define the model. As reported in Section 2.3.3.1.3, the model has been discussed elsewhere as conservatively predicting values of f'_{cc}. Predicted curves showing the changes in the stress-strain relationship with respect to confining pressure for a 90 MPa concrete is illustrated in Figure 2.8.

$$f_c = f'_{cc}(1-(1-\varepsilon/\varepsilon_o)^A \qquad \text{when} \quad \varepsilon < \varepsilon_o \tag{2.19}$$

$$f_c = f'_{cc}[\exp.(-k(\varepsilon-\varepsilon_o)^{1.15})] \, \text{when} \quad \varepsilon > \varepsilon_o \tag{2.20}$$

where

$$f'_{cc} = \lambda_2.[f'_c + (1.15+\frac{21}{f'_c}).f_r] \tag{2.21}$$

$$\varepsilon_o = 1.4895x10^{-5} f'_c + 0.0296\lambda_2 \frac{f_r}{f'_c} + 0.00195 \tag{2.22}$$

$$A = E_c \frac{\varepsilon_o}{f'_{cc}} \tag{2.23}$$

$$k = 24.66 f'_c.\exp(-1.45\frac{f_r}{\lambda_1}) \tag{2.24}$$

$$\lambda_1 = 1 + 25\frac{f_r}{f'_c}(1-\exp[(-f'_c/44.29)^9] \tag{2.25}$$

$$\lambda_2 = 1 + 15.(\frac{f_r}{f'_c})^3 \tag{2.26}$$

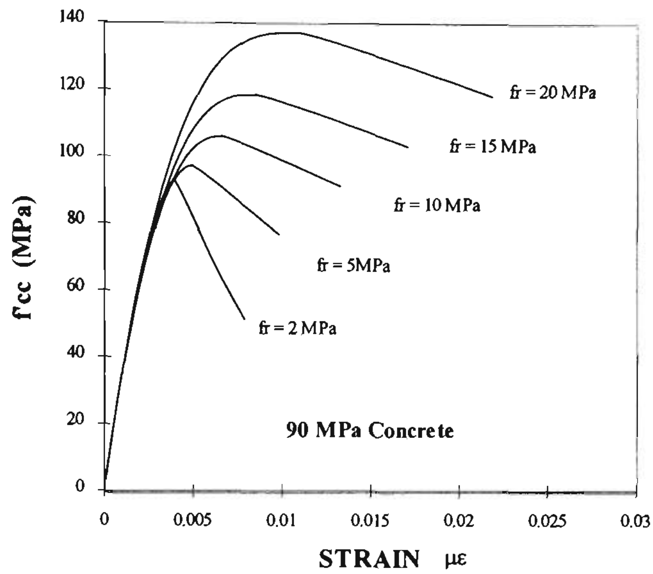

Figure 2.8: *Stress-strain relationship of laterally confined HSC as proposed by Fafitis and Shah (1986).*

2.3.3.2.2 Mander et al. (1988).

The stress-strain model as proposed by Mander et al. was based on an earlier model proposed by Popovics (1973). Unlike Fafitis and Shah's model, the entire σ-ε curve is represented by a continuous function (Eqn. 2.27). Derivation of this function (Eqn's. 2.28 to 2.31) incorporates the peak stress and strain, confining pressure and Elastic and Secant Modulus of the concrete.

$$f_c = \frac{f'_{cc} X r}{r - 1 + X^r} \quad \textbf{(2.27)}$$

where f'_{cc} is defined by Eqn. 2.12

$$X = \varepsilon / \varepsilon_o \quad \textbf{(2.28)}$$

$$\frac{\varepsilon_o}{\varepsilon_{co}} = 1 + 5\left(\frac{f'_{cc}}{f'_c} - 1\right) \quad \textbf{(2.29)}$$

$$r = \frac{E_c}{E_c - E_{sec}} \quad \textbf{(2.30)}$$

$$E_{sec} = f'_{cc} / \varepsilon_o \quad \textbf{(2.31)}$$

2.3.3.2.3 Setunge et al. (1992).

The stress-strain relationship proposed by Setunge et al., was based on an earlier model by Yong et al. (1988). Yong's model was derived from experimental results for SRC with compressive strength between 83 to 93 MPa and expressed the curve as a continuous function defined by Eqn. 2.32. A feature of this model is that expressions were given to derive two points on the descending curve branch as shown in Figure 2.9.

$$Y = \frac{AX + BX^2}{1 + CX + DX^2} \tag{2.32}$$

where $Y = f'_{cc} / f'_c$ and $X = \varepsilon / \varepsilon_o$

A, B, C, D are constants

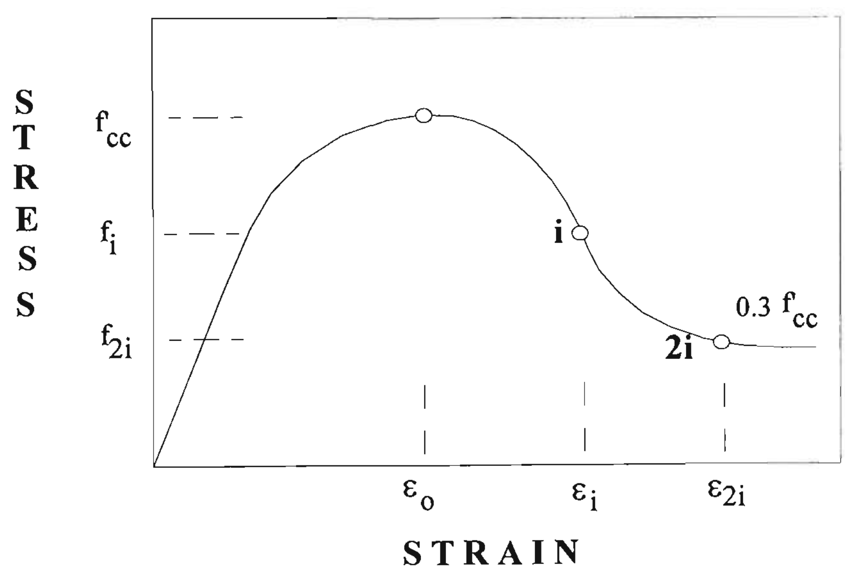

Figure 2.9: *Stress-strain relationship for laterally confined HSC as proposed by Yong et al. 1988 and Setunge et al. 1992.*

Unlike other models, Yong et al. derived peak stresses and strains based on a volumetric ratio of lateral to longitudinal steel, spacing of lateral steel, and several other factors strictly related to the SRC application. Subsequently, Setunge et al. derived empirical equations based on the experimental investigation to determine curve parameters. As discussed in Section 2.3.3.1.4, three failure criteria were proposed by the authors to predict the effective strengths f'_{cc} of various concrete mixes (Eqn's. 2.16 to 2.18). The empirical equations for deriving the peak strains at failure, the stress and strain at each of the points on the descending curve branch were defined by Eqn's. 2.33 to 2.37. In the proposed model separate functions are given for the use of dense and vesicular aggregates however only those functions related to dense aggregate are addressed in this text. The equations for predicting strains are based on the assumption that the peak strain of unconfined HSC (ε_{co}) has a mean value of 2800 $\mu\varepsilon$.

Peak Strain

$$\varepsilon_0 = ((\frac{f'_{cc}}{f'_c})^3 0.67 + 2.13)x10^{-3} \quad (2.33)$$

Point 'i'

$$(\frac{f_i}{f'_c})^2 = 2.858\frac{f'_{cc}}{f'_c} - 2.797 \quad (2.34)$$

$$\varepsilon_i = (4.79\frac{\varepsilon_o}{\varepsilon_{co}} - 0.896)x10^{-3} \quad (2.35)$$

Point '2i'

$$(\frac{f_{2i}}{f'_c})^2 = 1.939\frac{f'_{cc}}{f'_c} - 1.905 \quad (2.36)$$

$$\varepsilon_{2i} = 2\varepsilon_i - \varepsilon_o \quad (2.37)$$

Constants A, B, C, D determined in accordance to expressions given in Appendix of the aforementioned reference.

2.3.4 Poisson's Ratio

To date, there has only been limited experimental investigations into the Poisson's Ratio of HSC. As reported in the "*High Strength Concrete*" manual (NRMCA and CCA), it is widely accepted that in the elastic range of concrete behaviour, the Poisson's Ratio for both HSC and NSC are approximately 0.2. In the inelastic range, the increase in lateral strains for HSC have shown to be considerably less than that of NSC owing to the reduced extents of microcracking. However, further investigations are required to quantify the Poisson's effect in the inelastic range.

2.3.5 Elastic Modulus

Hwee and Rangan (1990) identified that the elastic modulus of concrete determined from NSC relationships, may be inadequate for higher compressive strengths. It was observed by this investigation, that the current design expression given in the Australian Standard AS3600 (Eqn. 2.38), overestimated test results for HSC by up to 30 %. Although having little bearing on the capacity of short CFST columns, this inaccuracy could have serious ramifications on the predicted capacities of slender columns. In the "*High Strength Concrete*" manual, two design expressions derived empirically from HSC results are given. The expressions proposed by Carrasqillo and Ahmad and Shah are defined by Eqn's. 2.39 and 2.40 respectively. In Figure 2.10 the predictions based on each formula are plotted for concrete strengths 50 to 150 MPa.

AS3600 $$E_c = 0.043\rho^{1.5}\sqrt{f'_c} \tag{2.38}$$

Carrasquillo et al. $$E_c = (3320\sqrt{f'_c} + 6900)(\rho / 2320)^{1.5} \tag{2.39}$$

Ahmad and Shah $$E_c = 3.38\rho^{2.5}(f'_c)^{0.325} x10^{-5} \tag{2.40}$$

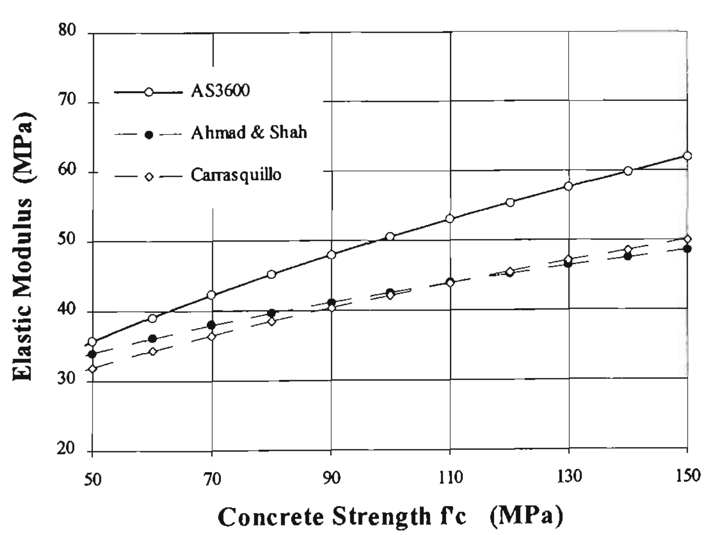

Figure 2.10: *Predicted relationships of elastic modulus of concrete.*

It is evident that the AS3600 equation overestimates the elastic modulus of the HSC expressions by approximately 20 % at compressive strength of 100 MPa. Throughout the 50 to 150 MPa range, both HSC equations give similar predictions with the correlation between 6.5 %. Preference is generally given to the Carrasquillo equation due to its simpler form and being widely accepted having been recommended in the earlier ACI Committee 363 publication.

2.3.6 Application of HSC on CFST Behaviour

Assessing the characteristics of HSC several factors are identified as potentially influencing the behaviour of a CFST column. Similar to SRC column applications, the reduced volumetric dilatancy of the HSC would result in a decrease in the confinement stresses (σ_{cr} σ_{st}) developing prior to ultimate load. The greater strain required to initiate concrete dilation would suggest the confinement conditions of the concrete core would not evolve until latter stages in the load sequence. This implies that the geometric ranges such as slenderness and D/t ratio to which confinement conditions are effective may vary. In the case of very thin walled sections, the strain required to cause dilation of HSC may be closer to the local buckling strain of the steel tube than in NSC. In the extreme situation, local buckling failure of the steel tube may occur in CFST-HSC columns, but not in NSC columns of the same configuration.

2.4 DETERMINATION OF CFST COLUMN STRENGTH

2.4.1 Types of Analysis

In reviewing existing design literature, the methods of determining the axial capacity of CFST columns can be broadly categorised by three general methods of analysis, or as a combination of approaches:

- **Triaxial Analysis:** In which allowances are made for the enhanced strength of the laterally confined concrete core.

- **Strength Super-Imposition:** Neglects the effects of lateral confinement and determines strengths based on a summation of the individual material components under uniaxial conditions.

- **Modified Euler Buckling (Tangent Modulus Analysis):** Where expressions are derived for determining the effective stiffness or tangent modulus of the composite section and modified Euler buckling formulae used to predict the critical buckling capacity of the column.

In general, strength superimposition and tangent modulus analysis neglect the influence of lateral confinement, thus giving conservative estimates of short column capacities. However, models based on modified column stiffness (or tangent modulus) such as Salani and Sims (1964), Gardner and Jacobson (1967) and Knowles and Park (1969-70), have shown to predict the axial capacities of slender columns reasonably. As the scope of this investigation concerns confinement effects in short columns, particular attention is focused on triaxial analytical procedures.

2.4.2 Historical Background of Triaxial Analysis

As discussed in Section 2.2.2 the fundamentals of triaxial analysis for CFST columns require the quantification of the effective steel tube stresses and concrete confining pressure at ultimate conditions. Therefore the longitudinal capacities of the steel tube (σ_{sl}) and concrete core (σ_{cl} or f'_{cc}) can then be determined by applying yield criteria for each material. The section capacity can then be determined using Eqn. 2.2.

In many early research investigations it was assumed that for short columns, the longitudinal steel stress diminished to zero at ultimate conditions, while transverse stresses increased to the yield strength of the steel (Kloppel and Godar, 1957; Salani and Sims, 1964; Gardner and Jacobson, 1967; Neogi et al., 1969). Hence, $\sigma_{st} = f_y$ and

$\sigma_{sl} = 0$. Therefore from Eqn's. 2.2 and 2.11, the strength of CFST section was represented as:

$$N_{pl} = A_c(f'_c + Kf_r) \tag{2.41}$$

By solving the equilibrium conditions of the cross section (Eqn 2.3) and assuming the approximated ratio of $A_s/A_c = 4t/d_c$, the cross sectional strength equation was represented in the form of:

$$N_{pl} = A_c f'_c + \frac{K}{2} A_s f_y \tag{2.42}$$

By taking the 'K' co-efficient as 4, it was shown that steel in the CFST cross section was twice as effective as under uniaxial conditions. Further experimental studies, in particular Sen (1969), found that under no circumstances did the longitudinal steel stresses diminish to zero as previously suggested rendering Eqn. 2.42 invalid. Knowles and Park (1969) suggested that even under the conditions where the concrete core alone is loaded, any presence of bond or frictional forces would produce longitudinal stress in the steel. As a consequence design models became more complex as different analytical methods were proposed for predicting the effective confinement pressures.

2.4.3 Implementation of Design Code Provisions

In reviewing International Design Standards for composite structures, it was found that only a limited number of codes incorporate design provisions incorporating strength enhancement of CFST short columns. They were:

- British Standard : BS5400 *"Steel, Concrete and Composite Bridges: Part 5: Code of Practice for the Design of Composite Bridges." (1979).*
- Canadian Standard : CAN3-S16.1-M84 *"Design of Steel Structures for Buildings." (1984).*

- Eurocode 4 : *"Design of Composite Steel and Concrete Structures." (1990 Draft).*
- German Standard : DIN 18806 *"The Design of Composite Structures." (1984).*

Although each of the aforementioned codes contain some differences in design methodology, they essentially stem from the same research origins.

In BS5400, the design of composite columns was based on work performed by Basu and Sommerville (1969) and latter by Virdi and Dowling (1976). For axially loaded rectangular encased and filled columns, Basu and Sommerville proposed that the design strength of a column N_d, was represented as a function of the cross sectional capacity N_o and a slenderness reduction factor K_1 obtained from a column buckling curve where:

$$N_d = K_1 N_o \tag{2.43}$$

Further K co-efficients (K_2 K_3) were also applied to take into account the effects of eccentricity of loading, ratio of column end moments and concrete contribution ratio.

Virdi and Dowling (1976) noted several limitations of Basu and Sommerville's design methods:

1. no allowance was made for the increased strength of circular filled columns.
2. design loads determined from very slender columns gave very conservative predictions.

Therefore Virdi and Dowling proposed a unified design model which incorporated design procedures for circular filled sections based on earlier work performed by Sen (1969).

Sen proposed an expression for determining the ultimate capacity of the CFST section, derived from findings of his extensive experimental program. The design equation incorporated a number of numerical co-efficients to account for the reduction in steel tube capacity and the enhancement of the concrete strength. These co-efficients were determined empirically from Sen's results which were for NSC columns. The equation was given by:

$$N_{pl} = A_s f_y / \overline{\varphi} + A_c (f'_c + \frac{2t\delta\varphi f_y}{d\overline{\varphi}}) \quad \textbf{(2.44)}$$

where δ is a numerical co-efficient ranging between 4 to 10.

φ is a numerical co-efficient ranging between 0.2 to 0.5.

and
$$\overline{\varphi} = \sqrt{1 + \varphi + \varphi^2} \quad \textbf{(2.45)}$$

Virdi and Dowling made the assumption that the effects of confinement were only existent up to a column L/D ratio of 25. The authors then proposed relationships for predicting Sen's co-efficients as linear functions of column slenderness L/D, converging to uniaxial conditions at L/D = 25. The expressions were given by Eqn's 2.46 and 2.47.

$$\delta = 0.25(25 - L/D) \quad \textbf{(2.46)}$$

$$\varphi = 0.02(25 - L/D) \quad \textbf{(2.47)}$$

Virdi and Dowling also abandoned the method of classifying the slenderness ratio of the composite column by L_e/r due to problems in determining the effective radius of gyration of the composite section. A relative slenderness factor $\overline{\lambda}$, defined as the ratio of effective column length to its critical buckling length ($\overline{\lambda}=L_e/L_{cr}$) was proposed. This factor was later represented as a function of the sections nominal section capacity to the column critical buckling capacity given by Eqn. 2.48 (Eurocode 4, 1990). Determining slenderness in this manner enabled column sections to be related to a singular buckling curve independent of material properties. In BS5400, DIN 18806 and Eurocode 4, three curves have been adopted depending on the type of the composite section. The curves are shown in Figure 2.11 where Curve 'a' applies to CFST sections.

$$\bar{\lambda} = \sqrt{N_o / N_{cr}} \tag{2.48}$$

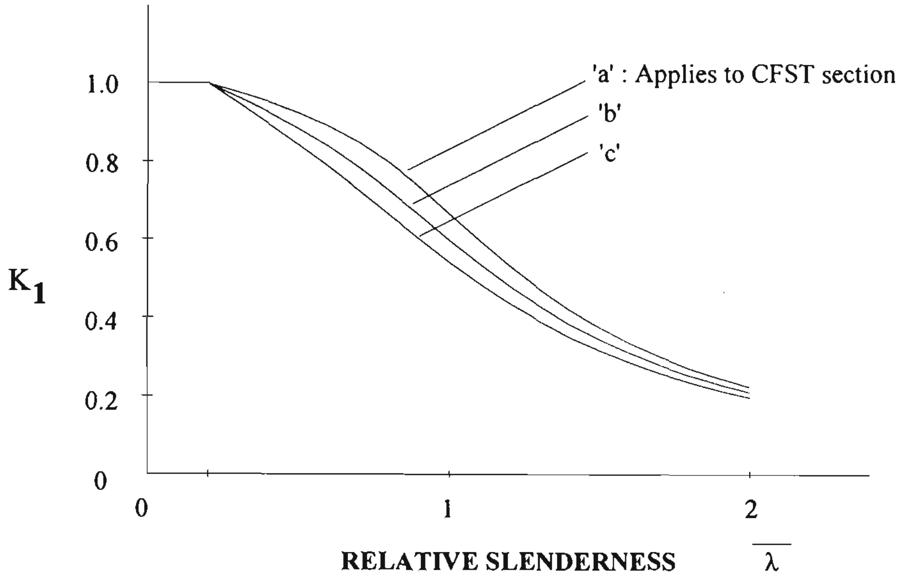

Figure 2.11: *Column buckling curves for composite columns.*

It may be stated that the design codes emanating from the proposals by Virdi and Dowling are largely empirical for a number of reasons. Firstly the values of design co-efficients are derived solely as functions of L/D ratio. Studies by Tomii et al. (1977) found that in fact the stresses within the steel varied with respect to changes in strength and geometrical properties of the cross section. Furthermore, the values for the co-efficients originate from studies on columns with normal strength concretes. It has been discussed that volumetric dilation of concrete is decreased with increases in compressive strength. For this reason transverse stress levels which develop in the tube are variable with respect to concrete compressive strength. Consequently the relevance of existing co-efficients to CFST-HSC columns is questionable.

2.4.4 Effective Steel Tube Stresses - Plasticity Function

To account for changes in CFST cross sectional properties on the steel tube stresses at ultimate conditions, Tomii et al. (1977) proposed a semi-empirical plasticity function. The method was based on establishing the relationship between longitudinal and transverse strains $\varepsilon_{st}/\varepsilon_{sl}$ and then determining values of σ_{st} and σ_{sl}. This approach was latter applied by Zhong and Maio (1987).

2.4.4.1 Derivation of Plasticity Function - Tomii et al. (1977)

For inelastic strains, it was assumed that the relationship between incremental stress $\{d\sigma\}$ and strain increment $\{d\varepsilon\}$ for the steel tube be represented by:

$$\{d\sigma\} = [D^P]\{d\varepsilon\} \tag{2.49}$$

where D^P denotes the plasticity matrix

$$\{d\sigma\} = \{d\sigma_{sl} \;\; d\sigma_{st}\}^T \tag{2.50}$$

$$\{d\varepsilon\} = \{d\varepsilon_{sl} \;\; d\varepsilon_{st}\}^T \tag{2.51}$$

It was adopted that the relationship between transverse and longitudinal strains throughout the stages of loading be represented as a ratio of the change in strain in the transverse direction, to that of the longitudinal direction. This is essentially a measure of incremental Poisson's Ratio ($d\upsilon$) and is a negative constant represented by Eqn. 2.52. (Note the notation of $d\upsilon$ used in the original reference was that of a constant β).

$$d\upsilon = d\varepsilon_{st} / d\varepsilon_{sl} \tag{2.52}$$

The assumption was made that values of σ_{st} and σ_{sl} under the volumetric dilation of the composite section, converge to specific values at ultimate strength. Hence:

$$d\sigma_{sl} = d\sigma_{st} = 0 \tag{2.53}$$

By substituting Eqn. 2.52 and 2.53 into 2.49, the incremental Poisson's Ratio $d\upsilon$ was represented in terms of both σ_{st} and σ_{sl} where:

$$d\upsilon = \frac{2\sigma_{st} - \sigma_{sl}}{2\sigma_{sl} - \sigma_{st}} \tag{2.54}$$

Applying Von Mises yield criteria (Eqn. 2.55) for steel tube subjected to a biaxial stress state to Eqn. 2.54, expressions for σ_{sl} and σ_{st} in terms of $d\upsilon$ and f_y were derived.

$$\sigma_{sl}^2 + \sigma_{st}^2 - \sigma_{sl}\sigma_{st} = f_y^2 \tag{2.55}$$

$$\sigma_{sl} = \frac{d\upsilon + 2}{\sqrt{3(d\upsilon^2 + d\upsilon + 1)}}.f_y \quad (2.56)$$

$$\sigma_{st} = \frac{2d\upsilon + 1}{\sqrt{3(d\upsilon^2 + d\upsilon + 1)}}.f_y \quad (2.57)$$

By solving Eqn. 2.57 with Eqn 2.3, the concrete confining pressure can be represented in similar form, given by:

$$\sigma_{cr} = \frac{2t}{d_c}.\frac{2d\upsilon + 1}{\sqrt{3(d\upsilon^2 + d\upsilon + 1)}}.f_y \quad (2.58)$$

It should be noted that for constant volume conditions where $d\upsilon = -0.5$, the steel stresses converge to uniaxial conditions where $\sigma_{sl} = f_y$ and $\sigma_{st} = 0$.

2.4.4.2 Empirical Models for Determining $d\upsilon$

Tests results obtained by Tomii et al. (1977) and Zhong and Maio (1987) for short column having $L/D \leq 3.5$, observed values of $d\upsilon$ to vary with respect to cross sectional parameters A_c, A_s, f'_c and f_y. Each investigation derived empirical equations for $d\upsilon$ based on statistical assessment of results. Tomii et al. proposed an empirical equation relating $d\upsilon$ to the steel contribution ratio δ_s of a section given by:

$$d\upsilon = 0.9(\delta_s) - 1.4 \quad (2.59)$$

$$\text{where } \delta_s = A_s f_y / N_o \quad (2.60)$$

Zhong and Maio chose to represent the cross sectional properties in terms of a Confinement Index Φ ($\Phi = A_s f_y / A_c f'_c$) with the Eqn. 2.61.

$$d\upsilon = -\frac{1}{2} - \frac{1}{2(\Phi + 1)} \quad (2.61)$$

The proposed equations are illustrated in Figure 2.12 and are observed to converge to values of -0.5 for increases in δ_s and Φ respectively.

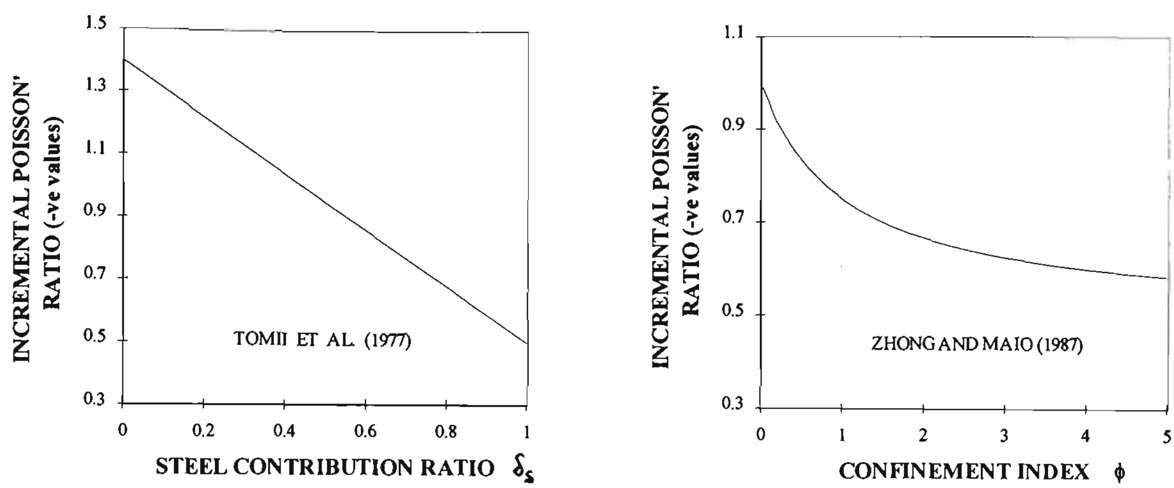

a) Tomii et al. *b) Zhong and Maio*

Figure 2.12: *Empirical models for determining the $d\upsilon$ - δ_s relationship as proposed by Tomii et al. (1977), and $d\upsilon$ - ϕ relationship as proposed by Zhong and Maio (1987).*

Both the definition of $d\upsilon$ and the experimental parameters investigated by the two studies require some discussion. In each case tests were performed on CFST columns having NSC and D/t ratios below 75. The section parameters δ_S and Φ were predominantly in excess of 0.4 and 0.5 respectively. As previously noted in Section 2.2.3 specimens having low D/t and L/D ratio, no ultimate load was observed for some specimens. As a consequence, the definition of column strength used by Tomii et al. and Zhong and Maio was at a transition point between the elasto-plastic and strengthening stages as represented in Figure 2.13. Empirical equations for $d\upsilon$ have therefore been derived from values at this point. Tests performed by Campbell et al. on CFST-HSC columns failed to exhibit any distinct transition between stages and ultimate load was obtained. It should be noted that the empirical relationships have not been verified at low values of δ_S and Φ, or for HSC columns applications. Subsequently, the application of these expressions to CFST-HSC columns is subject to findings of further experimental investigations.

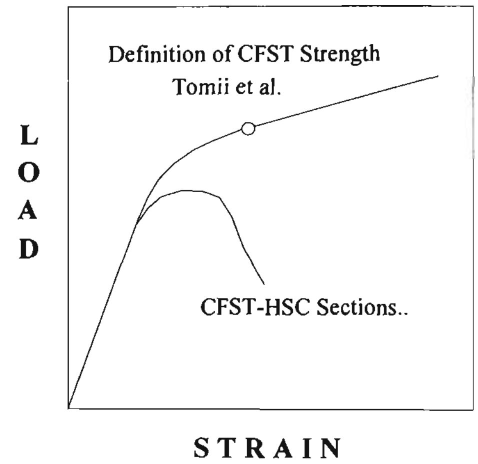

Figure 2.13: *Definition of column strength by Tomii et al. and Zhong and Maio.*

2.4.5 Application of Concrete Failure Criteria

Once steel tube stresses at ultimate conditions have been established, the effective strength of the concrete component (N_c) can be obtained by using the predicted confining pressure f_r, and adopting a relevant failure criteria for the confined concrete as detailed in Section 2.3.3.1.

2.5 CONCLUDING COMMENTS

In this review it has been shown that the properties and characteristics of HSC are distinctly different to those of normal NSC. The reduced volumetric dilation of the higher grade concrete was identified as having significant influence on the confining action in a CFST section, however literature for CFST-HSC columns is sparse. Existing International Design Code provisions were reviewed and found to be derived predominantly from the characteristics of NSC. It is therefore imperative to undertake further experimental studies to appraise existing design procedures for their suitability to high strength materials.

CHAPTER 3 EXPERIMENTAL PROGRAM

3.1 GENERAL SCOPE

The test program was designed to ascertain the effects of material and geometric properties on the extent of the confinement action and subsequent enhancement in the ultimate axial capacity of short CFST columns. Attention was focused on column slenderness ratios in which the effects of column instability are minimal. It was discussed in the preceding chapter that the enhanced strength is primarily dependent on the quantity of steel in the cross section, and the compressive strength of the concrete infill. Bearing this in mind, the following parameters and their experimental ranges were investigated:

1.	Compressive Strength of Concrete	$f'c$	46.3 - 100.6 MPa
2.	Steel Tube Grade	f_y	239 & 495 MPa
3.	Tube Diameter to Wall Thickness Ratio	D/t	38 - 87.8
4.	Column Slenderness Ratio	L/D	3 - 9.72

In all, 62 scale model CFST-HSC specimens were tested beyond failure under short term load. Column cross sectional parameters (f'_c, f_y, & D/t) were classified in terms of a steel contribution factor (δ_S), defined as the proportion of load attributed to the steel tube, to the nominal section capacity (N_o) given by Eqn. 3.1. This factor varied from 0.107 to 0.493 for the parametric ranges.

$$\delta_s = A_s f_y / N_o \tag{3.1}$$

In conjunction with CFST experiments, tests were performed on specimens on hollow steel tube (HST), unrestrained concrete cores, and standard concrete cylinders. Such tests enabled the material characteristics and behaviour of the constituent materials under isolated conditions to be assessed.

Two series of experiments consisting of 13 casting groups were performed. Series I experiments (Castings CA3-CA10), were conducted within the Department of Civil and Building Engineering's Concrete Testing Laboratory, Victoria University of Technology (VUT). In these tests, the ultimate load capacity and column load-displacement relationships were recorded for each specimen. In proceeding Series 11 experiments (Castings CA11-CA13), the investigation was extended to monitor the longitudinal and circumferential strains measured on the surface of the steel tube. These experiments were performed at the BHP Research Laboratories - Melbourne, utilising the superior data acquisition facilities made available.

3.2 MATERIAL PROPERTIES

3.2.1 Steel Tube

Two grades of steel tube were considered, one a mild strength steel (MS), and the other a high tensile strength steel (HSS). The dimensions of the tube cross sections were selected on the basis of their nominal wall slenderness (D/t), machining characteristics, and the maximum capacity of the compression testing apparatus used for CFST tests (200 tonne - 'Mori' Compression Testing Apparatus). The MS tube was an electrically resistance welded (ERW) variety, manufactured from rolled flat plate with nominal external diameter and wall thickness of 76.1 and 1.6 mm respectively. The HSS tube was a seamless extruded section with corresponding dimensions of 76.1 and 2.0 mm. To ensure that the quantity of each tube acquired exhibited similar material properties, tubes were obtained in 6 metre lengths out of identical batches from the supplier.

Due to the fabrication and transportation processes of the steel tube, potential shape and length irregularities required examination. As a consequence, each tube specimen was required to undergo a stringent geometric assessment of imperfections prior to being accepted for the experimental program. The inherent imperfections for the tube specimens had to be within desired tolerances for:

- Concentricity of the tube diameter
- Uniformity of nominal wall thickness
- Overall straightness of the tube length

The MS tube (ERW) was more susceptible to shape irregularities, in particular the out-of-roundness of the tube diameter. As a result, many sections of tube were rejected on this basis. Once accepted, each tube specimen was cut to approximate size, and accurately machined to the specified length and wall thickness. The tolerances stipulated for the machining of specimens were that the required tube thickness be within ± 0.02 mm, and the column length ± 0.5 mm..

3.2.1.1 Tensile Testing of Steel Tube Properties

To determine the yield and tensile strengths of each tube, tests were carried out on tensile coupons extracted from tube segments in accordance with Australian Standard AS1391 "*Methods for Tensile Testing of Metals*" (1990). Coupon specimens were removed at random from various segments of tube and shaped in accordance with the dimensional proportions illustrated in Figure 3.1. A 'Shimadzu' 300 kN type RH-30 Universal Testing Machine with friction grip supports was used for this experimental application. The ends of the coupon specimens were flattened in a press to provide a uniform surface for the friction grip supports. Tests were controlled at a constant displacement rate of 0.5 mm/min. which corresponded to a strain rate of 1.25×10^{-4} /s for a 65 mm gauge length. This strain rate was maintained until fracture of each specimen occurred. Longitudinal extensions were recorded by means of a mechanical displacement gauge fixed between the jaws of each support. This procedure provided only an approximation of the stress-strain relationship as some slippage was observed between the gripping jaws and the specimens. As a consequence, the elastic modulus of the steels (E_s) could not be determined accurately. A value of 200,000 MPa was therefore adopted.

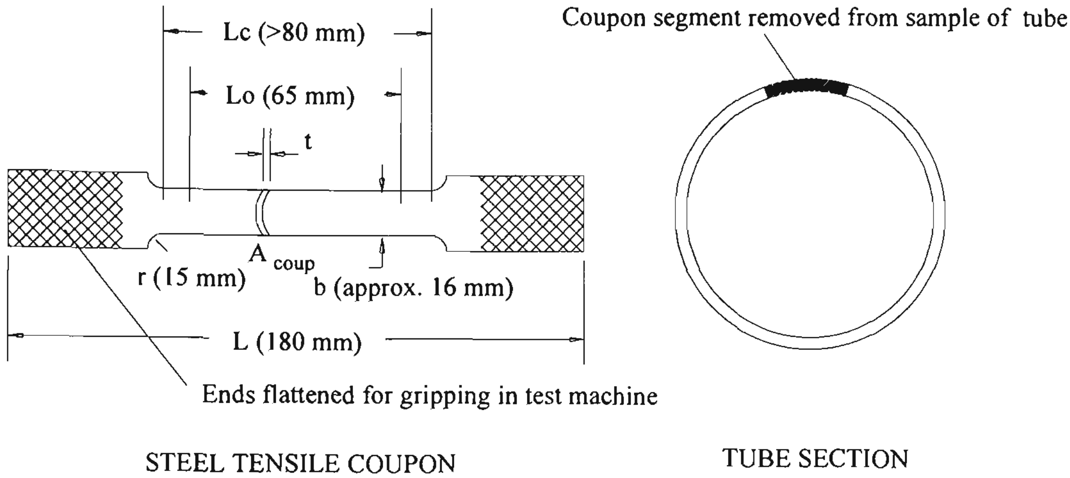

Figure 3.1: *Longitudinal steel tensile coupons cut from circular tube. Where 'b' and 't' are the respective width and thickness of the specimen, 'Lo' gauge length, 'Lc' minimum parallel distance, 'A_{coup}' cross sectional area and 'r' the transition radius.*

$$A_{coup} = ab.\left|1 + \frac{b^2}{6D.(D-2a)}\right| \tag{3.2}$$

The material properties obtained for each tube type are summarised in Table 3.1 with actual test results given in Table A.1 of Appendix A. The observed stress-strain relationships from tensile tests are illustrated in Figure 3.2 The mild steel stress-strain relationships exhibited elastic behaviour up to approximately 80% of the ultimate tensile strength. After initial yielding, the relationship exhibited a ductile plastic range until fracture of the specimen occurred, The percentage elongation (e_f) at fracture had a mean value of 20.8%. The stress-strain relationships for the HSS coupons represented linear elastic behaviour up to ultimate load. The yield and ultimate strengths for the HSS were equivalent as brittle fracture occurred without significant yielding of the material. This less ductile behaviour can be attributed to the strain hardening of the steel which occurs during the extrusion process.

TABLE 3.1: Strength Properties of Steel Tubes.

Steel Tube Type:	Code	f_y (MPa)	f_u (MPa)	E_s (MPa)	e_f (%)	f_u / f_y
Seam Welded (ERW)	MS	239	300	200,000	20.8	1.25
Drawn Tube (seamless)	HSS	495	495	200,000	3.4	1.00

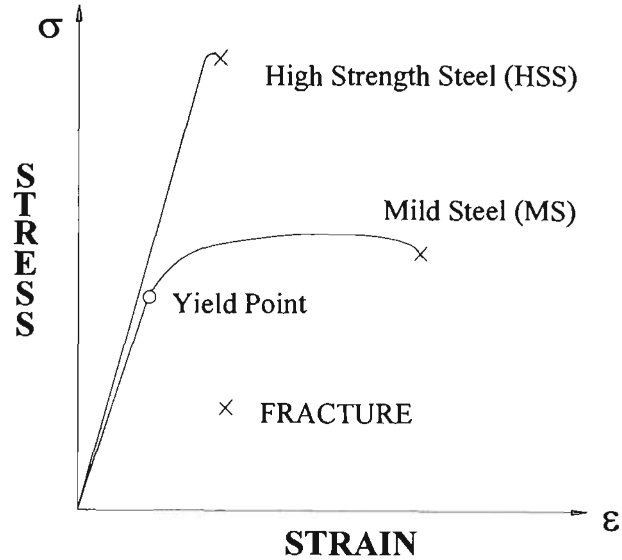

Figure 3.2: *Generalised stress-strain relationships observed from tensile tests.*

3.2.2 Concrete Properties

Two HSC mix designs designated 'A' and 'B' with nominal compressive strengths of 60 and 90 MPa were adopted. Each mix comprised of ordinary Type A - Portland Cement, local aggregates and commercially available concrete additives. The performance criteria for each concrete mix was they were to achieve specified strengths at 28 days, and to satisfy initial workability and setting time requirements. Details of the concrete mixes are given in Table 3.2 The respective contents of cementitious materials (cement + flyash) were 420 and 600 kg/m^3 with corresponding water/cement ratios of 0.42 and 0.28.

AS1012 "*Methods for Testing of Concrete*" (1988) specifies that for a 100 mm diameter concrete cylinder, the maximum aggregate size should be limited to 20 mm. Scaling this value with respect to the internal dimensions of CFST specimens, gives a nominal aggregate size of 14 mm. To prevent any potential compaction problems or load bridging mechanisms of the aggregate, a nominal aggregate size of 11 mm was selected. Initial sieve analysis showed that the basalt aggregate used contained a small quantity of 14 mm aggregate.

TABLE 3.2: Concrete Mix Design.

AGGREGATE / ADMIXTURES			MIX A (60^+ MPa)	MIX B (90^+ MPa)	UNITS
Cement Content (Portland Cement type A)			320	500	kg/m^3
Flyash			100	100	kg/m^3
Water			170	150	lt/m^3
11 mm Aggregate (Max. 14 mm)			620	600	kg/m^3
7 mm Aggregate			330	300	kg/m^3
Sand			890	700	kg/m^3
	Darattard	**(1) (Note 1.)**	600	540	(Note 1.)
Admixtures:	**Force 100**	**(2)**	10	50	lt/m^3
	Daracem	**(3)**	4	4-6	lt/m^3
Water / Binder Ratio		**(Note 2.)**	0.42	0.28	

(1) Darattard : Set Retarding Admixture
(2) Force 100 : Condensed silica fume liquid which increases bond strength between particles and enables higher concrete strengths to be obtained. The admixture contains 50 % by weight condensed silica fume.
(3) Daracem : Superplasticizer Admixture.
Additives available through W.R.GRACE LTD. AUST.

Note 1. : Admixture dosage rate is in mls/100 kg cementitious material (cement + flyash + silica fume)
Note 2. : Water cement ratio is determined by assuming that the water volume is equal to the contents of water given plus 50 % of the Force 100 dosage and the cement content determined as Note 1.

3.2.2.1 Casting and Curing of HSC Cylinders

To obtain the characteristic compressive strength of the concrete used for each CFST casting group, standard 100 mm diameter by 200 mm high cylinders were cast in accordance with AS1012 Part 9 "*Methods for Determining the Compressive Strength of Concrete*" (1988). To provide results with adequate confidence limits, a minimum sample size of four cylinders were cast for each group. Cylinders were filled in two equal layers and compacted progressively to ensure uniformity of concrete properties. The steel moulds were then sealed and allowed to stand for 24 hours. After this initial setting period, cylinders were removed from their moulds and transferred into a lime saturated water bath, within a humidity controlled fog room. The conditions of the fog room were kept at a constant temperature of 23°C and relative humidity of 95 - 100%. At the age of testing (generally 28 days), specimens were removed, weighed and their geometric properties recorded. The curing conditions of the concrete cylinders were adopted after preliminary testing reported in Section 3.5.

3.2.2.2 Preparation of End Capping

The appropriate means of end capping for HSC cylinders has been treated with some uncertainty as highlighted in recent research performed by Mak and Attard (1992). Currently, AS1012 allows concrete cylinders with compressive strength of up to 80 MPa to be capped using either a sulphur capping compound or an unbonded restrained rubber cap. When concrete strengths exceed 80 MPa, the standard prohibits the use of the rubber capping technique and stipulates that the strength of the sulphur capping compound be at least 50 MPa. For concrete Mix A (60 MPa) specimens, 4 cylinders were taken and tested using the unbonded rubber capping technique. In concrete Mix B (90 MPa) tests, 6 cylinders were cast, three to be tested by both rubber capping and high strength sulphur capping techniques.

Practical difficulties were encountered with the use of the rubber capping system for a small number of high strength (Mix B) cylinders. It was observed that the proportion of rubber overhanging the concrete had a tendency to lock the end of the cylinder within the cap's steel restraining ring. Mak and Attard discussed that this phenomenon could contribute to possible end confinement of the cylinder effecting the ultimate strengths obtained. The authors proposed that the number of times the rubber (neoprene) insert had been used, its general condition, and the compressive strength of the concrete, can significantly influence the nature of the test. Consequently, a visual inspection of the cap was performed on a regular basis. It was observed in comparisons between the two capping techniques that the cylinders capped using the unbonded rubber capping technique had greater variability than their high strength sulphur capped counterparts. However, this did not tend to vary the mean strength substantially.

3.2.2.3 Compressive Strengths

Concrete cylinders were tested in an 'ELE' 3000 kN capacity universal testing machine. Load was applied at a constant stress rate of 20 MPa/min. (2.62 kN/sec. for 100 mm diameter cylinders), as specified in AS1012. As load was applied at a continuous load rate, the unloading behaviour of the HSC could not be monitored. The end conditions of the concrete cylinder experiments were pinned (upper support), fixed (lower support) as shown in Figure 3.3. Average compressive strengths obtained for each casting are tabulated in Table 3.3 and further details of results given in Appendix A.

TABLE 3.3: Characteristic Strength of Concrete for Castings

Casting No.	Mix	f'_c	Casting No.	Mix	f'_c	Casting No.	Mix	f'_c
CA3	A	65.4	CA7	A	46.3	CA11	B	100.6
CA4	B	92.2	CA8	B	82.4	CA12	A	58.0
CA5	A	67.4	CA9	B	94.4	CA13	B	87.9
CA6	B	93.45	CA10	A	57.7			

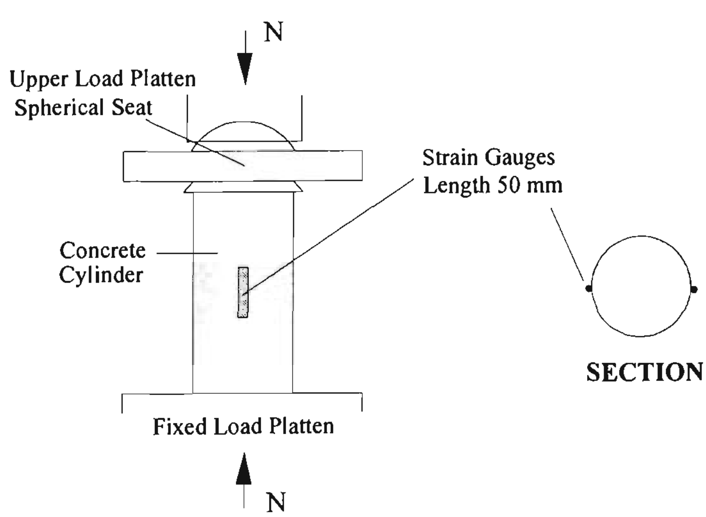

Figure 3.3: *Strain gauge arrangement for concrete cylinders.*

To examine the stress-strain relationship of the HSC mixes, selected cylinders from castings CA11 and CA12 were instrumented with strain gauges and tested at the BHP Laboratories. Two strain gauges having nominal gauge lengths of 50 mm were attached at midheight of each cylinder and linked to a Hewlett Packard data acquisition system. Gauge locations are represented schematically in Figure 3.3. Initial attempts to record the radial strain and Poisson's ratio of the concrete cylinders were inconclusive. The results of these experiments are detailed in Section 4.2.

3.2.2.4 Discussion of Concrete Properties

In all HSC cylinders, an explosive mode of failure occurred simultaneously with ultimate load. The rapid release of energy was intensified for the higher strength Mix B cylinders which left only a scatter of debris after fracture. Typical cone type failure as expected in normal grade concrete (Mak and Attard, 1990) was not clearly identified in the tests undertaken by this program.

It was noted that castings CA7 and CA8 yielded significantly lower strengths than expected. This decrease in strength was attributed to the sand (new delivery) having excessive moisture content at the time of casting. This problem was rectified for proceeding castings by allowing the sand to dry to acceptable moisture contents. For casting CA11, the compressive strength of the concrete reached over 100 MPa by thoroughly cleansing the 11 mm and 7 mm aggregates prior to their use. This variation between results emphasises the need for strict controls when using HSC.

Statistically the standard deviation of concrete cylinder strengths for each casting were predominantly below 3% of the mean. The greatest standard deviation of 4.8% was obtained for casting CA4 as a result of a single cylinder yielding a marginally lower value (refer to Table A.2 Appendix A). On the basis of the close correlation between cylinder results for each casting group, the characteristic strength of the concrete f'_c was taken as the mean of cylinder results f_{cm}.

3.3 TEST PROCEDURES

3.3.1 Testing of CFST Columns

The composite columns were cast in the vertical position with an impermeable membrane capping applied to the base of the steel tubes to prevent bleeding of the concrete infill during initial placement. The concrete filling was performed in equal layers with depths corresponding to the diameter of the tube. Compaction was performed progressively for each layer in accordance to AS1012 procedures to ensure homogeneity within the core. The upper surface of the concrete was then smoothed to a level surface and sealed so that the concrete was under hermetic conditions. The CFST specimens were allowed to set for a 24 hour duration before being transferred into the fog room (detailed in section 3.2.2.1). Preliminary tests observed the combination of moisture and air inside the fog room resulted in a build up of surface rust on the exterior of the steel. By submerging the CFST specimens in a lime saturated water bath the formation of rust was minimised. Specimens remained submerged to cure until testing at 28 days.

Prior to testing, each end of the column specimen was capped to ensure even load distribution to the steel and concrete given longitudinal strain compatibility ($\varepsilon_{cl}=\varepsilon_{sl}$). A high strength sulphur capping compound was used for the majority of test specimens, however this material was observed to exhibit a minor degree of compressibility. An alternative method using high strength epoxy resin (130 MPa) was used for the latter part of the test program. Plastic inserts of 2 mm thickness were cast into each end of the CFST columns. Once removed the remaining void was over-filled with the high strength epoxy resin. The resin once set, was machined back to a flush surface with the ends of the tube. The two capping procedures are illustrated in Figure 3.4 A comparison between each technique verified the epoxy resin capping as the superior option.

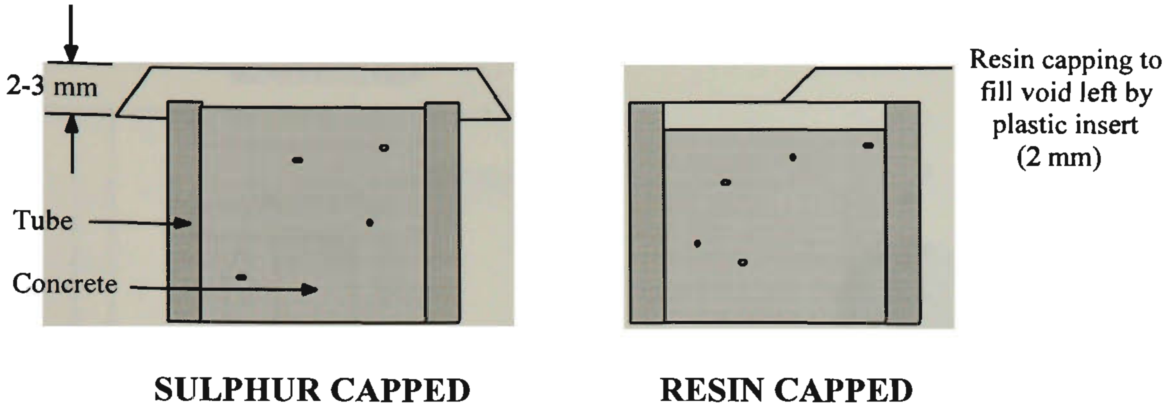

Figure 3.4: *Capping techniques for CFST specimens.*

3.3.1.1 Loading Arrangement and Instrumentation - Series I (VUT).

CFST specimens tested at Victoria University (CA3-CA10) were concentrically loaded in a 'Mori' 200 tonne capacity hydraulic testing machine as illustrated in Figure 3.5. The apparatus consisted of a lower load platen being fixed to the hydraulic loading ram, and the upper platen fixed to the machine cross head through a spherical bearing seat replicating pinned conditions. Longitudinal deformations of the specimens were measured by means of three displacement gauges placed between the load platens at 120° spacing around the tube perimeter.

Once specimens were aligned centrally within the centroid of the load platens, a small load was applied to the specimen and removed to allow for any settlement of surface grit on the end capping, and to verify the alignment of the column. Axial load was applied at constant displacement rate of 0.15 mm/min. with values of longitudinal displacement taken at regular load increments. This process was continued well beyond the attainment of ultimate load until specimens were grossly deformed, clearly defining the mode of failure. At this stage the load resistance of the column nearly receded to between 60-70% of the ultimate capacity. Depending on the ductility and residual strength exhibited by specimens in the post ultimate range, the displacement rates for some tests were increased up to 0.6 mm/min. The duration of loading times for each test ranged between 20 to 50 min.

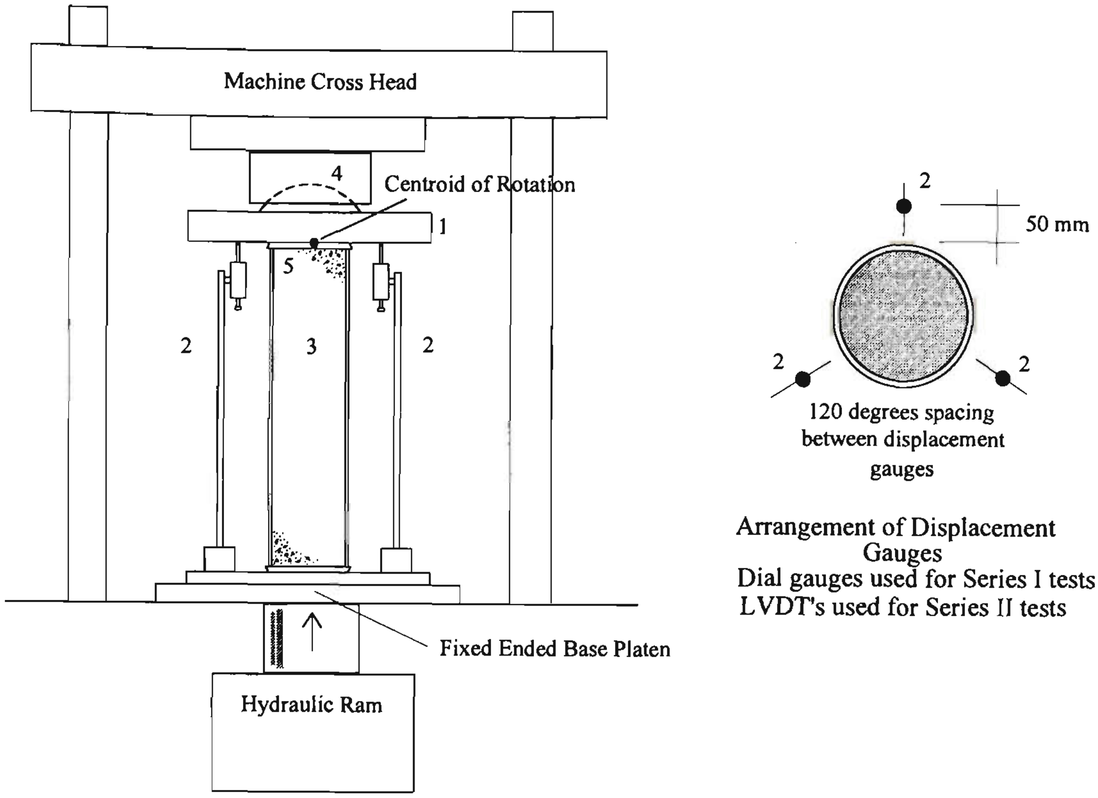

Figure 3.5: *Composite test specimen set-up: 1. Loading platens, 2. Displacement gauges, 3. Composite specimens, 4. Spherical bearing seat, 5. Capping compound.*

3.3.1.2 Loading Arrangement and Instrumentation - Series II (BHP)

In selected Series II tests, electrical resistance strain gauges with biaxial elements measuring longitudinal and transverse strains were attached to the steel tube. Three gauges were attached at midheight of each specimen on axis spaced apart by 120°. Further gauges were attached at various heights to examine the uniformity of the strains along the specimens. Gauge locations and numbering sequences are represented schematically in Figure 3.6. Overall longitudinal displacements were recorded by three linear variable displacement transducers (LVDT) a shown in Figure 3.5. Load tests were performed in an 'Instron' 1 MN capacity Servo-Hydraulic Universal Testing Machine with end conditions replicating the earlier VUT tests. Specimens were centralised by applying small increments of load and monitoring midheight strain gauges to ensure uniformity. Load was applied by means of a constant machine ramp rate corresponding to displacement rate used in Series I experiments. A Hewlett

Packard data acquisition and control system was used to record measurements of applied load, strain and displacements at 5 second intervals. Specimens tested under strain gauge instrumentation included: CA11-47.6-MB-1, CA11-47.6-MB-2, CA11-47.6-MB-4, CA13-38-HB-1 and CA13-38-HB-4.

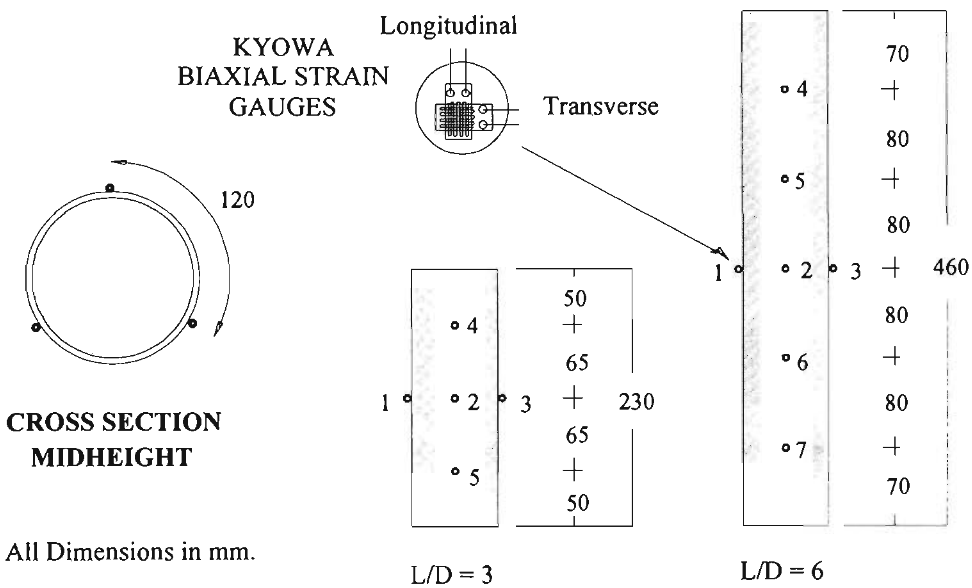

Figure 3.6: *Strain gauge arrangement for BHP test specimens from castings CA11 and CA13.*

3.3.2 Hollow Steel Tube Tests

Tests were performed on hollow steel tube (HST) columns to obtain their squash load capacities and behaviour under uniaxial compression. Two specimens, for each tube geometry used in CFST columns, were tested under exact procedures described in Section 3.3.1.1 for CFST columns. These results are presented in Section 4.3.

3.3.3 Concrete Core Tests

To compare the compressive strength of the concrete determined from standard cylinders and the actual core strength within a CFST column, two types of tests were per formed on cores removed from their steel encasement.

3.3.3.1 Type A Core Tests

Type A core tests were performed to examine the potential scaling effects between the 100 mm diameter cylinders and the 72.9 mm diameter concrete cores. Cores were removed from the steel encasement after being cast and cured as CFST columns. Specimens were cut to L/D ratios of 2, replicating the geometric ratio of the cylinders. Cores were then capped using high strength sulphur capping and tested to failure under a constant stress rate of 20 MPa/min. (1.39 kN/sec.).

3.3.3.2 Type B Core Tests

Type B core tests consisted of full length core samples tested under constant displacement rates of 0.15 mm/min. used for CFST specimens. These tests were to examine the effects of load rate and column slenderness on the comparative strengths of concrete cores/cylinders.

3.4 GEOMETRIC PROPERTIES OF TEST SPECIMENS

A summary of the geometric and material properties for the various test specimens are presented in Tables 3.4 to 3.6. In each table and throughout the thesis, specimens have been designated by the following notation:

CFST TEST SPECIMENS

CA3-47.6-MA-1

Casting No.

D/t Ratio

Specimen No.

Concrete Mix

Steel Strength
(M - Mild, H - High)

Note: When referring to average values of a group of specimens with identical experimental parameters, specimen numbers are replaced with the corresponding column lengths

HOLLOW STEEL TUBE TESTS

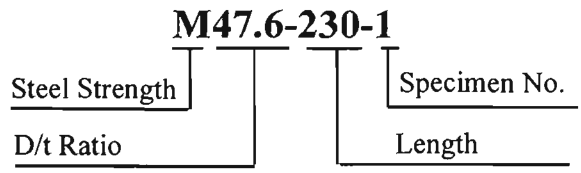

CONCRETE CORE TESTS

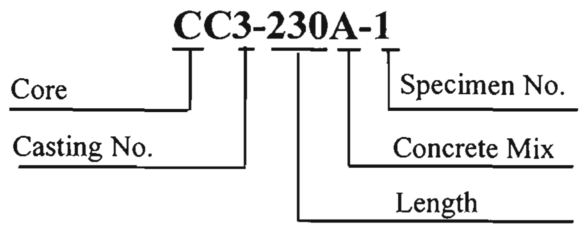

TABLE 3.4: Geometric Properties of CFST Specimens

Casting Code	Specimen No. (s)	D (mm)	t (mm)	D/t ratio	L (mm)	L/D	f'_c (MPa)	f_y (MPa)
Series I								
CA3	1 - 3	76.1	1.6	47.6	230	3.02	65.4	239
CA3	4 - 6	76.1	1.6	47.6	460	6.04	65.4	239
CA4	1 - 3	76.1	1.6	47.6	230	3.02	92.2	239
CA4	4 - 6	76.1	1.6	47.6	460	6.04	92.2	239
CA5	1 - 3	76.1	1.6	47.6	600	7.88	67.4	239
CA5	4 - 6	76.1	1.6	47.6	740	9.82	67.4	239
CA6	1 - 3	76.1	1.6	47.6	600	7.88	93.45	239
CA6	4 - 6	76.1	1.6	47.6	740	9.82	93.45	239
CA7	1 - 3	75.4	1.25	60.3	230	3.05	46.3	239
CA7	4 - 6	74.6	0.85	87.8	230	3.08	46.3	239
CA8	1 - 3	75.4	1.25	60.3	230	3.05	82.4	239
CA8	4 - 6	74.6	0.85	87.8	230	3.08	82.4	239
CA9	1 - 3	75.4	1.25	60.3	460	6.10	94.4	239
CA9	4 - 5	74.6	0.85	87.8	460	6.17	94.4	239
CA10	1 - 3	75.4	1.25	60.3	460	6.10	57.7	239
CA10	4 - 5	74.6	0.85	87.8	460	6.17	57.7	239
Series II								
CA11	1 - 3	76.1	1.6	47.6	230	3.02	100.6	495
CA11	4	76.1	1.6	47.6	460	6.04	100.6	495
CA12	1 - 3	76.1	2.0	38.05	230	3.02	58.0	495
CA12	4 - 6	76.1	2.0	38.05	460	6.04	58.0	495
CA13	1 - 3	76.1	2.0	38.05	230	3.02	87.9	495
CA13	4 - 6	76.1	2.0	38.05	460	6.04	87.9	495

TABLE 3.5: Geometric Properties of Hollow Steel Tubes

Specimen Code	Specimen No. (s)	D (mm)	t (mm)	L (mm)	f_y (MPa)	f_u (MPa)
MS						
47.6M-230	1 - 2	76.1	1.6	230	239	297
47.6M-460	1 - 2	76.1	1.6	460	239	297
47.6M-600	1 - 2	76.1	1.6	600	239	297
47.6M-740	1 - 2	76.1	1.6	740	239	297
60.3M-230	1 - 2	75.4	1.25	230	239	297
60.3M-460	1 - 2	75.4	1.25	460	239	297
87.8M-230	1 - 2	74.6	0.85	230	239	297
87.8M-460	1 - 2	74.6	0.85	460	239	297
HSS						
38H-115	1 - 3	76.1	2.0	115	495	495
38H-230	1 - 2	76.1	2.0	230	495	495
38H-460	1 - 2	76.1	2.0	460	495	495

E_s : Adopted as 200,000 MPa

TABLE 3.6: Geometric Properties of Concrete Core Tests

Specimen Code	No. of Specimens	d_c (mm)	L (mm)	f'_c (MPa)
Type A				
CC7-230A	3	72.9	144	46.3
CC8-230B	3	72.9	144	82.4
CC9-460B	3	72.9	144	94.4
CC10-460A	3	72.9	144	57.7
Type B				
C7-230A	3	72.9	230	46.3
C8-230B	3	72.9	230	82.4
C9-460B	3	72.9	460	94.4
C10-460A	3	72.9	460	57.7

3.5 VERIFICATION OF EXPERIMENTAL PROCEDURES

One questionable aspect of the experiment program was whether the characteristic strength of the concrete determined from cylinder tests gave an accurate representation of the uniaxial strength of the concrete prism within a CFST column. To substantiate the comparative strengths of cylinders to cores, tests were performed to verify the effects of curing condition and specimen size.

3.5.1 Effects of Curing Condition on Concrete Strengths

Urpani et al. (1991), found that the compressive strength of HSC cylinders was shown to be effected considerably by the curing regime to which the concrete was subjected. The degree of water penetration or egress under each environment, size effects and ratio of exposed surface area to volume, were shown to influence the compressive strength of test cylinders. The authors recorded up to 25% difference in strengths determined from moist cured and dry cured cylinders. In CFST columns with sealed ends, the concrete infill is in essence hermetically sealed, while concrete cylinders cured in accordance with AS1012 are completely exposed. Therefore, preliminary tests were carried out to verify experimental curing conditions whereby the strengths of concrete cylinders and cores were equivalent.

For two trial concrete mixes, specimens of 100mm diameter cylinders (**CYL**) and CFST columns were cast and subjected to various curing conditions described below and designated by the prefixes given.

1. Dry cured specimens left in a room environment for 28 days. **(EXP)**
2. Moist cured specimens placed in a humidity controlled fog room for 28 days (23°C and 95-100% RH.). **(FR)**
3. Specimens cured submerged in a lime saturated water bath within a fog room. **(WB)**

Prefixes '**U**' and '**S**' have also been used to define core specimens taken from CFST columns with unsealed ends and sealed ends respectively.

After curing for 28 days, core samples (**CORE**) were removed from the CFST sections and trimmed to L/D ratios of 2. A minimum of four samples were taken for each curing criteria. Compressive tests were performed using procedures detailed in Section 3.2.2.3. Average results obtained for each concrete mix and specimen type are presented in Table 3.7.

TABLE 3.7: Effects of Curing Conditions on the Compressive Strength of Concrete

SPECIMEN TYPE	TRIAL MIX 1 CURING CONDITION			TRIAL MIX 2 CURING CONDITION		
	EXP	**FR**	**WB**	**EXP**	**FR**	**WB**
CYL	47.6	57.9	**60.2**	59.6.	79.8	**81.9**
CORE	56.1 /S 53.2 /U		**59.2 /U**	80.2 /S 68.4 /U		**82.8 /U**

The results indicated that concrete strengths determined from cylinder and core specimens cured in the water bath environment compared favourably with strength variations below 1.7 percent. Consequently, these curing procedures were adopted as the preferred option for the experimental program.

3.5.2 Effects of Specimen Size and Load Rate

Type A and B core tests outlined in Section 3.3.3 were performed to examine potential variations in concrete strength due to specimen size and load rates applied. Details of results are represented in Tables A.3 and A.4 of Appendix A. It was observed from Type A tests that the ratio between core and cylinder strengths, varied between 0.947 to 1.043. As the results were generally within 5% and failed to exhibit any distinct pattern, it was assumed that the scale effects between 100 and 72.9 mm diameter were negligible.

In Type B core tests, squash load capacities were predominantly less than f'_c. For the 230 mm long cores (L/D $\approx$3), the ratio of core to cylinder strength varied between 0.998-1.013 for Mix A, and 0.918 to 0.953 for Mix B specimens. In 460 mm long cores (L/D $\approx$ 6), the corresponding ratios ranged between 0.896-0.937 and 0.889-0.901 for Mix A and B tests respectively. It was apparent that column slenderness had a marked effect on the compressive strength of the concrete with core strengths reducing by approximately 10% as specimen lengths increased to 460 mm. With the ratio of core/cylinder strengths for Mix A - 230 mm specimens equivalent to unity, it would suggest that differences in load rates between test procedures, did not substantially effect the compressive strength of the concrete.

CHAPTER 4: TEST RESULTS AND OBSERVATIONS

4.1 OVERVIEW

In this chapter, the results obtained from axial compressive tests described in the previous chapter are presented. The various types of tests performed are addressed in the following order:

- Unconfined Concrete Specimen Tests
- Hollow Steel Tube Tests
- Concrete Filled Steel Tube Tests

4.2 EXPERIMENTAL RESULTS - UNCONFINED HSC

4.2.1 Behaviour of Unconfined HSC

From preliminary test results reported in Section 3.5, it was found that the compressive strength obtained from concrete cylinders compared favourably with the uniaxial strength of the concrete prism within a CFST column. Consequentially, the stress-strain relationships and elastic modulus (E_c) of the two concrete grades were obtained from standard 100 mm diameter cylinders tested in accordance to AS1012 Part 9.

The experimental stress-strain relationships obtained are shown in Figure 4.1, in which each curve is representative of an average of two gauge readings. The recorded peak stresses (f'_c) and strains (ε_{co}), and measured elastic modulus (E_c) are listed in Table 4.1. With the load applied at a constant load rate in preference to a constant strain rate, the unloading branch of the σ-ε relationship could not be obtained. Hence the experimental curves are only representative of the ascending concrete behaviour as brittle fracture occurred at peak stress. Examining the disbursed fragments of the HSC specimens indicated that failure had occurred under the combined actions of both vertical tensile splitting and oblique shear crack patterns. A description of such failure patterns for unconfined concrete can be found in Neville (1981).

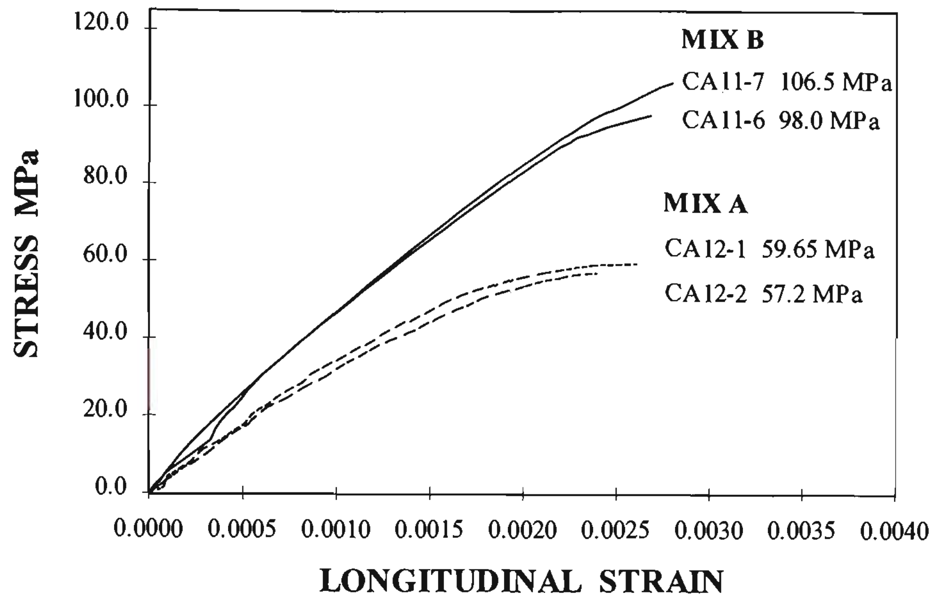

Figure 4.1: *Experimental stress-strain relationship for HSC cylinders - castings CA11 (Mix B) and CA12 (Mix A).*

TABLE 4.1: Stress-Strain Test Results of Unconfined Concrete.

Cyl No.	Mix	f'c MPa	ε_{co} ($\mu\varepsilon$)	E_c (exp) MPa
CA11-6	B	98.0	2685	47,380
CA11-7	B	106.5	2805	48,750
		Mean	**2750**	**48,070**
CA12-1	A	57.2	2340	33,990
CA12-2	A	59.65	2610	36,510
		Mean	**2480**	**35,250**

For the higher grade concrete Mix B, divergence from the initial linear elastic behaviour was not evident until stress levels beyond 90% of the ultimate strength. The corresponding proportion was considerably less (70-75%) for the lower strength Mix A concrete. The shape of the stress strain curves is consistent with that explained from micro cracking studies detailed in Section 2.3.1.

4.2.1.1 Strain at Peak Stress

The strain ε_{co} at peak stress recorded for the tests undertaken, increased with increases in compressive strength. The average peak strains recorded for concrete Mix A and Mix B were 2480 $\mu\varepsilon$ and 2750 $\mu\varepsilon$ respectively. Investigations by Fafitis and Shah (1986) and Ahmad and Shah (1985) proposed linear relationships to predict ε_{co} for increases in concrete compressive strength as defined by Eqn. 4.1 and 4.2 respectively. For the nominal concrete strengths of 60 and 90 MPa, Fafitis and Shah's equation predicts values of ε_{co} equal to 2840 and 3290 $\mu\varepsilon$, and Ahmad and Shah 2640 and 3130 $\mu\varepsilon$ respectively. The predicted values were observed to overestimate experimental strain by between 6 to 20 percent with the greatest discrepancy observed for the 90 MPa concrete.

Fafitis and Shah $$\varepsilon_{co} = 0.00195 + 1.4895x10^{-5} f'_c \quad \textbf{(4.1)}$$

Ahmad and Shah $$\varepsilon_{co} = 0.001648 + 1.65x10^{-5} f'_c \quad \textbf{(4.2)}$$

Experimental investigations reported by Setunge et al. (1992) found that concretes having similar compressive strength but different compositions, may not necessarily exhibit the same characteristics. For concrete strengths of 90-130 MPa using different types of aggregate and silica fume content, the authors recorded values of peak strain (ε_{co}) between 2400 $\mu\varepsilon$ to 3750 $\mu\varepsilon$. This is the most probable cause for the discrepancy between the Mix A and B experimental strains and those predicted using Eqn.'s 4.1 and 4.2. Setunge et al. proposed that, in the absence of experimental data for each particular concrete, a mean value of 2800 $\mu\varepsilon$ should apply to HSC using Basalt aggregate. Based on the inconsistency of empirical models for peak strain, the averaged experimental results are used in further discussions and analysis.

4.2.1.2 Elastic Modulus E_c

The measured values of E_c were determined in accordance with AS1012 Part 17 by taking a chord between the origin and the curve intersect, at a stress equivalent to 40 % peak stress. In Table 4.2, experimental values are compared with predicted values from Australian Standard - AS3600 (Eqn. 4.3), and empirical models for HSC as derived by Carrasquillo et al. and Ahmad and Shah (Eqn's 4.4 and 4.5 respectively).

$$E_c = 0.043\rho^{1.5}\sqrt{f'_c} \quad \textbf{(4.3)}$$

$$E_c = (3320\sqrt{f'_c} + 6900).(\rho/2320)^{1.5} \quad \textbf{(4.4)}$$

$$E_c = 3.38\rho^{2.5}(f'_c)^{0.325}x10^{-5} \quad \textbf{(4.5)}$$

The ratio of experimental to predicted values based on the existing code expression varied between 0.87 to 0.97, suggesting Equation 4.3 overestimates the effective E_c of HSC. Predictions based on Eqn.'s 4.4 and 4.5 were generally below the experimental results with ratios between 1.01 to 1.13 and 0.96 to 1.12 respectively. These HSC empirical formulae are conservative by more than 10 percent for the higher grade Mix B concrete.

TABLE 4.2: Elastic Modulus of HSC Cylinders.

Cyl No.	Mix	f'c MPa	$E_{c\ exp}$	AS3600	$\frac{E_{c\ exp}}{AS3600}$	Eqn 4.4	$\frac{E_{c\ exp}}{Eqn\ 4.4}$	Eqn 4.5	$\frac{E_{c\ exp}}{Eqn\ 4.5}$
CA11-6	B	98.0	47,380	52,170	0.91	41,840	1.13	42,320	1.12
CA11-7	B	106.5	48,750	50,050	0.97	43,310	1.13	43,480	1.12
CA12-1	A	57.2	33,990	39,050	0.87	33,680	1.01	35,530	0.96
CA12-2	A	59.65	36,510	38,240	0.96	34,230	1.06	36,020	1.01

4.2.1.3 Modified Stress-Strain Model for HSC - Uniaxial Conditions

In Figure 4.2, the experimental stress-strain curves for HSC are compared against predicted relationships using the model proposed by Fafitis and Shah (1986). The model consisted of two functions defining the ascending and descending σ-ε curves for both unconfined and laterally confined HSC. For the uniaxial condition, the functions are defined by Eqn's. 4.6 to 4.9. It was noted in Section 4.2.1.1 that the author's empirical equation used for determining the peak strain overestimated the experimental values. Consequently the predicted curves have been modified using experimental peak strains in preference to Eqn. 4.1. From the figure it is shown that the modified Fafitis and Shah relationship depicts the ascending branch of the experimental curves to a high degree of accuracy.

$$f = f'_c[1-(1-\varepsilon/\varepsilon_{co})^A] \qquad \varepsilon < \varepsilon_{co} \tag{4.6}$$

$$f = f'_c \exp[-k(\varepsilon-\varepsilon_o)^{1.15}] \qquad \varepsilon > \varepsilon_{co} \tag{4.7}$$

$$k = 24.7f'_c \tag{4.8}$$

$$A = E_c(\varepsilon_{co}/f'_c) \tag{4.9}$$

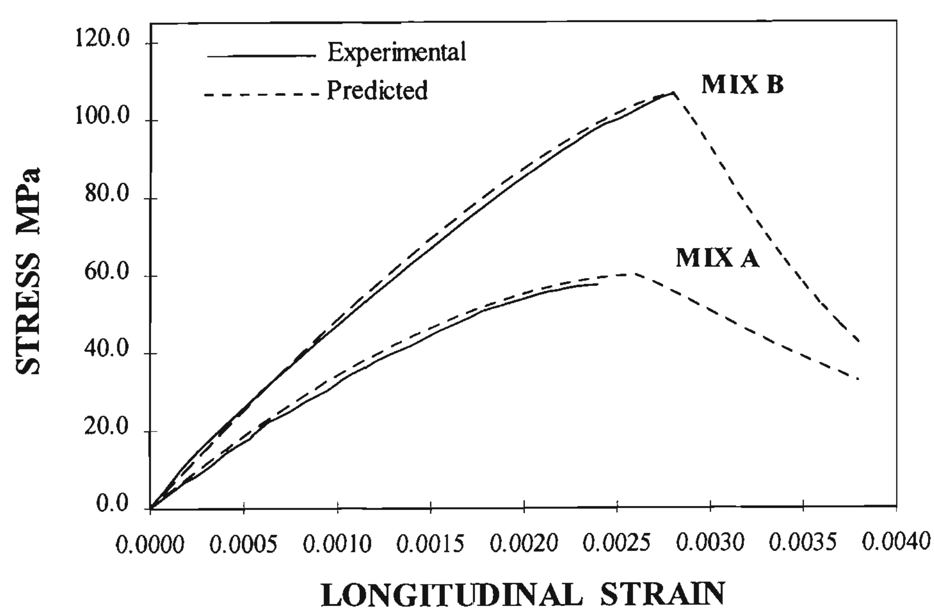

Figure 4.2: *Experimental stress-strain curves for HSC (uniaxial conditions) as compared with modified predictions by Fafitis and Shah (1986).*

4.3 EXPERIMENTAL RESULTS - HOLLOW STEEL TUBES

4.3.1 Ultimate Squash Load Capacity - Hollow Steel Tubes

The results of axial compressive tests on Hollow Steel Tube (HST) columns are summarised in Table 4.3. A comparison between the ultimate load capacity of steel columns and values predicted based on tensile coupon yield strengths are also included. For stub columns (L/D = 3), the ratio N_{stub}/N_{coup} ranged between 0.988 to 1.036 disregarding the remote result of specimen M87.8-230-1 (1.073). This indicates that the effective strengths determined from tensile coupon tests are adequate for design purposes for uniaxial compression. When slenderness of column sections increased, the measured ratio of N_{stub}/N_{coup} declined. The slenderness reduction was greatest in the thin walled sections. For Mild Steel Tube with D/t ratio of 87.8 the value of N_{stub}/N_{coup} reduced from 1.01 to 0.81 as column length increased from 230 mm to 460 mm. As this value is less than unity, it suggests that the column strength has been influenced by inelastic local buckling mechanisms.

The concept of 'effective width' determination to predict the reduced capacity of thinwalled plate elements due to local buckling mechanisms, was performed in accordance with Australian Standard AS4100 "The Design of Steel Structures" (1990). The code applies an effective form factor 'k_f' given as a ratio of the reduced area to the nominal cross sectional area (A_e/A_s). With the exception of one tube type, the tube cross sections were considered fully effective ($k_f = 1$). For the M87.8 tube the k_f factor was calculated to be 0.989. This reduced section does not significantly modify predicted capacities based on nominal areas and has been omitted from further consideration.

Peak strains (ε_o) recorded at ultimate load were observed to vary between 2300 $\mu\varepsilon$ to 10300 $\mu\varepsilon$ for the Mild Steel columns, and between 8000 $\mu\varepsilon$ to 14000 $\mu\varepsilon$ for the High Strength Steel columns. The strains were by far greater for specimens having lesser values of wall slenderness (D/t) and column slenderness (L/D). For the MS tube the mean yield strain (ε_y) was 0.0026 with a standard deviation of 0.0003. The corresponding values for the HSS tube were 0.0036 and 0.0006 respectively.

TABLE 4.3: Hollow Steel Column - Squash Load Capacities

Tube Notation	f_y (MPa)	A_s (mm2)	L/D	N_{exp} (kN)	σ_{exp} (MPa)	ε_o	$\frac{N_y (0.1\%)}{N_{exp}}$	$\varepsilon_{y(0.1\%)}$	$\frac{N_{exp}}{N_{coup}}$
Mild Steel									
M47.6-230-1	239	374.48	3.02	**90.7**	**242.2**	0.0103	0.843	0.0023	1.013
M47.6-230-2	239	374.48	3.02	**91.7**	**244.9**	0.0083	0.872	0.0025	1.025
M47.6-460-1	239	374.48	6.04	**89.8**	**239.8**	0.0070	0.902	0.0024	1.003
M47.6-460-2	239	374.48	6.04	**90.7**	**242.2**	0.0065	0.899	0.0027	1.013
M47.6-600-1	239	374.48	7.88	**87.8**	**234.5**	0.0055	0.900	0.0024	0.981
M47.6-600-2	239	374.48	7.88	**87.3**	**233.1**	0.0065	0.905	0.0024	0.975
M47.6-740-1	239	374.48	9.72	**87.8**	**234.5**	0.0057	0.934	0.0027	0.981
M47.6-740-2	239	374.48	9.72	**84.9**	**226.7**	0.0061	0.913	0.0026	0.949
M60.3-230-1	239	291.19	3.05	**72.1**	**247.6**	0.0054	0.945	0.0026	1.036
M60.3-230-2	239	291.19	3.05	**69.7**	**239.4**	0.0061	0.941	0.0029	1.002
M60.3-460-1	239	291.19	6.10	**67.7**	**232.5**	0.0035	0.962	0.0027	0.973
M60.3-460-2	239	291.19	6.10	**67.2**	**230.8**	0.0035	0.958	0.0029	0.966
M87.8-230-1	239	196.94	3.08	**50.5**	**256.4**	0.0044	0.875	0.0032	1.073*
M87.8-230-2	239	196.94	3.08	**47.1**	**239.2**	0.0035	0.936	0.0032	1.001
M87.8-460-1	239	196.94	6.17	**39.7**	**201.6**	0.0033	0.927	0.0023	0.843
M87.8-460-1	239	196.94	6.17	**38.3**	**194.5**	0.0023	1.000	0.0023	0.814
High Strength									
H8-115-1	495	465.58	1.51	**232.5**	**499.4**	0.0140	0.898	0.0043	1.009
H38-115-2	495	465.58	1.51	**227.6**	**488.9**	0.0125	0.841	0.0041	0.988
H38-230-1	495	465.48	3.02	**229.6**	**493.1**	0.0110	0.904	0.0027	0.996
H38-230-2	495	465.48	3.02	**227.6**	**488.9**	0.0080	0.912	0.0037	0.988
H38-460-1	495	465.48	6.04	**232.5**	**499.4**	0.0090	0.925	0.0036	1.009
H38-460-2	495	465.58	6.04	**227.1**	**487.8**	0.0090	0.914	0.0035	0.985

4.3.2 Load-Strain Relationships

Average load versus strain curves obtained for steel column tests are illustrated in Figures 4.3 a) to d). The values of strain were obtained as a measure of column shortening / column length and are the mean of three displacement gauge readings for each test. In Figure 4.4, the measured relationships for stub columns (L/D = 3) are presented in terms of Stress and Strain. This relationship is representative of the gross column deformation, and assumes uniform distribution of longitudinal strain throughout the column length.

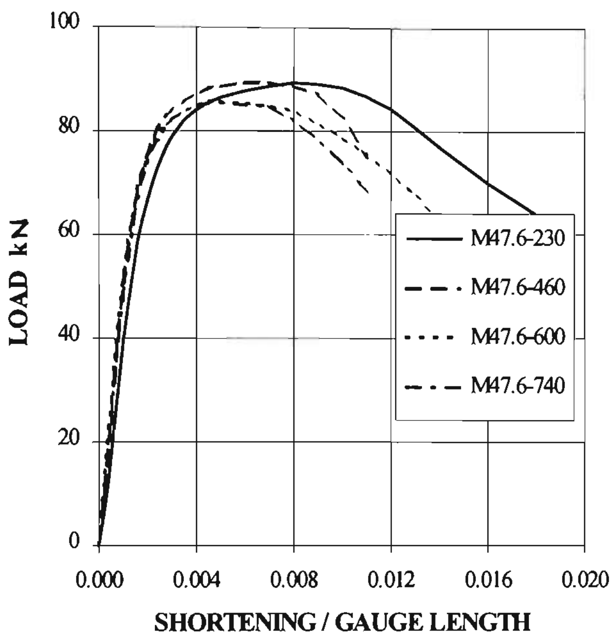

a) *Mild Steel D/t 47.6*

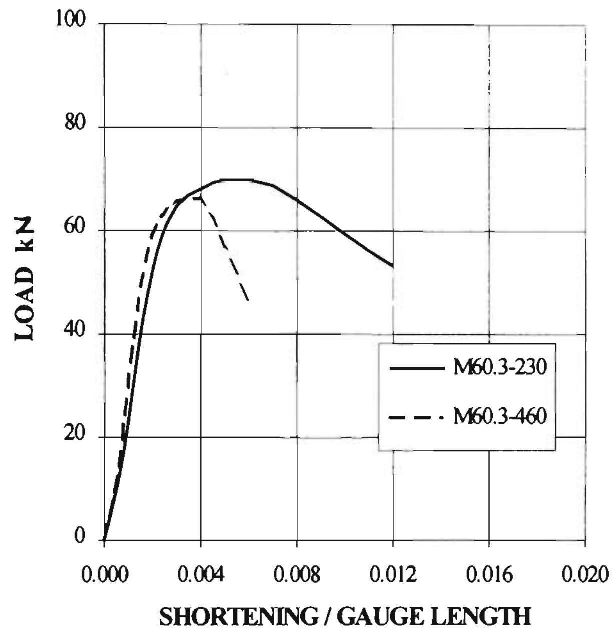

b) *Mild Steel D/t 60.3*

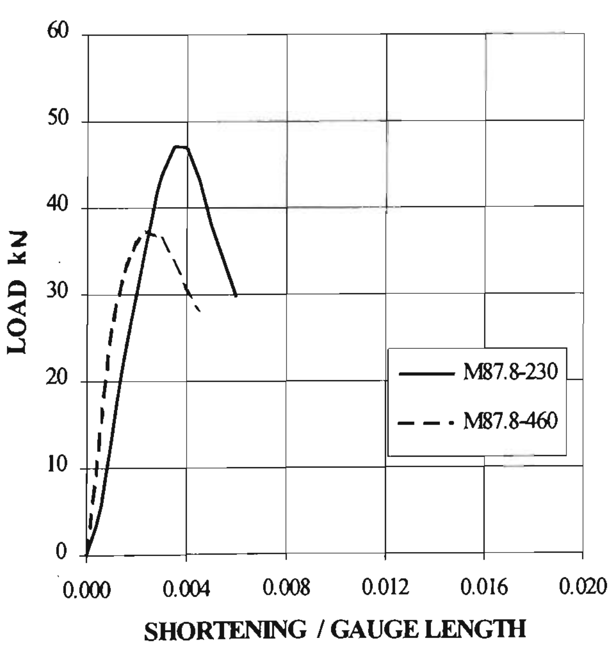

c) *Mild Steel D/t 87.8*

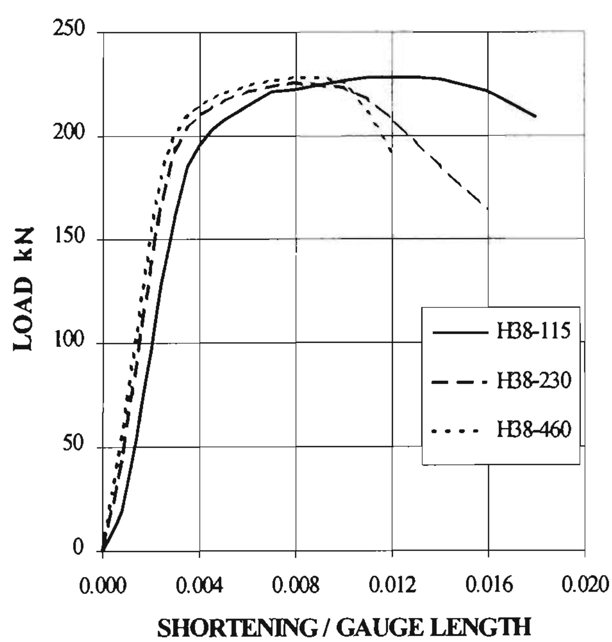

d) *High Strength Steel D/t 38.05*

Figures 4.3 a) to d): *Load - strain relationships for Hollow Steel Tube sections.*

Although exhibiting unique characteristics, each curve could be classified as consisting of three successive stages:

1. Linear Elastic stages
2. Elasto-Plastic plateaus
3. Unloading Behaviour in the post ultimate domain.

It can be observed from the Figures 4.3 a) to d), that the H38 and M47.6 tube sections exhibit distinct improvements in ductile behaviour and strain capacities over that of M60.3 and M87.8 sections. As there was no clearly defined yield point, proportional yield limits were specified as proof stress values (percentage strain offsets) as applied for tensile tests. Initial strain offsets of 0.2 % were observed to intersect experimental curves beyond ultimate conditions. Therefore yield limits have been specified at 0.1 % offset strains. From Table 4.3 the measured proportional limits of $N_{y(0.1\%)}$ / N_u varied between 0.843 to 1.000 for the MS tube and 0.840 to 0.925 for the HSS tube. The corresponding values of yield strain $\varepsilon_{y(0.1\%)}$ varied between 2300 - 3600 $\mu\varepsilon$ and 3500 - 4700 $\mu\varepsilon$ for the MS and HSS tube columns respectively.

Figure 4.5 is a reproduction of Figure 4.4 using a normalised stress format of σ_{exp} / σ_y. Here the reduced ductility of the thinwalled sections having D/t ratios of 87.8 is apparent. These columns behave elastically up to ultimate load without notable elasto-plastic behaviour, and exhibit steeper unloading characteristics. This behaviour is attributed to the fact that in thin walled sections the strain required to cause local buckling of the tube wall approach the yield strain of the material. This prevents the development of elasto-plastic stages typified by the experimental results.

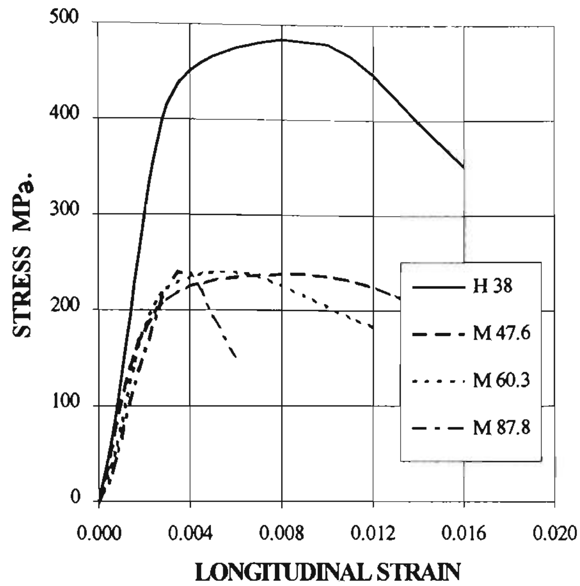

Figure 4.4: *Stress-strain relationship steel stub columns (L/D = 3).*

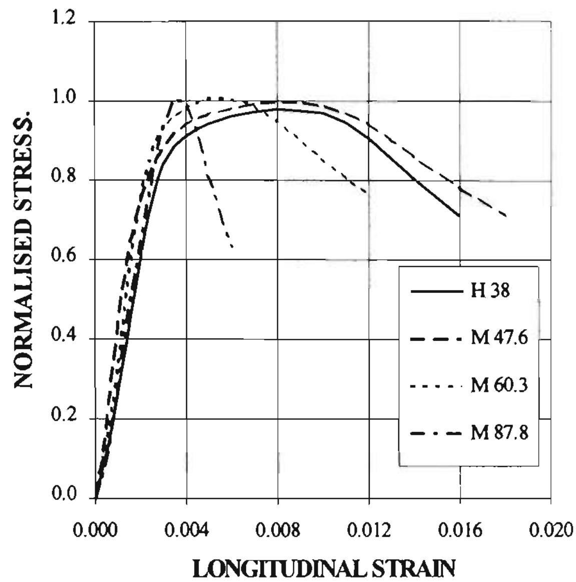

Figure 4.5: *Normalised stress-strain relationship steel stub columns (L/D = 3).*

4.3.3 <u>Modes of Failure</u>

In all HST tests, no visible evidence of failure was observed prior to the specimens achieving their ultimate load capacities. In the post ultimate range, the structural failure processes became evident. The modes of failure for the hollow tube specimens could be classified as one of two mechanisms:

- Local buckling of the tube wall.
- Overall column instability.

In all specimens with column length ≤ 460mm, the failure of the tube was characterised by the formation of a continuous concentric local buckle around the tube diameter as shown in Plate's 1 a) and b). The buckle occurred generally within 30 mm of the top of the column and the magnitude of lateral deformation was greatest in thicker walled sections. The appearance of such failure mode was observed to occur only as the ultimate axial capacity was reached. This leads to the conclusion that the strains corresponding to ultimate load ε_0 as given in Table 4.3, are representative of the local buckling strains for each HST column.

For specimens with length ≥ 600 mm, the mode of failure was characterised as an overall column buckling mode as shown for two slender specimens in Plate 4.1 a). The buckling of the column occurred through the formation of an inward plastic collapse mechanism of the tube wall, within the mid height of the section. Local buckling was also observed to occur at the end of these longer specimens on opposing sides to the inward collapse region.

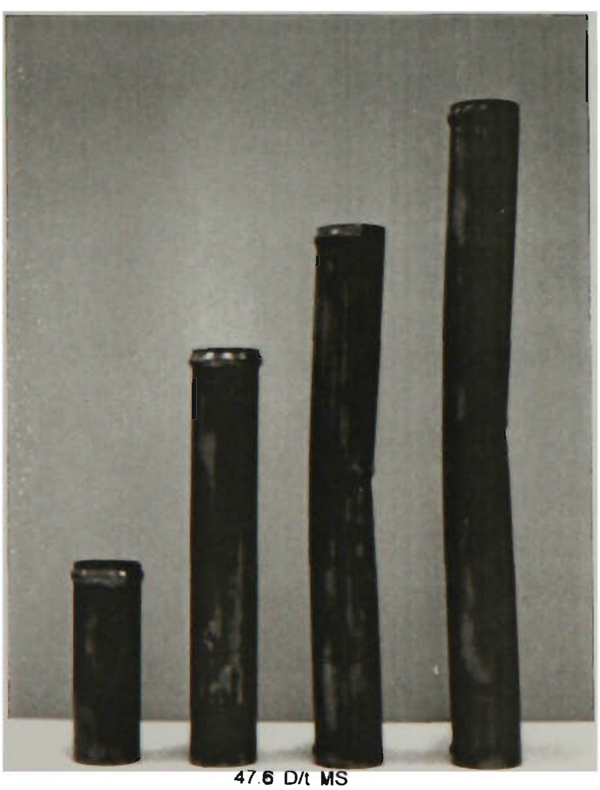

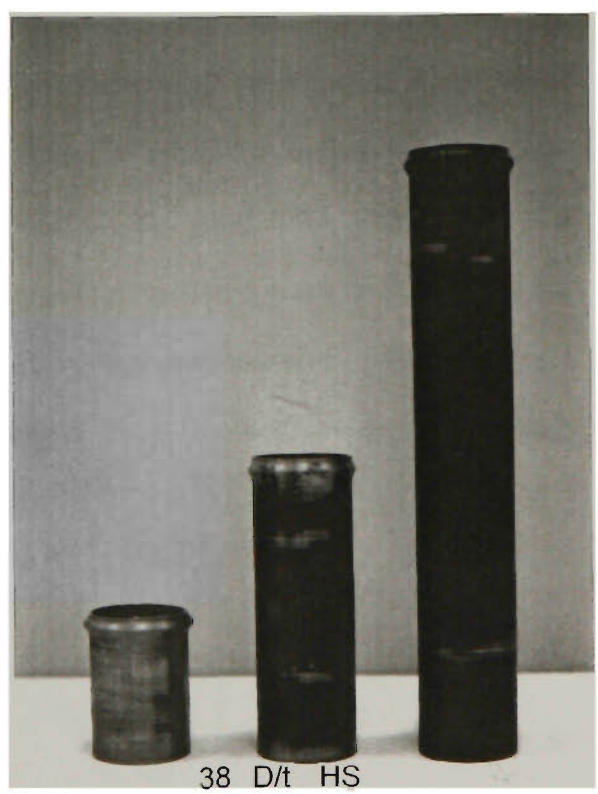

a) b)

Plate 4.1: *Failure modes hollow steel columns. a) Mild Steel tube D/t 47.6 b) High Strength tube D/t 38.05.*

4.4 EXPERIMENTAL RESULTS - CFST COLUMNS

4.4.1 General Behaviour

For each composite column test, a relationship between the applied load and the specimen deformation was obtained. In SERIES I experiments, the load-strain relationship was obtained as a measure of applied load against gross column shortening. In proceeding SERIES II experiments, actual load-strain relationships for both longitudinal and circumferential directions were recorded at various locations on the steel tube.

For all CFST-HSC specimens, the observed relationship between applied load and measured strain exhibited three distinct stages as illustrated in Figure 4.6. In the initial stages of loading, the experimental curves exhibited linear load-strain relationship designated by segment 'OA' where 'A' represented proportions between 65 to 95 % of the ultimate load. Beyond point 'A', yielding of the steel occurred and an elasto-plastic behaviour was observed up to ultimate load denoted by point 'B'. Proceeding the ultimate load, the failure mechanisms of the composite specimens were detected and the curves exhibited unloading branches 'BC'. Tests were terminated once the load resistance of the column declined to approximately 70 % of the ultimate capacity. Each test required between 20 to 50 minutes to complete.

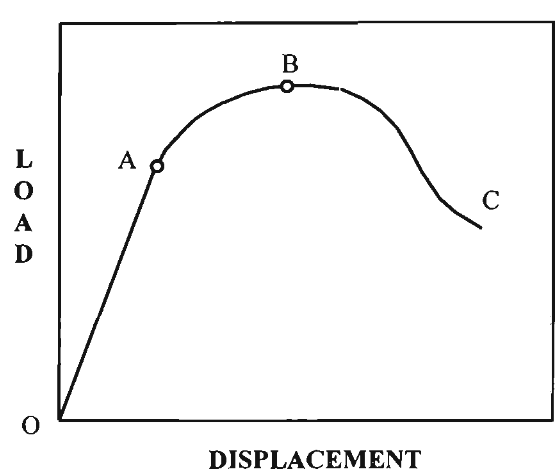

Figure 4.6: *Generalised load - displacement relationship for HSC-CFST columns.*

4.4.2 Failure Loads

The failure loads for CFST specimens from both Series I and Series II tests are summarised in Tables 4.4. and 4.5. The nominal section capacity N_o, peak strain ε_o, and the proportional strength and strain limits, are also presented in these tables. The measured peak strains ε_o are determined from displacement gauge readings as discussed in Section 3.3.1.1. Geometric and strength properties of the column sections have been classified in terms of the steel contribution factor δ_s, defined in Eqn. 3.1.

To investigate the failure loads of each specimen irrespective of material characteristics, the experimental axial capacities have been normalised by the uniaxial capacity (N_o) in column 6 of each table. Ratios of N_{exp}/N_o greater than unity imply an enhancement in strength due to triaxial confining actions on the concrete core. For the majority of each column configuration, three test results were obtained. The exceptions were CFST column groups CA9-87.8-MB-460 and CA10-87.8-MB-460 (2 tests), and CA11-47.6-MB-460 (Singular test).

The experimental failure loads for CFST column specimens having L/D = 3, were consistently greater than the nominal section capacity. The ratio of N_{exp}/N_o was observed to vary from 1.004 to 1.405 with values corresponding to the minimum and maximum experimental steel contribution ratios δ_s of 0.120 and 0.493 respectively. For CFST columns having identical steel tube configurations, the enhanced strengths due to confinement were consistently greater for the lower strength Mix A concrete. The effects of the various experimental parameters are covered in detail in following sections.

TABLE 4.4: Experimental Failure Loads and Peak Strain CFST Specimens - Mild Steel Tube.

Specimen Notation	δ_s	N_{exp} kN	N_o kN	ε_o $\mu\varepsilon$	N_{exp} / N_o	N_y / N_{exp}	ε_y / ε_o
CA3-47.6-MA-1	0.247	396.3	362.48	0.0112	1.0934	0.82	0.32
CA3-47.6-MA-2	0.247	388.5	362.48	0.0090	1.0717	0.91	0.52
CA3-47.6-MA-3	0.247	390.4	362.48	0.0100	1.0771	0.86	0.41
CA3-47.6-MA-4	0.247	392.4	362.48	0.0083	1.0826	0.91	0.45
CA3-47.6-MA-5	0.247	386.5	362.48	0.0063	1.0663	0.86	0.4
CA3-47.6-MA-6	0.247	382.6	362.48	0.0069	1.0555	0.87	0.45
CA4-47.6-MB-1	0.189	522.9	474.34	0.0070	1.1023	0.93	0.76
CA4-47.6-MB-2	0.189	502.3	474.34	0.0074	1.0589	0.95	0.76
CA4-47.6-MB-3	0.189	496.4	474.34	0.0074	1.0465	0.91	0.73
CA4-47.6-MB-4	0.189	493.4	474.34	0.0055	1.0403	0.03	0.76
CA4-47.6-MB-5	0.189	500.3	474.34	0.0055	1.0548	0.94	0.75
CA4-47.6-MB-6	0.189	490.5	474.34	0.0064	1.0341	0.94	0.66
CA5-47.6-MA-1	0.241	***348.3***	370.82	0.0073	0.9391	0.76	0.49
CA5-47.6-MA-2	0.241	369.1	370.82	0.0079	0.9973	0.89	0.47
CA5-47.6-MA-3	0.241	368.9	370.82	0.0072	0.9947	0.89	0.50
CA5-47.6-MA-4	0.241	358.1	370.82	0.0068	0.9656	0.86	0.40
CA5-47.6-MA-5	0.241	359.1	370.82	0.0057	0.9682	0.90	0.53
CA5-47.6-MA-6	0.241	356.1	370.82	0.0057	0.9603	0.90	0.54
CA6-47.6-MB-1	0.187	475.8	479.55	0.0051	0.9921	0.93	0.75
CA6-47.6-MB-2	0.187	478.7	479.55	0.0053	0.9983	0.94	0.75
CA6-47.6-MB-3	0.187	482.7	479.55	0.0049	1.0065	0.97	0.82
CA6-47.6-MB-4	0.187	475.8	479.55	0.0049	0.9921	0.94	0.76
CA6-47.6-MB-5	0.187	468.9	479.55	0.0048	0.9778	0.96	0.81
CA6-47.6-MB-6	0.187	467.0	479.55	0.0048	0.9737	0.94	0.71
CA7-60.3-MA-1	0.265	280.6	262.85	0.0076	1.0674	0.98	0.61
CA7-60.3-MA-2	0.265	282.5	262.85	0.0100	1.0749	0.71	0.35
CA7-60.3-MA-3	0.265	288.4	262.85	0.0070	1.0973	0.85	0.46
CA7-87.8-MA-4	0.196	259.0	240.32	0.0060	1.0777	0.87	0.57
CA7-87.8-MA-5	0.196	252.1	240.32	0.0060	1.0491	0.89	0.55
CA7-87.8-MA-6	0.196	256.0	240.32	0.0075	1.0654	0.79	0.43
CA8-60.3-MB-1	0.168	435.6	413.53	0.0060	1.0533	0.88	0.68
CA8-60.3-MB-2	0.168	446.4	413.53	0.0067	1.0794	0.75	0.64
CA8-60.3-MB-3	0.168	421.8	413.53	0.0072	1.0201	0.87	0.60
CA8-87.8-MB-4	0.120	396.3	391.00	0.0058	1.0136	0.94	0.69
CA8-87.8-MB-5	0.120	392.4	391.00	0.0056	1.0036	0.96	0.71
CA8-87.8-MB-6	0.120	393.4	391.00	0.0058	1.0061	0.92	0.78

TABLE 4.4 (Cont.): **Experimental Failure Loads and Peak Strain CFST Specimens - Mild Steel Tube.**

Specimen Notation	δ_s	N_{exp} kN	N_o kN	ε_o $\mu\varepsilon$	N_{exp} / N_o	N_y / N_{exp}	ε_y / ε_o
CA9-60.3-MB-1	0.150	476.8	463.61	0.0051	1.0284	0.95	0.80
CA9-60.3-MB-2	0.150	474.8	463.61	0.0054	1.0241	0.98	0.81
CA9-60.3-MB-3	0.150	483.6	463.61	0.0048	1.0432	0.96	0.85
CA9-87.8-MB-4	0.107	447.3	441.09	0.0045	1.0142	0.95	0.89
CA9-87.8-MB-5	0.107	453.2	441.09	0.0049	1.0275	0.96	0.80
CA10-60.3-MA-1	0.224	327.7	310.43	0.0052	1.0555	0.92	0.62
CA10-60.3-MA-2	0.224	315.9	310.43	0.0052	1.0176	0.92	0.58
CA10-60.3-MA-3	0.224	333.5	310.43	0.0057	1.0744	0.92	0.56
CA10-87.8-MA-4	0.163	294.3	287.9	0.0045	1.0222	0.93	0.69
CA10.87.8-MA-5	0.163	304.1	287.9	0.0045	1.0563	0.93	0.69
CA11-47.6-MB-1	0.176	533.8	509.40	0.0048	1.0479	0.98	0.96
CA11-47.6-MB-2	0.176	***497.6***	509.40	0.0055	0.9768	1.00	0.93
CA11-47.6-MB-3	0.176	545.4	509.40	0.0048	1.0707	0.97	0.94
CA11-47.6-MB-4	0.176	522.5	509.40	0.0030	1.0257	0.99	0.89

xxx Denotes suspect values

TABLE 4.5: **Experimental Failure Loads and Peak Strain CFST Specimens - High Strength Steel Tube.**

Specimen Notation	δ_s	N_{exp} kN	N_o kN	ε_o $\mu\varepsilon$	N_{exp} / N_o	N_y / N_{exp}	ε_y / ε_o
CA12-38-HA-1	0.493	637.7	467.27	0.0148	1.3647	0.85	0.36
CA12-38-HA-2	0.493	656.3	467.27	0.0180	1.4045	0.60	0.27
CA12-38-HA-3	0.493	647.5	467.27	0.0152	1.3857	0.62	0.28
CA12-38-HA-4	0.493	613.1	467.27	0.0144	1.3121	0.80	0.24
CA12-38-HA-5	0.493	620.0	467.27	0.0160	1.3269	0.75	0.30
CA12-38-HA-6	0.493	619.0	467.27	0.0132	1.3247	0.75	0.36
CA13-38-HB-1	0.391	739.1	589.34	0.0120	1.2541	0.89	0.58
CA13-38-HB-2	0.391	764.2	589.34	0.0120	1.2967	0.81	0.60
CA13-38-HB-3	0.391	770.1	589.34	0.0130	1.3067	0.81	0.54
CA13-38-HB-4	0.391	726.8	589.34	0.0090	1.2332	0.89	0.52
CA13-38-HB-5	0.391	725.0	589.34	0.0120	1.2302	0.78	0.47
CA13-38-HB-6	0.391	745.6	589.34	0.0123	1.2651	0.80	0.46

Two specimens were identified as having excessive low failure loads compared to their identical counterparts (CA5-47.6-MA-1 and CA11-47.6-MB-2). Post test inspection of the columns in question, with steel encasement removed, identified that both samples displayed significant void contents caused by inadequate compaction of the concrete. In such small scale columns the presence of concrete voids is detrimental to the resultant strength. Consequently these tests have been omitted from further analysis. A statistical assessment of results for individual column configurations is presented in Table 4.6. It is observed that the maximum standard deviation and sample ranges obtained for any test group, are 2.82 % and 5.66 % respectively. This indicates the degree of consistency of results obtained throughout the experimental program.

Table 4.6: Statistical Assessment of Experimental Results

Casting	No.s	f'c MPa	fy MPa	Average N_{exp}	sd %	Range %	Range kN
CA3-47.6-230	1-3	65.4	239	391.7	1.04 %	1.99 %	7.8
CA3-47.6-460	4-6	65.4	239	387.2	1.27 %	2.53 %	9.8
CA4-47.6-230	1-3	92.2	239	507.2	2.74 %	5.22 %	26.5
CA4-47.6-460	4-6	92.2	239	494.8	1.01 %	1.98 %	9.8
***CA5-47.6-600**	**1-3**	**67.4**	**239**	**369.4**	**0.17 %**	**0.24 %**	**0.9**
CA5-47.6-740	4-6	67.4	239	357.7	0.42 %	0.81 %	2.9
CA6-47.6-600	1-3	93.45	239	479.1	0.72 %	1.44 %	6.9
CA6-47.6-740	4-6	93.45	239	470.6	0.98 %	1.87 %	8.8
CA7-60.3-230	1-3	46.3	239	283.8	1.44 %	2.75 %	7.8
CA7-87.8-230	4-6	46.3	239	255.7	1.35 %	2.70 %	6.9
CA8-60.3-230	1-3	82.4	239	434.6	2.82 %	5.66 %	24.6
CA8-87.8-230	4-6	82.4	239	394.0	0.52 %	0.99 %	3.9
CA9-60.3-460	1-3	94.4	239	478.4	0.97 %	1.84 %	8.8
CA9-87.8-460	4-5	94.4	239	450.3	0.92 %	1.31 %	5.9
CA10-60.3-460	1-3	57.7	239	325.7	2.76 %	5.40 %	17.6
CA10-87.8-460	4-5	57.7	239	299.2	2.32 %	3.28 %	9.8
***CA11-47.6-230**	**1-3**	**100.6**	**239**	**539.6**	**1.52 %**	**2.15 %**	**11.9**
CA11-47.6-460	4	100.6	239	522.5	Note (1)		
CA12-38-230	1-3	58.0	495	647.2	1.44 %	2.87 %	18.6
CA12-38-460	4-6	58.0	495	617.4	0.60 %	1.12 %	6.9
CA13-38-230	1-3	87.9	495	757.8	2.17 %	4.09 %	31.0
CA13-38-460	4-6	87.9	495	732.5	1.56 %	2.81 %	20.6
				Max.	**2.82 %**	**5.66 %**	**31.0**
				Min.	**0.17%**	**0.24 %**	**0.9**

* Denotes suspect test result omitted.
Note (1): Only a singular column test performed.

4.4.2.1 Effects of Steel Contribution Ratio

The experimental results for column specimens having L/D ratio less than 4 are plotted against their respective steel contribution ratio δ_s in Figure 4.7. The slenderness ratio has been limited to examine the effects of cross section strength and geometric parameters independent of slenderness effects. By definition, the δ_s factor incorporates changes in D/t ratio, f'_c and f_y. Previous tests conducted at Victoria University of Technology (VUT) in 1990 and published by Campbell et al. (1991) are included in this comparison. These tests consisted of HSS tube columns, filled with concrete having compressive strength matching Mix A concrete. A summary of these results are tabulated in Appendix C.

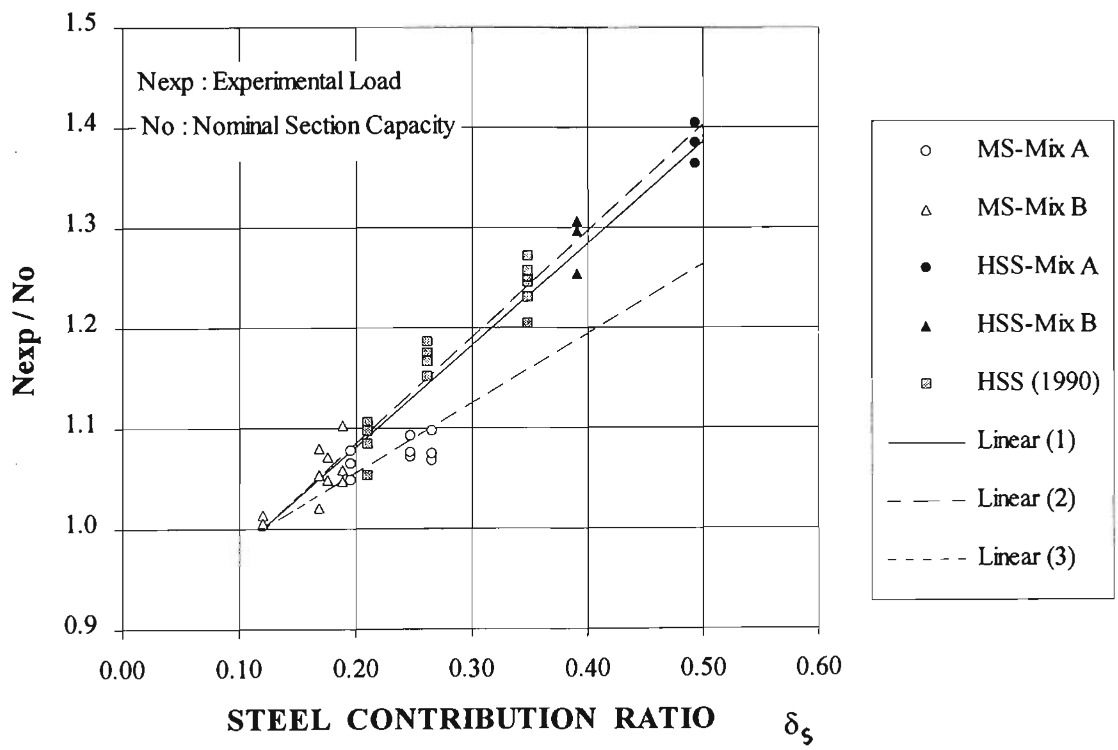

Figure 4.7: *Stub column load versus steel contribution ratio relationship (L/D).*

The experimental results illustrate clearly increases in the enhanced capacity N_{exp}/N_o with respect to δ_s. The observed relationship between N_{exp}/N_o and δ_s is potentially a linear function, converging to uniaxial conditions ($N_u/N_o = 1$) as the steel contribution ratio decreases to 0.12. Assuming values of strength increase below 3 % to be negligible, the regression of experimental results indicate that a minimum steel requirement δ_s of 0.15 is required to enhance the CFST-HSC column capacity. This compares favourably with the minimum requirement of 0.2 specified in the Eurocode 4 (1991) design provisions.

Linear regression of results was undertaken to obtain simplified empirical equations for the relationship between normalised column capacity (N_u/N_o) and steel contribution ratio (δ_s). It should be recognised that the presented data contains only a limited number of results for MS and HSS columns having similar values of δ_s. Examining Figure 4.7 for $\delta_s \approx 0.25$, insinuates the relationship for CFST columns using 60-90 MPa concrete may be influenced by the grade of steel tube. This observation is not in itself conclusive and is subject to further investigation. Bearing these factors in mind, linear regression was performed on results for three separate criteria: 1. All VUT Results, 2. HSS tube only and 3. MS tube only. The linear equations obtained are defined by Eqns. 4.10 to 4.12. Each equation passes through the point giving uniaxial conditions of $N_u/N_o = 1$ at $\delta_s = 0.12$. The equations have been graphically represented against experimental results in Figure 4.7.

(1) All VUT $$N / N_o = 1 + (\delta_s - 0.12)\ 1.016 \qquad \textbf{(4.10)}$$

(2) HSS tube $$N / N_o = 1 + (\delta_s - 0.12)\ 1.0612 \qquad \textbf{(4.11)}$$

(3) MS tube $$N / N_o = 1 + (\delta_s - 0.12)\ 0.695 \qquad \textbf{(4.12)}$$

The corresponding co-efficients of variations with regressed data for Eqns. 4.10 to 4.12 were 0.959, 0.975 and 0.611 respectively. From Figure 4.7 it is shown that Eqn 4.6 gives a reasonable estimate of the majority of column specimens, however it tends to overestimate some of the MS results. Applying the independent equations for each steel tube grade, it can be observed that the predictions using the HSS equation exhibits excellent correlation with results. On the other hand the MS equation was found to provide lower bound predictions to experimental results. A further aspect which must be taken into consideration is that CFST specimens using MS were only tested up to δ_s of 0.265, hence there is some uncertainty regarding the N_u/N_o - δ_s relationship beyond this value. By definition the δ_s ratio has two extremities of 0 and 1, which represent unconfined concrete and solid steel sections. At these extremities the normalised capacity must converge to uniaxial conditions. From Figure 4.7 it was observed that for $\delta_s \leq 0.15$, uniaxial conditions existed (N_u/N_o=1). As δ_s increased, there was a ascendancy in the N_u/N_o - δ_s relationship. In order for uniaxial conditions to exist at the upper limit of $\delta_s = 1$, there must exist a transition point at which the N_u/N_o descends to unity. This aspect fell outside the scope of this experiment investigation as only thin walled sections were examined ($\delta_s \leq 0.493$).

4.4.2.2 Effects of Concrete Compressive Strength

From results given in Tables 4.4 and 4.5, it was identified that the normalised experimental capacities were consistently greater in the lower grade Mix A concrete specimens than in the corresponding Mix B specimens. This effect is best represented by examining the results of CFST tests from castings CA12 and CA13 using the HSS tube. For CA12 (Mix A) tests, the ratio of N_{exp}/N_o ranged between 1.36 to 1.41 while in the CA13 (Mix B) columns the ratio ranged between 1.25 - 1.31. In this scenario confinement effects of the 60 MPa concrete were 11% more effective than in the 90 MPa concrete. Similar trends were also observed for the MS specimens with D/t = 47.6, where the range of N_{exp}/N_o reduced from 1.07 - 1.09 to 1.04 - 1.06 as the compressive strength of the concrete increased from 67.4 to 92.2 MPa.

These results are consistent with findings of previous investigations on confined HSC in spirally reinforced columns and under hydrostatic confinement, as discussed in Section 2.3.2 of the literature review chapter. In summary, it can be stated that confinement in HSC is less effective than in lower grade concretes for two reasons:

1. The reduced volumetric dilation in HSC leads to the development of lower transverse stress levels in the steel tube. As a result the confining pressure f_r is reduced and so is the effective strength of the laterally confined HSC f'_{cc}.

2. In HSC, shear failure occurs through an increasing proportion of aggregate. Therefore, interlocking mechanisms of the aggregate which contribute to the shear resistance of the concrete are not as effective as in NSC.

4.4.2.3 Effects of Column Slenderness

The relationship between normalised failure loads N_{exp}/N_o and column relative slenderness $\bar{\lambda}$, defined by Eqn. 4.13, are shown in Figure 4.8. Relative slenderness is defined as a function of N_o and the column critical buckling capacity N_{cr}, given by Eqn 4.14. The appropriate European Buckling Curve from Eurocode 4 for circular filled sections (defined in Appendix D.3) is included to illustrate the design strengths for the CFST columns based on uniaxial capacity N_o.

$$\bar{\lambda} = \sqrt{\frac{N_o}{N_{cr}}} \tag{4.13}$$

$$\text{where } N_{cr} = \frac{\pi^2 (EI_e)}{L_e^2} \tag{4.14}$$

(EI_e is defined in Appendix (D.3)

The results clearly indicate that for $\bar{\lambda} < 0.3$, experimental loads are in excess of the nominal capacities due to triaxial confining actions. As the relative slenderness of columns increase, the influence of confinement forces diminish and the CFST capacities converge to uniaxial conditions as defined by the European Buckling Curve. For all experimental specimens using MS tube, this $\bar{\lambda}$ ratio was in the order of 0.4 to 0.5. This slenderness range is in agreement with the Eurocode 4 specification which limits confinement effects up to $\bar{\lambda}$ = 0.5. In the case of HSS tube specimens, tests were only performed upon L/D ratios below 6 ($\bar{\lambda}$ < 0.3), therefore the range at which the enhanced capacity of such columns diminished to unity could not be extrapolated from results.

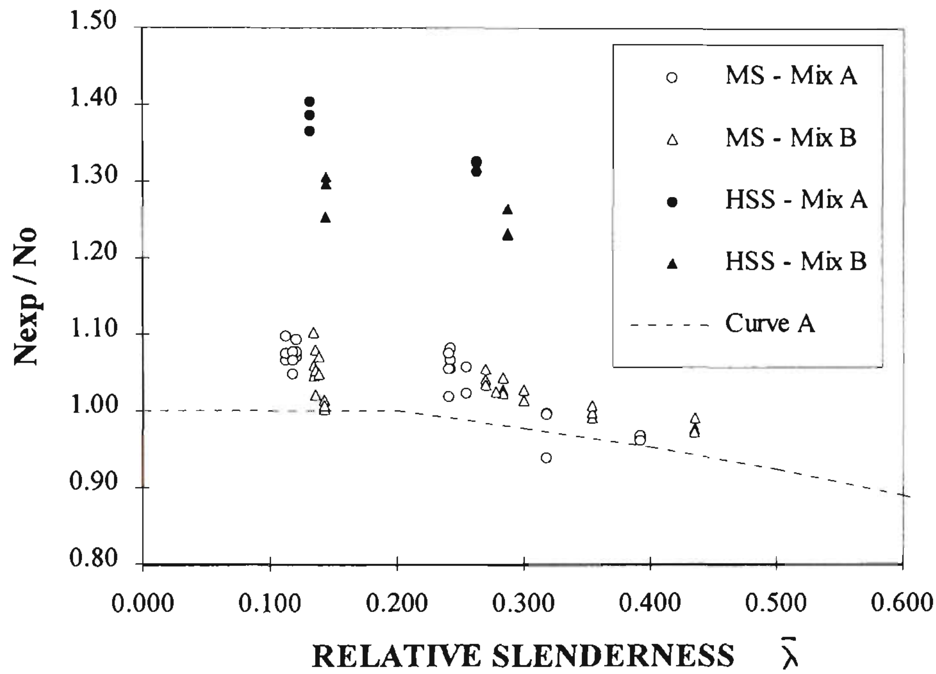

Figure 4.8: *Load - relative slenderness relationship.*

4.4.3 Load-Displacement Relationship

Averaged load-displacement curves for selected stub column specimens are shown in Figures 4.9 and 4.10. In the latter figure, applied loads are presented in the normalised format of N_{exp}/N_o for comparison purposes. Stub column relationships are only examined due to the volume of curves obtained by this study. A complete set of the raw experimental curves are included in Appendix B.

As defined in Section 4.4.1 the load-displacement relationships for the CFST columns could be divided into three stages of loading. They are Elastic, Elasto-plastic and Unloading behaviour as illustrated earlier in Figure 4.6. The distinguishing differences between each curve can be summarised in terms of several factors:

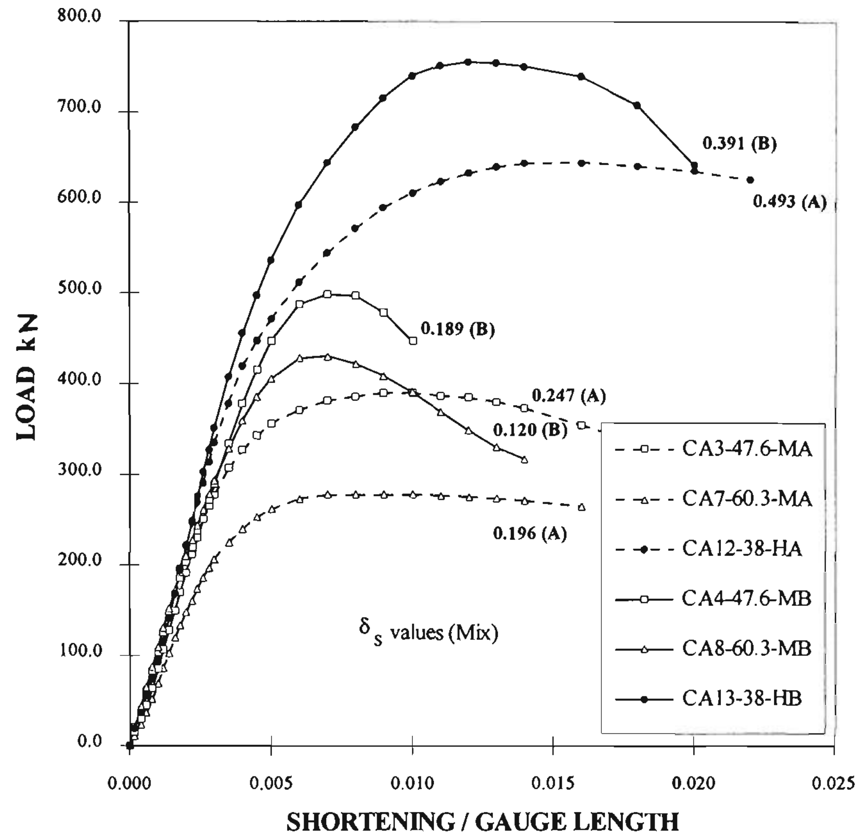

Figure 4.9: *Load-displacement relationships - short columns L = 230 mm.*

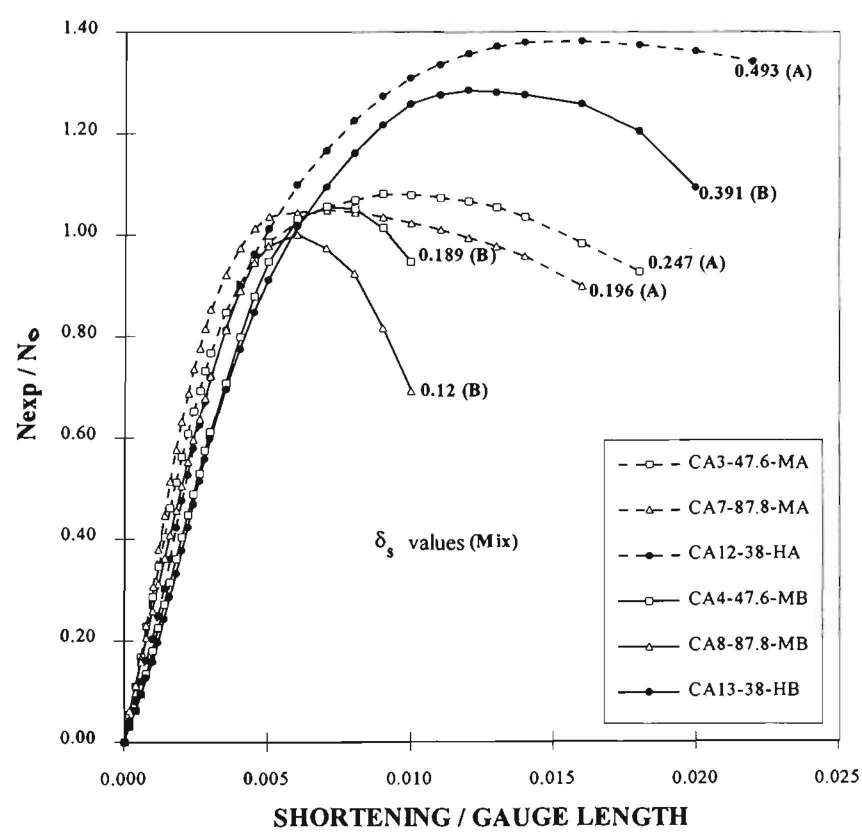

Figure 4.10: *Dimensionless load-displacement relationships - short columns L = 230 mm.*

- The initial slope and proportion of linearity of the curve
- The range of the elasto-plastic zone
- The peak strength and strain at ultimate conditions
- The slope of the unloading behaviour in the post ultimate range.

Figure 4.10 indicates clearly that for a given concrete strength there is an improvement in the ductility of the load-displacement relationship for specimens having greater δ_s ratio. This is signified by elongated elasto-plastic plateaus, higher peak strains at failure and less dramatic unloading behaviour. If it is assumed that the greater quantity of steel tube in the section (δ_s) represents increases in the confining pressure on the concrete core, the improved behaviour of the composite specimens can be explained by examining the behaviour of the concrete infill. For unconfined concrete, failure occurs as a result of the combined action of both vertical and oblique crack patterns forming in its microstructure. In a CFST column the propagation of such micro cracking is resisted by the confining effect of the steel tube. This results in higher strengths and strains required to initiate failure under increasing confinement pressures. The prolonged elasto-plastic behaviour is a response to this resistance. Ultimate load of confined concrete occurs as failure plane(s) develop within its structure and destructive processes take place. It is well documented that for confined concrete, failure traditionally occurs by the formation of an oblique shear plane. The unloading characteristics of the specimens occur as the concrete segments bisected by failure planes slide against each other. In thicker walled section possessing larger confinement pressures, resistance to this movement is intensified and load reduction is not as rapid.

In addition to the effects of the quantity of the steel in the composite section, the observed load-displacement relationship was influenced by the compressive strength of the concrete. In all circumstances increased ductile behaviour was associated with lower strength as compared to the higher grade concretes. Steeper unloading phases for Mix B specimens typified the brittle behaviour of the HSC.

4.4.3.1 Strains at Ultimate Conditions

The relationship between peak strain ε_0 and the steel contribution ratio δ_s is shown in Figure 4.11, which clearly indicates an increase in peak strain with respect to the steel contribution ratio. In the Figure the experimental strains are determined from the peak shortening of specimens recorded at ultimate load by displacement gauges, and divided by the original gauge length. Assuming the peak experimental strains of the unconfined concretes ε_{co} given in Section 4.2.1.1, the ratio $\varepsilon_0/\varepsilon_{co}$ varied from 1.17 to 6.15.

These results are suspect to experimental errors caused by the compressibility of the sulphur capping compound which is discussed in the following section. It is anticipated that the actual values of ε_0 would be less than those shown and converge to unconfined concrete strains ε_{co} at low values of δ_s. Without the ability to provide specific correctional factors to values of ε_0, proposing empirical equations based on the data is not appropriate.

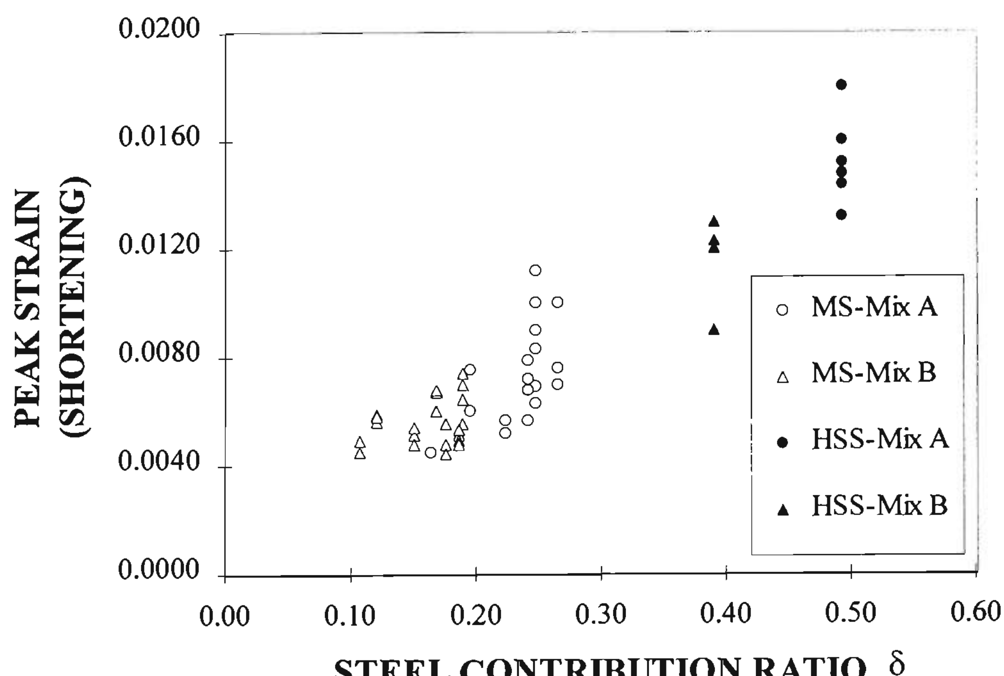

Figure 4.11: *Peak strain - steel contribution ratio relationship.*

4.4.3.2 Discussion - Compressibility of Sulphur Capping

It was identified during the experimental program that the use of high strength sulphur compound (>50 MPa) for capping of CFST specimens, exhibited a small degree of compressibility under loading. With column displacements measured between load platens, experimental results incorporate this additional shortening. From castings CA11 onwards, specimens were tested using both sulphur and resin capped techniques described in Section 3.3.1. It was observed from these comparative tests that typical 5 mm thickness of sulphur capping (2.5 mm both ends) compressed between 0.1 to 0.6 mm. This effect was greatest in columns having large experimental failure loads. However, there was insufficent results to quantify this shortening and to modify the experimental displacements.

The effect of sulphur capped and resin capped specimens on the load-displacement relationships is graphically presented in Figure 4.12. The discrepancies observed for the initial slope of the experimental curves prohibited an assessment of the stiffness of the composite columns.

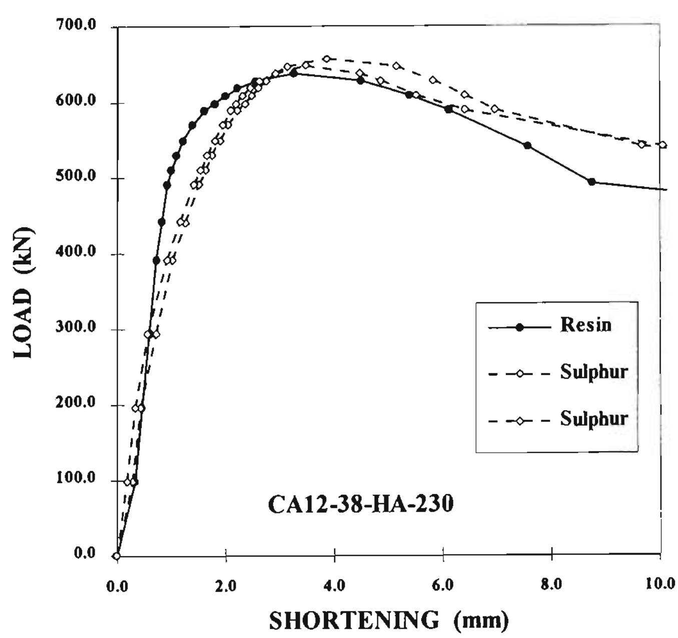

Figure 4.12: *Comparative load-displacement curves for different capping techniques.*

4.4.3.3 Column Ductility

To quantify the various ductile responses observed from the CFST load-displacement curves, a Ductility Index (D_I) as adopted by Zhao and Hancock (1991) for hollow steel columns was applied. The Ductility Index is derived as a singular numeric ratio relating to the difference in deformation of the specimen in both loading and unloading curve branches for a particular proportion of ultimate axial capacity. D_I is defined by:

$$D_I = (\Delta_2 - \Delta_1) / \Delta_1 \tag{4.15}$$

where Δ_1 is the axial displacement on the ascending branch of the curve corresponding to 90 % ultimate load

Δ_2 is the corresponding value on the descending curve

This is illustrated in Figure 4.13. To some extent the D_I factor is an indication of the energy absorption capacity of the section, as it is a measure of sustained load capacity (90%) for a displacement.

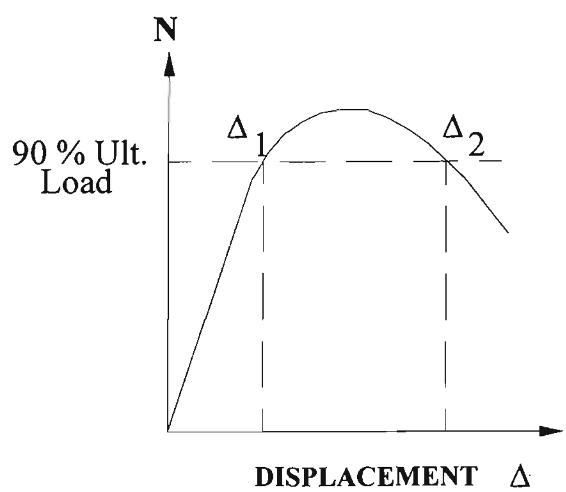

Figure 4.13: *Definition of ductilty index.*

The D_I results for all composite specimens are graphically represented in Figure 4.14. The results indicate that the degree of ductility is primarily dependent on the concrete strength and the quantity of the confining steel tube (δ_s). Mix A specimens exhibited D_I ratios between 2 to 4 whereas Mix B specimens were significantly lower in the range of

0.5 to 2. Ductility increased as expected with δ_S for a particular concrete mix being depicted. Assuming the modified stress-strain relationship by Fafitis and Shah (discussed in Section 4.2.1.3) is applicable to the unconfined HSC, the D_I ratio for the respective Mix A and Mix B concretes were 0.38 and 0.25. Subsequently, the ratios of D_I obtained from CFST tests to corresponding values for the unconfined concrete varied between 4.34 - 9.67 for Mix A specimens, and 2.04 - 8.12 for Mix B specimens. It is worth noting that, for $\delta_s < 0.15$, the steel tube provides an improvement in the ductility of the HSC behaviour although not contributing to any increase in strength. The explanation for this is that even though failure of the concrete infill has occurred prior to the confining action being established, the destructive processes of the core are still resisted to some extent by the tube encasement.

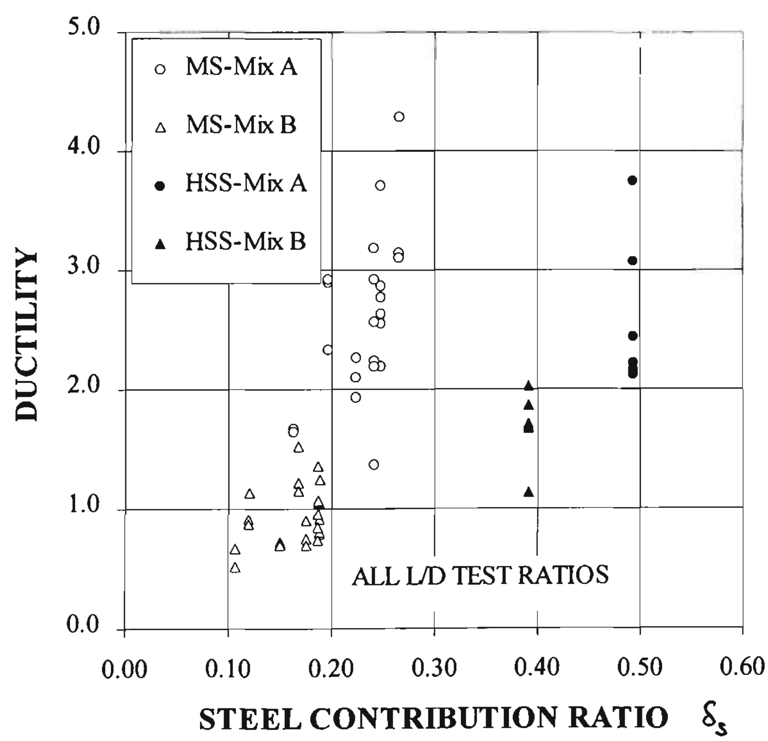

Figure 4.14: *Ductility index of CFST column.*

4.4.4 Modes of Failure

4.4.4.1 Concrete Shear Failure

The ultimate load capacity was associated with the formation of a classical shear plane at an oblique angle within the concrete core for all columns tested except specimens CA5-5 and CA5-6. The initial indication of the failure was signified by the appearance of small lateral bulging on the exterior of the steel tube corresponding with the achievement of ultimate load. As specimens were loaded well into the post ultimate range, the angle of inclination became clearly visible with local buckling and stretch lines appearing on the tube exterior. This inelastic failure mechanism predominantly occurred within the mid region of the column. No inelastic local buckling mechanisms were detected in the steel tube until well into the post ultimate phase.

The measured inclinations of the failure plane to the vertical axis (θ) for short columns ranged between 25-44 degrees. The relationship between the shear failure angle and δ_s is illustrated in Figure 4.15. It can be seen that the measured angle approaches 45 degrees with increasing δ_s corresponding to higher confinement stresses. The variation of such failure planes can be observed in Plates 2 - 5.

Post test examinations of specimens with segments of steel encasing removed were performed. In the majority of cases, the two core elements bi-sected by the shear plane maintained their structural integrity with the exception of slight micro-cracking and spalling of the concrete in the vicinity of the plane. Shear plane failures for the HSC were clear with failure occurring through both the mortar matrix and a large fraction of aggregate as shown in Plate 3. In specimens of increasing D/t ratio, a notable increase in the amount of vertical cracking was observed.

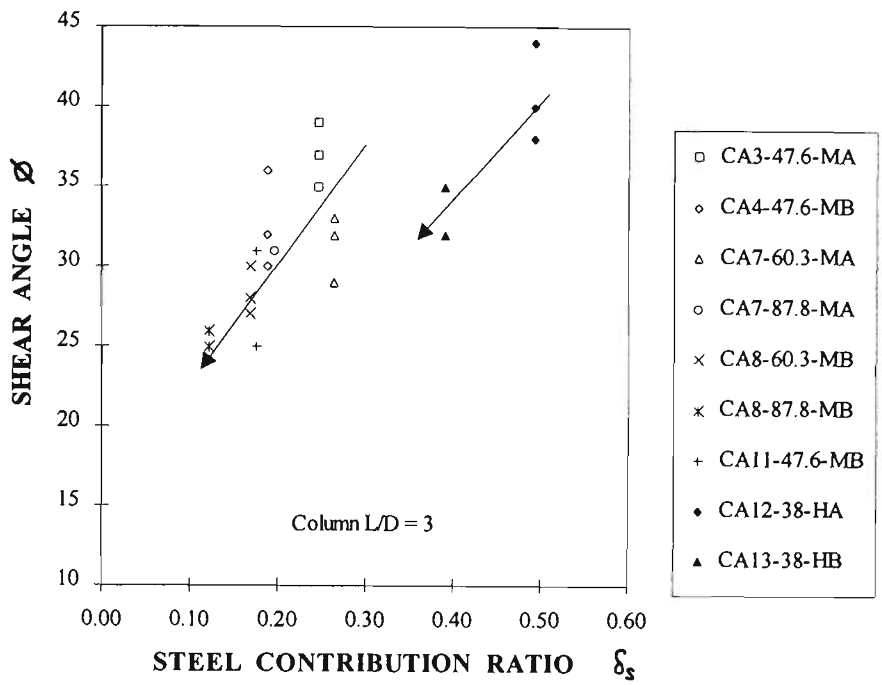

Figure 4.15: *Shear failure angles of CFST specimens.*

The variation in the shear failure angle may be explained in terms of micro cracking theory as described by Luksha and Nesterovich (1991). In plain concrete, vertical tensile and oblique shear cracks form. As cracks propagate, the vertical cracks link with existing oblique cracks to form failure planes. In triaxially stressed concrete, the vertical cracks are resisted by the growing presence of confinement forces, and reduce in number and size. Oblique cracks, on the other hand, are enhanced by the shearing action of the confinement forces, and contribute vastly to the formation of a principal failure plane. Based on this interpretation of crack formations, it is obvious that under increasing confinement pressures, the formation of oblique failure planes approach 45° to the vertical axis as observed for tests reported by this study.

Plate 2: *Typical shear failure - CFST stub column (steel removed).*

Plate 3: *Shear plane of concrete core through both mortar and aggregate.*

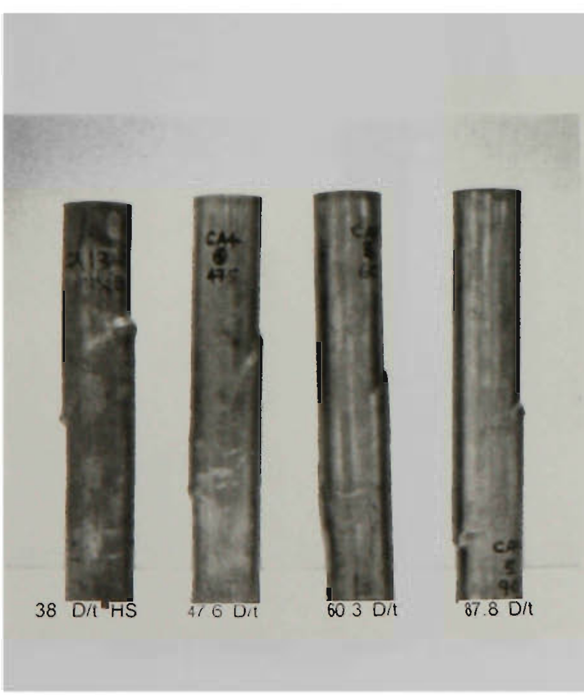

Plate 4: *Variation in shear failure angles for all D/t ratios (L/D = 460 mm).*

Plate 5: *Shear failure observed for very thinwalled (D/t=87.8) CFST specimens.*

4.4.4.2 Column Buckling

Two specimens CA5-5 and CA5-6, with L/D ratio of 9.72 filled with Mix A, exhibited an overall buckling failure mode more characteristic of column instability than material failure (Plate 6). This failure type was not observed for the corresponding Mix B specimens of similar slenderness which failed under shear actions. It is understood that HSC has a larger elastic modulus and therefore greater resistance to column buckling than in lower strengths concrete. Predictions of column buckling capacities based on the modified Euler buckling formula defined by Eqn 4.14, were shown to over predict the experimental failure loads substantially. This suggests that the most probable cause for failure resulted from combined actions of material and stability failure, with cracking of the concrete weakening the resistance of the column to buckling mechanisms. This effect may have been further enhanced by eccentricity of the applied load, or column imperfections.

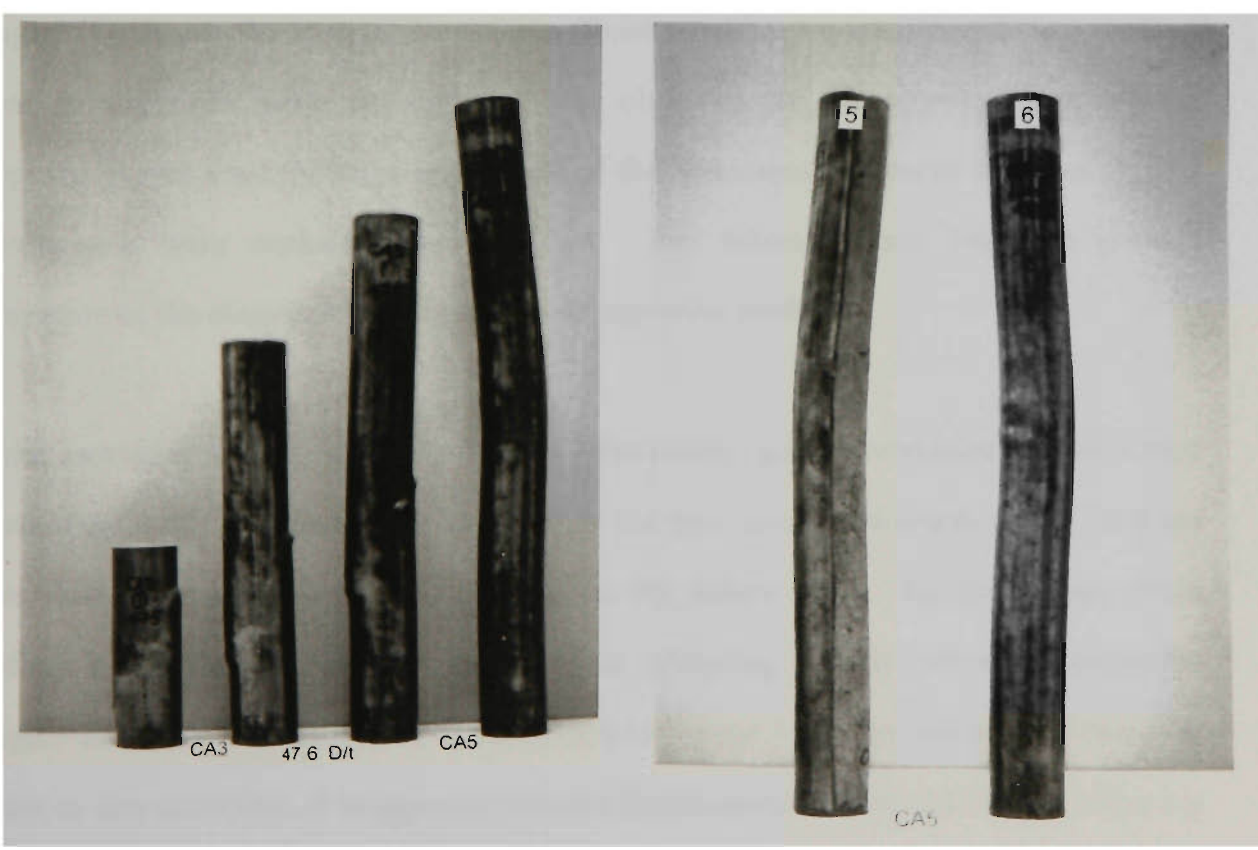

a) *All slenderness ratios* **b)** *Column buckling*

Plate 6: *Column failure for various slenderness ratios and column buckling*

4.4.5 Load-Strain Relationships - SERIES II Tests

In Figures 4.16 to 4.19, the experimental load-strain relationship for strain gauged specimens (SERIES II) are shown. In each figure the experimental relationships for longitudinal and transverse strains are shown. Longitudinal compressive strains and transverse tensile strains have been plotted as positive and negative values respectively. Figures also include load-displacement relationships recorded from LVDT's. Initially five strain gauged columns were tested, however for reasons detailed in Section 4.4.2, results for Specimens No. CA11-47.6-MB-2 have been omitted. A summary of the peak load and strains recorded are given in Table 4.7.

In each figure only strains recorded at column midheight are illustrated for two reasons. Firstly, it was observed that in both 230 and 460 mm long specimens, the strains recorded at the upper and lower column extremities varied with respect to midheight gauges. Strains at the base of the column (fixed condition) were generally in excess of those at midheight while the opposite was observed for the upper gauges (pinned support). It was presumed that end effects of the specimens influenced these values and subsequently were excluded from analysis. The second reason being to prevent congestion of the diagrams where gauge readings were similar.

In the ascending branch of the load-strain relationship, good correlation was observed between each of the experimental curves. In the post ultimate domain, gauge readings were shown to vary due to their location to the failure plane. In some cases strain readings became erratic with the failure plane occurring directly below the particular gauge. This was true for Strain Gauge No.2 in Figure 4.16. In comparing measured strains to displacements, it is apparent that the displacement readings although reflecting similar curve shapes up to ultimate load, were consistently in excess of the strains recorded. Initial settlements of displacement were observed to occur on the application of load for the displacement gauge readings.

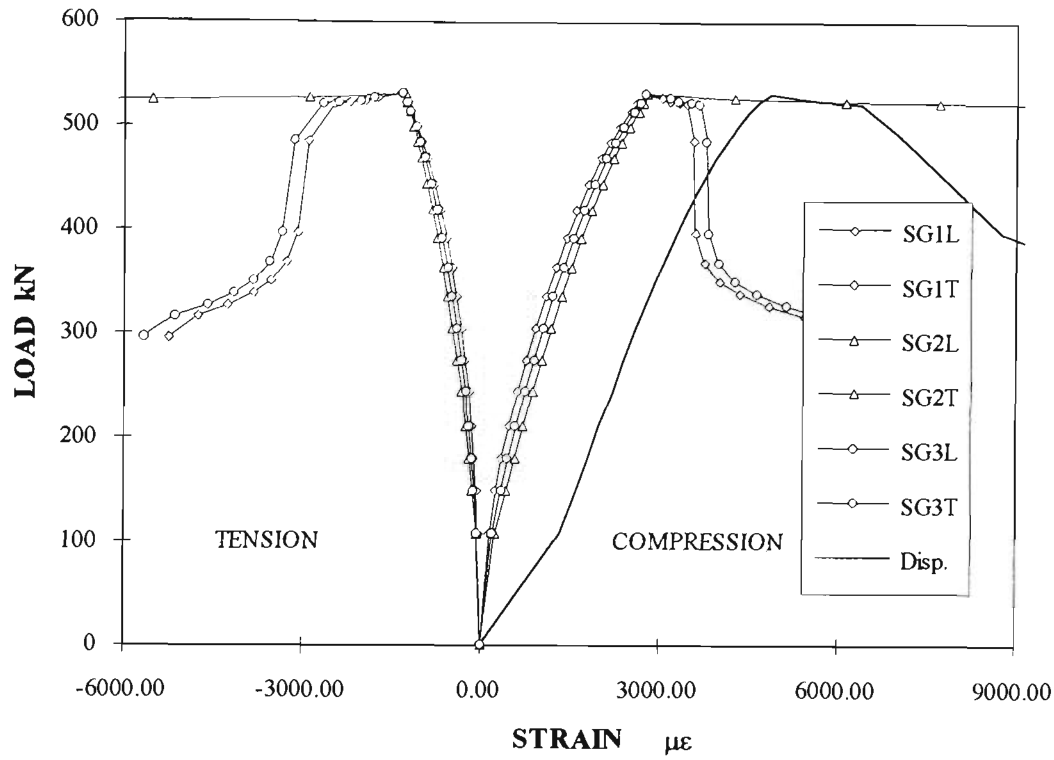

Figure 4.16: *Load-strain relationships : CA11-47.6-MB-1 (length = 230 mm).*

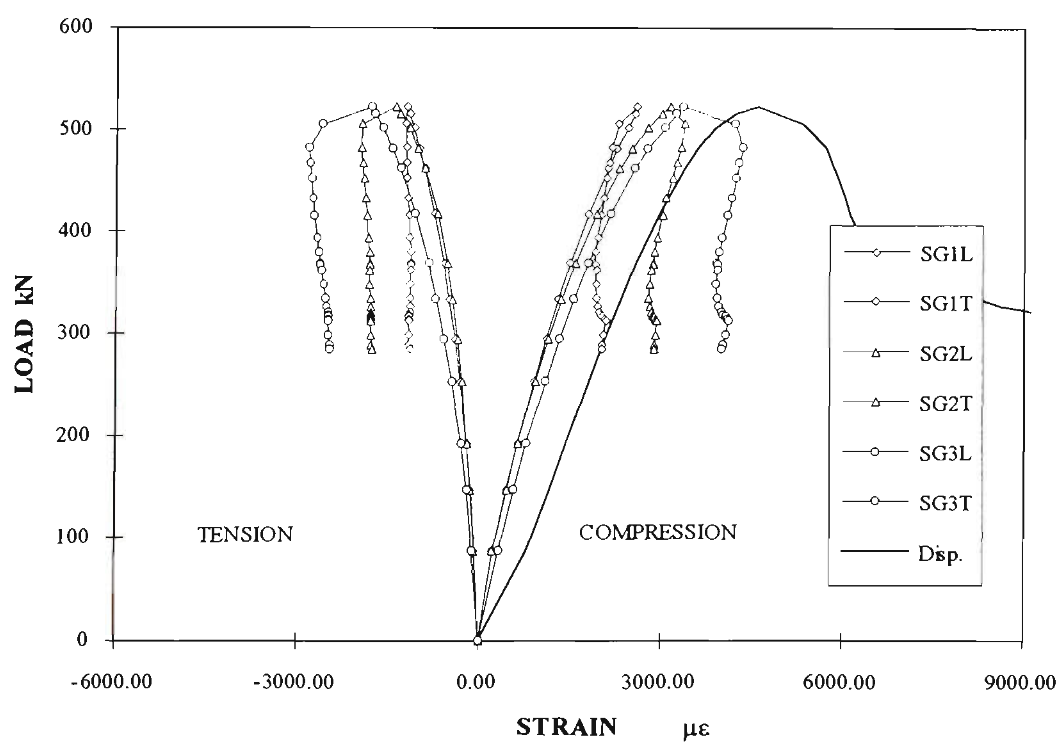

Figure 4.17: *Load-strain relationships : CA11-47.6-MB-4 (length 460 mm).*

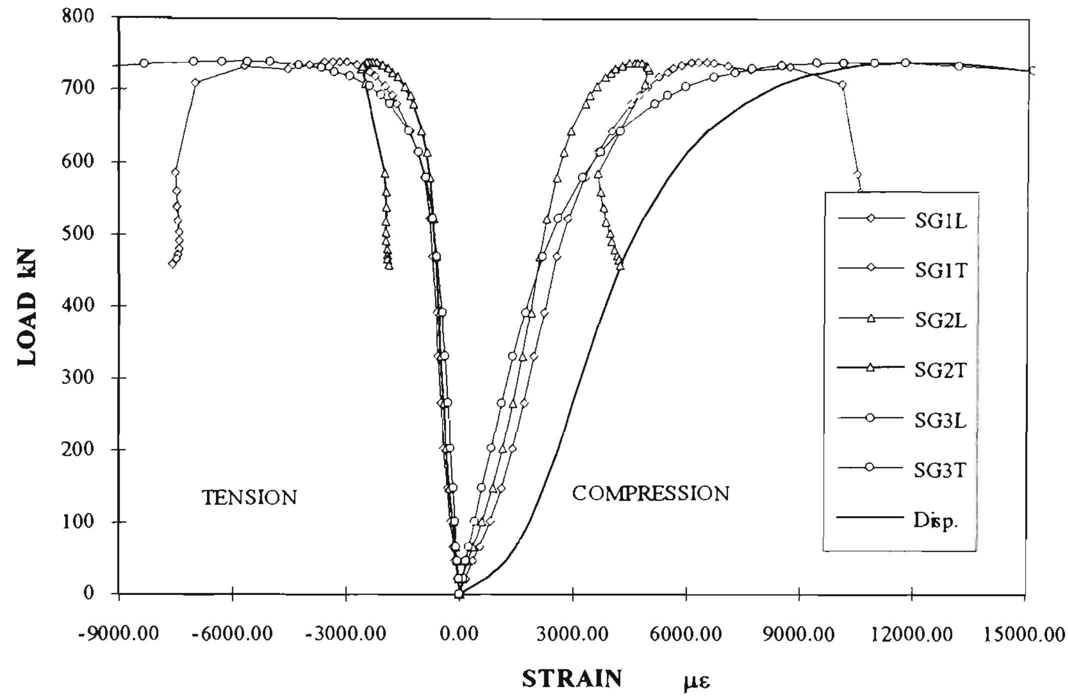

Figure 4.18: *Load-strain relationships : CA13-38-MB-1 (length = 230 mm).*

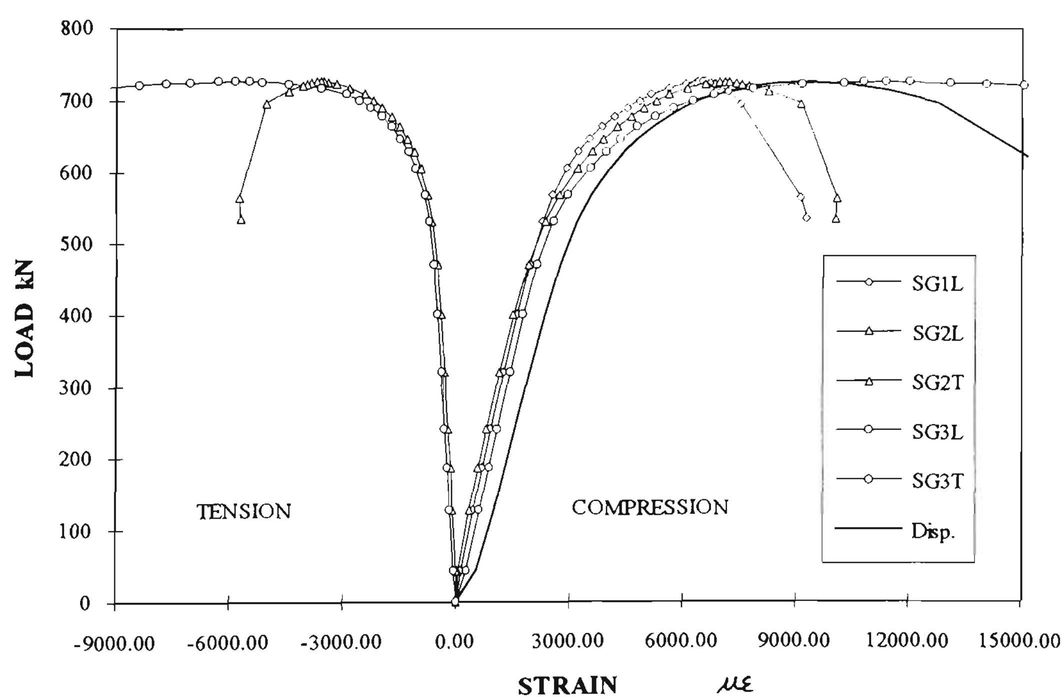

Figure 4.19: *Load-strain relationships - CA13-38-MB-4 (length = 460 mm).*

In some situations strain reversal from gauge readings was observed in the post ultimate range. This effect can be attributed to slippage occurring between the steel sheath and the concrete core as the segments of concrete bisected by the shear plane slide against each other. A resulting relaxation in the steel strains could then occur.

Table 4.7: Summary of SERIES II CFST Results.

No.	N_{exp} kN	ε_{sl} $\mu\varepsilon$	ε_{st} $\mu\varepsilon$	υ	υ_{inc}	E_{sc} MPa
CA11-1	533.8	2810	1370	0.487	0.67	77,613
CA11-4	522.5	2860	1370	0.500	0.612	56,780
CA13-1	739.1	8340	4560	0.520	0.83	53,900
CA13-4	726.8	7870	4180	0.510	0.72	54,350

4.4.6 Relationship Between Transverse and Longitudinal Strains

The relationship between transverse and longitudinal strains for both Mild Steel and High Strength Steel columns are shown in Figures 4.20 and 4.21. In Figures 4.20 a) to d) the Poisson's ratio (υ), is given as the cumulative ratio of transverse to longitudinal strains $\varepsilon_{st}/\varepsilon_{sl}$. In latter Figures, Incremental Poisson's Ratio ($d\upsilon$) defined as the ratio of the respective strain increments $d\varepsilon_{st}/d\varepsilon_{sl}$ is illustrated. The distinct difference between each relationship is that the incremental Poisson's Ratio gives values throughout the load sequence independent of the preceding strain history. In each Figure individual gauges readings are plotted with lines of best fit superimposed. Ultimate load conditions are denoted by the symbol **V**, and are summarised in Table 4.7.

The Figures indicate distinct characteristics for both υ and υ_{inc} relationships:

1: Relatively constant υ equal to approximately 0.3 corresponding to the elastic stage.

2: A sudden transition in the gradient of the measured value of υ ($d\upsilon$), indicating the rapid volumetric dilation of the concrete .

3: Convergence to a constant Poisson's ratio at large limits of strain only observed for CA13 specimens.

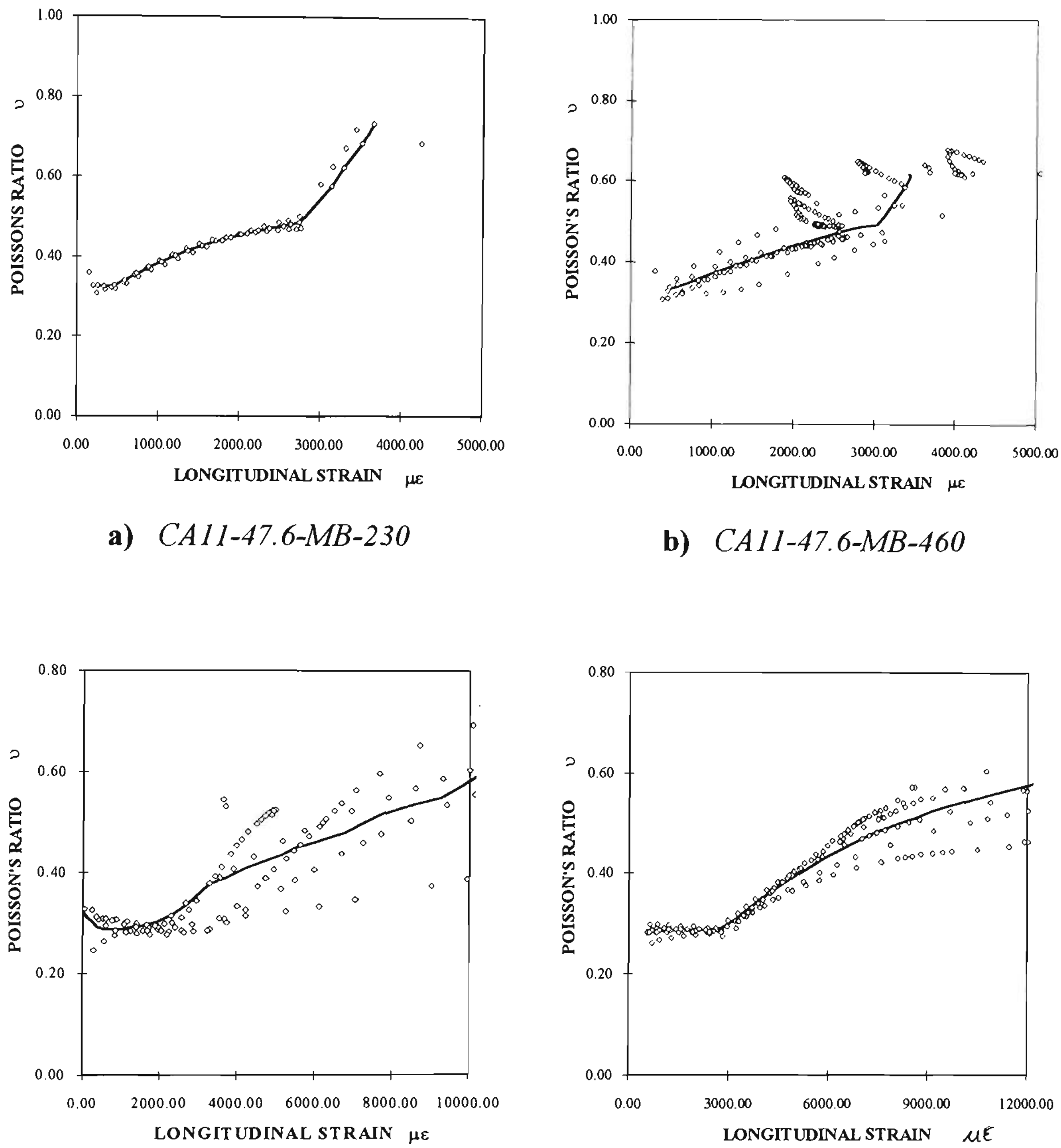

a) *CA11-47.6-MB-230* **b)** *CA11-47.6-MB-460*

c) *CA13-38-MB-230* **d)** *CA13-38-MB-460*

Figure 4.20: *Measure Poisson's Ratio υ - Series II tests.*

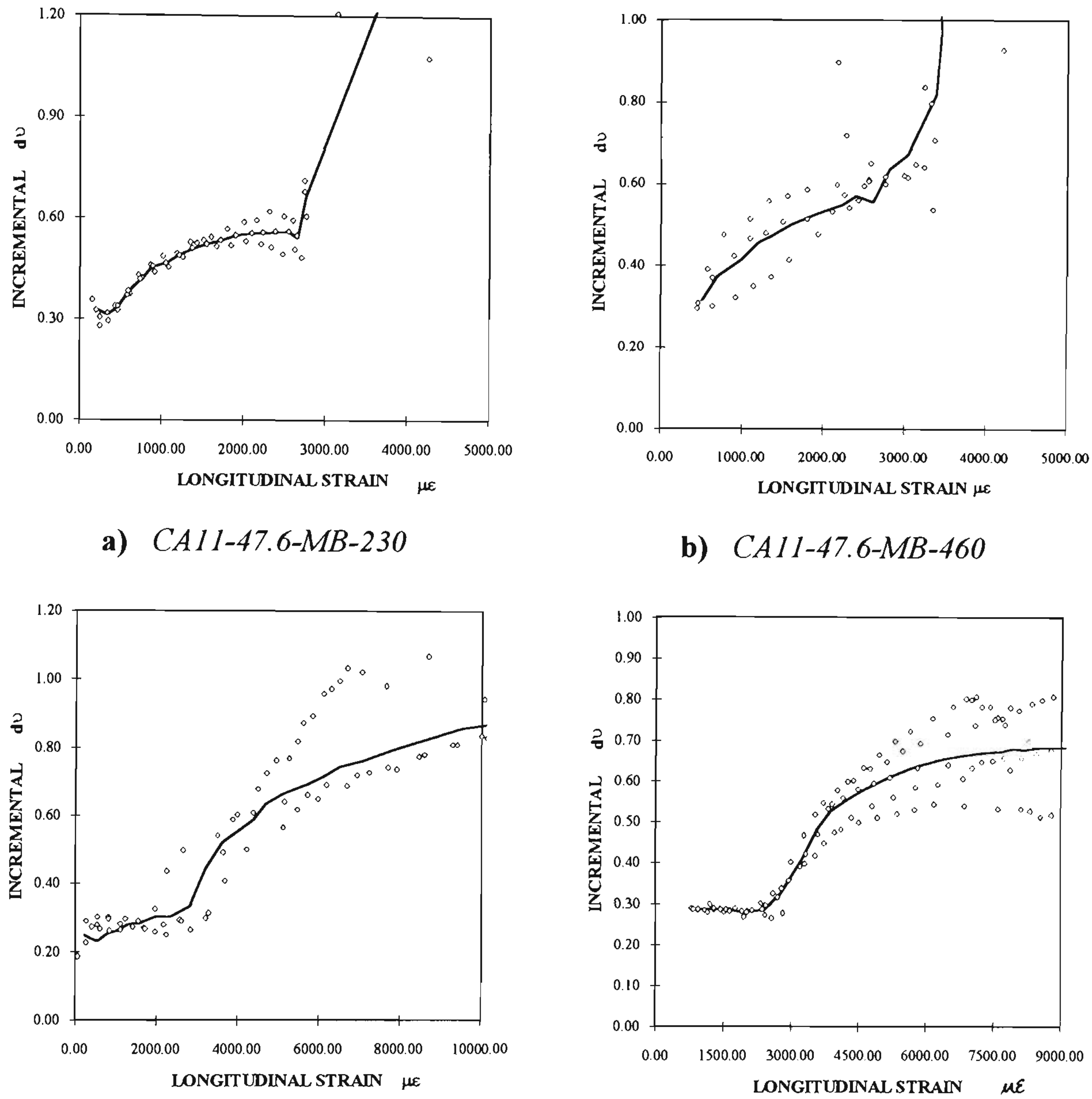

a) *CA11-47.6-MB-230*

b) *CA11-47.6-MB-460*

c) *CA13-38-HB-230*

d) *CA13-38-HB-460*

Figure 4.21: *Measure Incremental Poisson's Ratio dυ - Series II tests.*

In the initial stages of loading, the measured values of υ and dυ for both grades of steel tube were approximately equal to 0.3. As longitudinal strains intensified, the ratio remained constant for the High Strength tube, while increasing marginally for the Mild Steel specimens. Once longitudinal strains reached values in the order of 2500 to 2700 με, the measured Poisson's Ratio increased rapidly coinciding with the lateral expansion of the concrete core. This continued well beyond ultimate conditions into the plastic domain. For the HSS tube specimens, the incremental Poisson's Ratio was observed to converge to values in the order of 0.8. This effect was not distinguishable for MS tube specimens where the relationship continued to increase.

Experimental studies by Tsuji et al. (1991) and Sakino and Hayashi (1991) observed similar relationships to the HSS-CFST columns for columns tested using NSC and steel sections having D/t ratios below 58. This implies that in columns which provide greater confining pressures on the concrete, the incremental Poisson's ratio converges to specific values. Under low confinement pressures (MS-CFST specimens), the restraint of the steel tube to the destructive processes of the core is not substantial and the lateral expansion of the concrete continues to increase the measured transverse steel strain ε_{st} and subsequent values of υ ($d\upsilon$).

Considering the transition point in gradients of the υ - ε_{sl} relationship to reflect the initiation of lateral expansion of the concrete core, it can be concluded that, for confinement stress states in HSC Mix B specimens to exist, requires longitudinal strains of $\approx$2600 $\mu\varepsilon$. In comparison, Knowles and Park (1969) found that volumetric dilation in NSC occurred at 2000 $\mu\varepsilon$. This indicates that in CFST columns using concretes with greater compressive strengths, the mechanisms of confinement occur at a later stage in the load sequence. Based on this fact it can be anticipated that the confinement pressure developed prior to ultimate load would be reduced. The higher strain required would also reduce the values of column slenderness and eccentricity ratio of applied load, to which confinement influences are effective.

4.5 GENERAL DISCUSSION

From the results reported herein, several aspects of CFST-HSC behaviour were identified:

1. Strength enhancement relative to the uniaxial capacity of CFST stub columns with concrete strength 60-90 MPa, was observed to increase linearly with increases in steel contribution ratio δ_s. Such triaxial effects were observed to diminish with increases in column length, D/t ratio and the compressive strength of the concrete. It was found that a minimum steel requirement of $\delta_s \geq 0.15$ was necessary for the enhancement in CFST properties. A maximum increase in strength of 41 % was obtained for the column configuration utilising HSS and 60 MPa concrete.

2. The percentage increase in strength for columns having identical steel tube configurations, were greatest in the lower strength (Mix A) concrete specimens. This aspect was best demonstrated by comparing the normalised strengths of the HSS-CFST columns which had corresponding N_{exp}/N_o values of 1.36 - 1.41 for the 60 MPa concrete, and 1.25 - 1.31 for the 90 MPa concrete. This effect can be ascribed to the reduced volumetric dilation of the higher strength concrete.

3. Ductility and peak strain for the composite columns increased with respect to larger quantities of steel in the cross section. For similar column configurations, increases in the compressive strength of concrete, reduced ductility and brittle behaviour was demonstrated. By using the ductility index classification, the ratio of D_I for Mix A (60 MPa) to Mix B (90 MPa) specimens varied between 1.2 to 4.6.

4. The primary mode of failure for short CFST specimens is the formation of a shear failure within the concrete core. The inherent strength of the laterally confined concrete is the principle factor in determining the ultimate capacity of CFST columns. For the test specimens, the angle of failure to the vertical axis ranged between 25-44°.

5. The presence of concrete infill provides additional stability for the tube walls against the influences of local buckling mechanisms for the range of D/t ratio investigated.

6. The longitudinal strain at which the lateral expansion of the concrete infill is considerably greater in HSC. For the 90 MPa concrete mix investigated, the strain limit was in the order of 2600 $\mu\varepsilon$.

CHAPTER 5: THEORETICAL INTERPRETATION OF RESULTS

5.1 ULTIMATE AXIAL CAPACITY

In this section the experimental failure loads for stub columns L/D = 3 are assessed against various failure criteria for laterally confined HSC. The plasticity function described in Chapter 2 is used to determine the steel tube stresses and the effective confining pressure. Having adopted an appropriate failure criteria for the HSC used in this study, an empirical ultimate strength analysis is discussed in light of test results.

5.1.1 General Assumptions

To establish analytical procedures for CFST columns, several assumptions with respect to equilibrium and compatibility conditions are required:

1. The steel tube and concrete core are perfectly homogenous and isotropic materials.
2. At ultimate conditions the concrete and steel tube are under triaxial and biaxial stress states respectively
3. Longitudinal steel and concrete strains are compatibility $\varepsilon_{sl} = \varepsilon_{cl}$
4. Prior to ultimate load the lateral expansion of the concrete establishes tangential strain compatibility $\varepsilon_{st} = \varepsilon_{cr}$
5. Consistent with findings of Section 4.4.2.2, there is no strength enhancement for column sections having steel contribution ratios $\delta_s \leq 0.15$.
6. The design procedures do not apply to thinwalled sections in which the effects of local buckling of the tube is expected.

5.1.2 Plasticity Function - Steel Tube Stresses

Recapping the plasticity model proposed by Tomii et al. (1977), the effective steel stresses are derived as functions of the incremental Poisson's Ratio dυ where:

$$\sigma_{sl} = \frac{d\upsilon + 2}{\sqrt{3.(d\upsilon^2 + d\upsilon + 1)}}.f_y \tag{5.1}$$

$$\sigma_{st} = \frac{2d\upsilon + 1}{\sqrt{3.(d\upsilon^2 + d\upsilon + 1)}}.f_y \tag{5.2}$$

From equilibrium conditions of a cross section, the transverse steel stress can be represented as a concrete confining pressure given by:

$$f_r = \sigma_{cr} = \frac{2t}{d_c}.\sigma_{st} \tag{5.3}$$

5.1.2.1 dυ - δ_s Relationships

Empirical expressions for predicting the relationship between the incremental Poisson's Ratio dυ, and the cross sectional factors δ_s and Φ, as proposed by Tomii et al. and Zhong and Maio have previously been discussed in Section 2.4.4.2. A notable deficiency of these models is that at low values of δ_s and Φ, they assume dυ increases continuously. It has been established from test results that for δ_s below 0.15, uniaxial conditions exist. By definition of Eqn's. 5.1 and 5.2, uniaxial conditions (σ_{st} = 0 and σ_{sl}= f_y) are given when dυ equals ⁻0.5. Consequently at lower extremities, values of dυ must be constant (⁻0.5) up to δ_s = 0.15. It is anticipated that for δ_s > 0.15 the dυ - δ_s relationship must display ascending stages prior to displaying descending behaviour as observed by the aforementioned empirical models. In Figure 5.1, the relationship by Tomii et al. has been plotted against limited results obtained from this program. The results support the belief that at lower δ_s factors, the value of dυ converge to ⁻0.5 giving uniaxial conditions. This may be treated with some scepticism as the results are limited in number and experimental parameters examined.

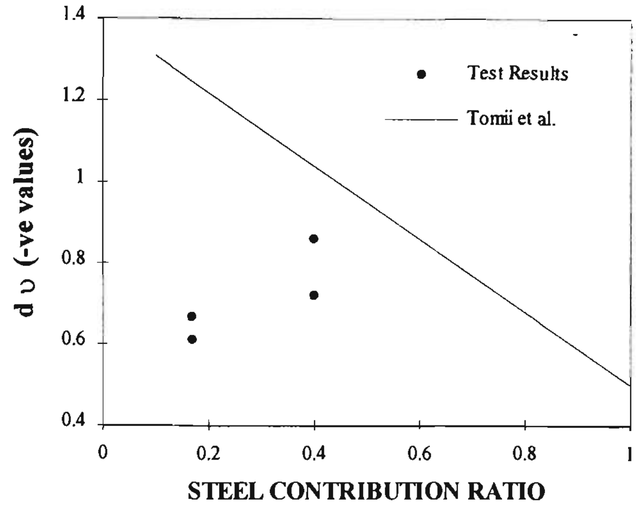

Figure 5.1: *Experimental results for $d\upsilon$.*

5.1.3 <u>Failure Criteria for Laterally Confined HSC.</u>

Based on the experimental values of $d\upsilon$ and the plasticity function, predicted column capacities have been obtained using various empirical failure criteria for confined HSC as defined by Eqn's. 5.4 to 5.9. The predicted capacities were then compared against experimental failure loads for concrete mix B (90 MPa) specimens. (strain gauged results only). These comparisons are summarised in Table 5.1.

Linear Relationship

$$f'_{cc} = f'_c + K.f_r \qquad \textbf{(5.4)}$$

Fafitis and Shah (1986)

$$f'_{cc} = \lambda_2.[f'_c + (1.15 + 21/f'_c).f_r] \qquad \textbf{(5.5)}$$

$$\lambda_2 = 1 + 15.(f_r / f'_c)^3$$

Mander et al. (1988)

$$f'_{cc} = f'_c(-1.254 + 2.254\sqrt{1 + 7.94\frac{f_r}{f'_c}} - 2\frac{f_r}{f'_c} \qquad \textbf{(5.6)}$$

Setunge et al. (1992) (1)

$$f'_{cc} = f'_c(13.07\frac{f_r}{f'_c} + 1)^{0.63} \qquad \textbf{(5.7)}$$

Setunge et al. (1992) (2) $$f'_{cc} = f'_c\,(14.67\frac{f_r}{f'_c} + 1)^{0.45} \tag{5.8}$$

Setunge et al. (1992) (3) $$f'_{cc} = f'_c\,(18.67\frac{f_r}{f'_c} + 1)^{0.45} \tag{5.9}$$

Setunge (1) : Applies to normal and medium strength concrete up to 60 MPa.
Setunge (2) : HSC without silica fume (90-120 MPa)
Setunge (3) : HSC with silica fume (90-130 MPa)

TABLE 5.1: Comparison of Experimental Failure Loads with Predicted Capacities based on Various Failure Criteria for Laterally Confined HSC.

Specimen	dυ	N_{exp} Note (1)	N_{exp} / N_{calc} (MIX B)					
			Linear K=4	Fafitis	Mander	Setunge (1)	Setunge (2)	Setunge (3)
CA11-1	0.67	539.6	1.006	1.066	0.954	0.931	0.964	0.935
CA11-4	0.612	522.5	0.988	1.027	0.951	0.934	0.957	0.936
CA13-1	0.83	757.8	1.088	1.352	0.971	0.883	1.020	0.948
CA13-4	0.72	732.5	1.114	1.330	0.999	0.929	1.037	0.973
		Mean	1.049	1.194	0.969	0.919	0.995	0.948

Note 1: Experimental failure loads given as average values of three tests specimens not singular results.

It was shown from Table 5.1, that the best correlation between predicted capacities and experimental results was obtained using the Setunge et al. failure criteria for HSC with no silica fume (Eqn. 5.8). In this case the mean ratio of N_{exp}/N_{calc} is 0.995 with a standard deviation of 0.040. Predicted values based on Fafitis and Shah were very conservative supporting observations by Setunge et al.. This was evident for the test specimens having greater δ_s (CA13). Predictions based on Mander et al. and the two other failure criteria proposed by Setunge et al. overestimated the experimental results by up to 11.7 %.

Although the Mix B concrete used in this investigation contained some content of silica fume, Setunge's HSC - silica fume failure criteria (Eqn. 5.9) was shown to overestimate experimental values by between 2.7 to 6.5 %. One reason for this may be attributed to the respective contents of silica fume used in each experimental program. Setunge's

HSC contained 45 kilograms of silica fume per cubic metre in comparison to 25 kg. for the Mix B concrete used in this program. This may account for the closer correlation of experimental results with the HSC without silica fume failure criteria.

Pertaining to these findings, it was adopted that the effective strength of the concrete core in CFST Mix B columns should be determined using Eqn. 5.8. For Mix A concretes, the failure criteria defined by Eqn. 5.7 was adopted. This was based on the fact that Setunge et al.'s (1) experimental results had similar strength and composition to the Mix A concrete used in this study. It should be noted that these assumptions are based on a limited number of available results and may be subject to further verification.

5.1.4 Analysis of Test Results

Due to the limited results for 'dυ' obtained from the test program, an analysis of expected values was performed to illustrate the probable shape of the dυ-δ_s relationship as discussed in Section 5.1.2.1. By assuming the plasticity equations for steel stresses and the two failure criteria adopted for respective Mix A and B concretes, predicted values of dυ were calculated from experimental failure loads. The determined values are plotted against their respective steel contribution ratio in Figure 5.2

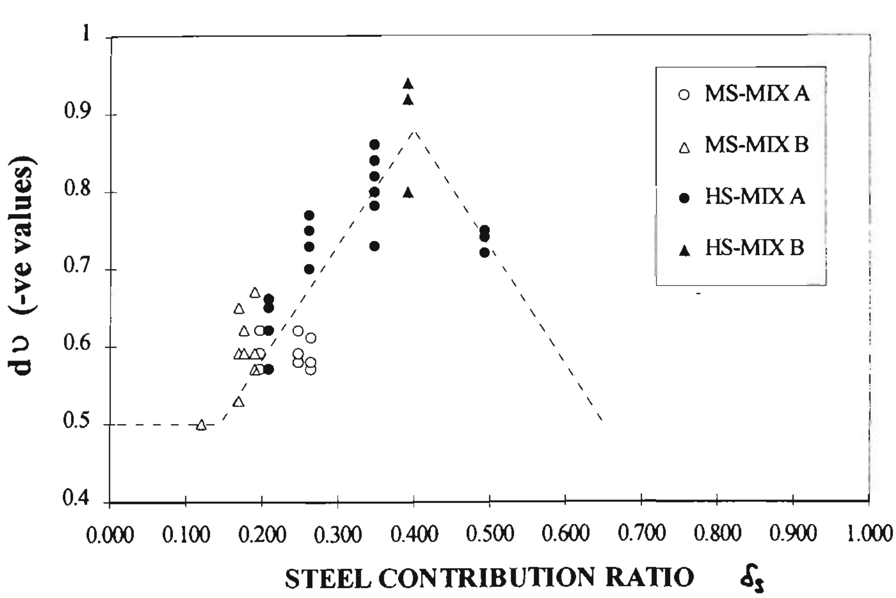

Figure 5.2: *Predicted values of dυ.*

In examining Figure 5.2, the calculated data indicates that the $d\upsilon$-δ_s relationship consists of varying stages. The values of $d\upsilon$ were observed to converge to $^{-}0.5$ as the δ_s ratio declined to 0.15. For δ_s between 0.15 and 0.4, the values of $d\upsilon$ increased in a linear manner. Results beyond $\delta_s = 0.4$ imply that at some stage a transition occurs and the values of $d\upsilon$ decend. Hence the relationship may consist of a number of linear segments, or possibly a curve function may apply. The accuracy of the empirical relationship is dependent on the exactness of failure criteria assumed for the concrete, therefore may only apply to the experiment parametric ranges covered within this study.

5.1.4.1 Empirical Model for $d\upsilon$

By establishing boundary conditions of the $d\upsilon$–δ_s relationship, empirical equations were obtained by taking linear regression with the data points as shown in Figure 5.2. It was assumed that:

- $0 \le \delta_s \le 0.15$ the corresponding $d\upsilon$ values are constant equal to $^{-}0.5$.
- $\delta_s = 0.4$ defines the transition point between increasing and decreasing values of $d\upsilon$.
- $\delta_s = 1.0$ $d\upsilon$ must be equal to uniaxial conditions $d\upsilon = {}^{-}0.5$.

The empirical relationship derived was defined by the following:

$$\begin{cases} d\upsilon = -0.5 & \text{when } \delta_s \le 0.15 \\ d\upsilon = -0.5 - 1.52\,(\delta_s - 0.15) & \text{when } 0.15 \le \delta_s \le 0.40 \\ d\upsilon = -0.88 + 1.52\,(\delta_s - 0.40) & \text{when } 0.40 \le \delta_s \le 0.65 \\ d\upsilon = -0.5 & \text{when } \delta_s \ge 0.65 \end{cases} \qquad \textbf{(5.10)}$$

This relationship is subject to further verification due to the limited experimental values of $d\upsilon$ obtained. There is also insufficient data to quantify exact relationships for column configurations having δ_s values in excess of 0.4. The empirical relationship is therefore restricted to CFST-HSC columns having concrete strengths between 60 to 90 MPa, and steel contribution ratio $\delta_s \leq 0.4$.

5.2 STRESS-STRAIN RELATIONSHIP OF CFST-HSC COLUMNS

The plasticity function for steel tube stresses and the incremental Poisson's Ratio may be used to determine the stress-strain relationship of the composite section. Load - strain relationships for both the steel tube and concrete core components under respective biaxial and triaxial stress states, can be superimposed to obtain the relationship of the composite section. This is shown schematically in Figure 5.3.

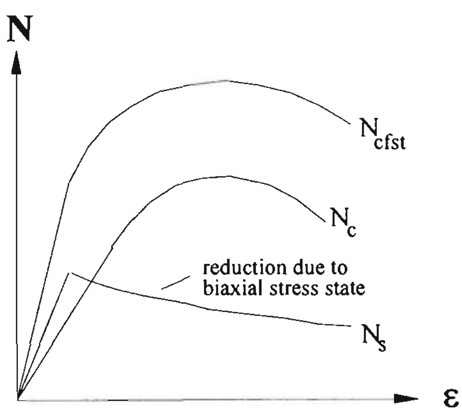

Figure 5.3: *Stress-strain relationship of composite materials.*

5.2.1 Load-Strain Relationship for the Steel Tube

The axial load-strain relationship for the steel tube component under confinement actions can be obtained by applying an associated flow rule for incremental Poisson's Ratio. Experimental results illustrated in Figure 4.21 indicate that the relationship between incremental Poisson's Ratio $d\upsilon$ and longitudinal strain can be represented in the general form shown in Figure 5.4. In the initial stages of loading, the $d\upsilon$ ratio remains constant around $^{-}0.3$ indicating the steel tube acts under uniaxial conditions. For HSC Mix B specimens $d\upsilon$ remained constant up to a mean longitudinal strain of 2600 $\mu\varepsilon$. At this strain, volumetric expansion of the concrete core initiated, increasing $d\upsilon$ and developing biaxial stress states within the steel tube. The $d\upsilon$ ratio was observed to increase in a parabolic manner after this point.

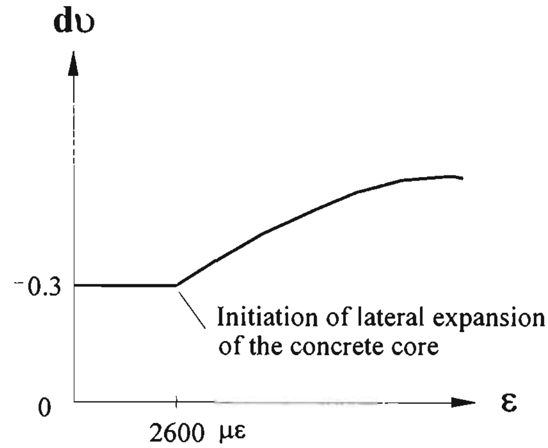

Figure 5.4: Incremental Poisson's Ratio ($d\upsilon$) and longitudinal strain (ε) relationship.

The load-strain curve for the steel tube component therefore consists of uniaxial and biaxial stages. To define the ascending load-strain relationship of the steel tube up to the initiation of confinement conditions, uniaxial relationships such as the Ramberg-Osgood function (Eqn 5.11) can be applied.

$$\varepsilon = \sigma / E + 0.002\ (\sigma / \sigma_y)^n \qquad \textbf{(5.11)}$$

As this equation is based on the steel having a nominal yield strain of 2000 $\mu\varepsilon$, the equation may be rewritten in the form of Eqn. 5.12 to accommodate variations in ε_y.

$$\varepsilon / \varepsilon_y = \sigma / \sigma_y + (0.002 / \varepsilon_y)(\sigma / \sigma_y)^n \qquad \textbf{(5.12)}$$

Examining the uniaxial experimental results for hollow steel tube stub columns reported in Section 4.3, it was found that Eqn. 5.12 gave best correlation for the ascending stress-strain relationship of the Mild Steel tube when ε_y was taken as 0.0026 and n = 10. For the High Strength Steel tube the corresponding values were ε_y = 0.0035 and n = 20. Figure 5.5 illustrates the comparison between predicted and experimental curves.

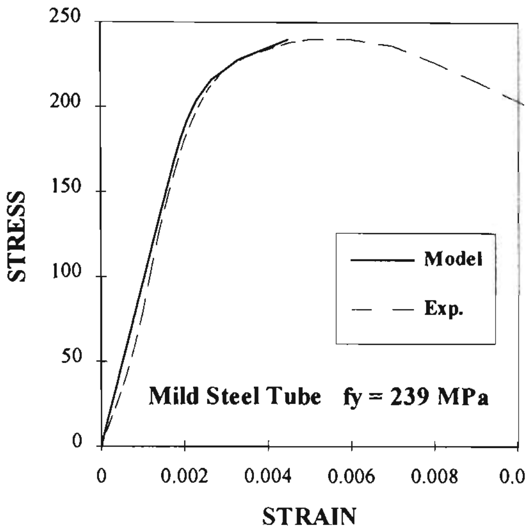

a) Mild Steel tube tests

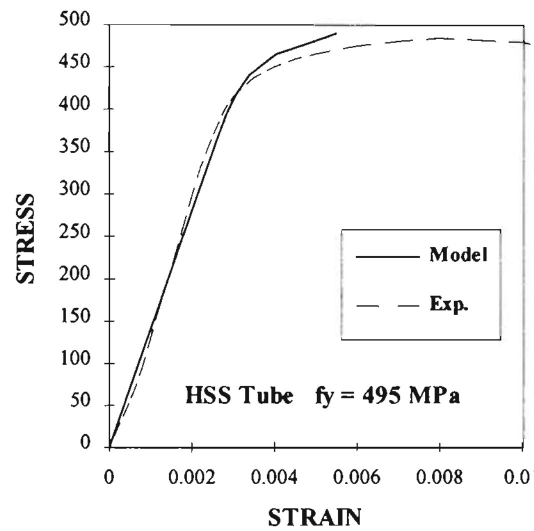

b) High Strength Steel tube

Figure 5.5: *Comparison of experiment stress-strain curves for hollow steel tube specimens and predictions based on modified Ramberg-Osgood functions.*

Establishing a relationship between the incremental Poisson's ratio $d\upsilon$ and longitudinal strain, the reduction in steel tube capacity due to biaxial stress states can be calculated using Eqn 5.1. The load-strain curve for the steel tube component is defined by the uniaxial relationship up to a point at which it intersects with the biaxial yield curve as illustrated in Figure 5.6. In the absence of appropriate empirical expressions for the $d\upsilon$-ε relationship, actual experimental values of $d\upsilon$ obtained from Series II experiments determined the steel tube load component for CFST specimen CA13-38-HB-1.

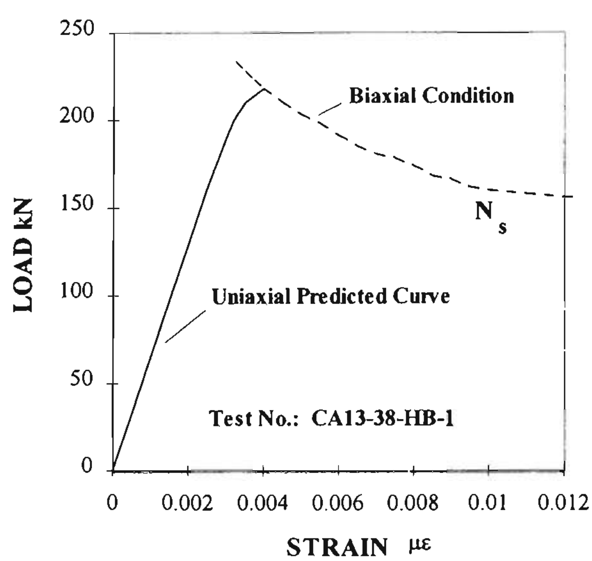

Figure 5.6: *Load-strain curve for steel tube component in a CFST section*

5.2.2 Load-Strain Relationship for the Concrete Core

Determining the effective confinement pressure f_r on the concrete at ultimate load based on the plasticity function enables the load-strain relationship of the concrete core to be determined, using available empirical models for laterally confined concrete. The majority of models represent the curve shape, peak stress and peak strain as functions of the confining pressure f_r and concrete strength f'_c. In appraising each of the empirical models detailed in Section 2.3.3.2 with experimental results from Series II (CFST) tests, it was found that great discrepancies exist between each model and the correlation with experimental curves. In the case of the CA13 specimens (HSS-HSC), model predictions for the peak strain at ultimate conditions were variable to a high degree. In the case of CFST specimen CA13-1, the experimental ε_o = 8340 $\mu\varepsilon$. The predictions based on Fafitis and Shah (Eqn. 2.22), Mander et al. (Eqn. 2.29) and Setunge et al. (Eqn. 2.33), were 7150 $\mu\varepsilon$, 12000 $\mu\varepsilon$, and 4980 $\mu\varepsilon$ respectively. This equates to a range of ± 44 % of the experimental value. It was not possible to recommend modifications or comment on the suitability of these empirical models in absence of further experimental results.

To illustrate the derivation of the composite curve, experimental values of ε_o and f'_{cc} were incorporated into the laterally confined concrete models by Fafitis and Shah (Eqn's. 2.19 to 2.26) and Setunge et al. (Eqn's 2.32 to 2.37). The load component attributed to the concrete (N_c) was then determined and combined with the steel tube component (N_s) to obtain the composite CFST load-strain relationship. In Figure 5.7 the predicted steel, concrete and composite curves based on the aforementioned procedures are compared against experimental results for CFST specimen CA13-38-HB-1. In each case a reasonable correlation between experimental and predicted curves was observed in the ascending curve range. In the post ultimate stage, the method applying Setunge's curve function underestimated the ductility of the column more than the Fafitis and Shah curve.

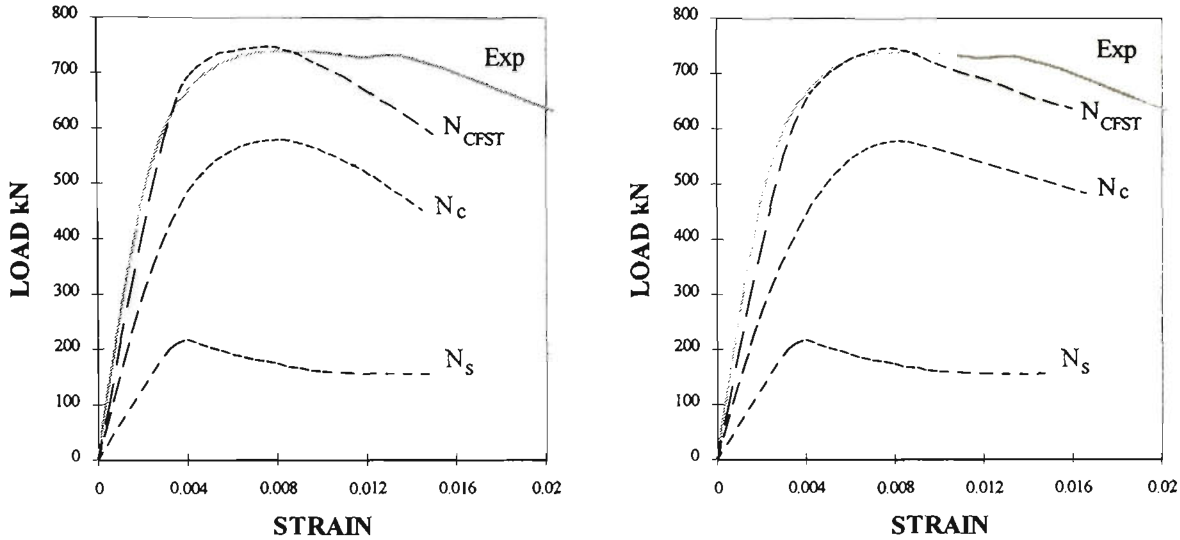

a) Modified Setunge et al. *b) Modified Fafitis and Shah*

Figure 5.7: *Derivation of composite load-strain relationships and experimental comparison.*

CHAPTER 6: DESIGN CODES AND COMPARISONS

6.1 INTRODUCTION

In this chapter, a comparison between the experimental failure loads and those predicted by three International design codes is performed.

- BS5400 (British Standard) *"Steel, Concrete and Composite Bridges: Part 5: Code of Practice for the Design of Composite Bridges." (1979).*
- CAN3-S16.1-M84 (Canadian Standard) *"Design of Steel Structures for Buildings." (1984).*
- EUROCODE 4 (European Standard) *"Design of Composite Steel and Concrete Structures." (1990 Draft).*

A comparative study is also presented on the predicted capacities of each code for a range of geometric and strength parameters.

6.2 OVERVIEW OF CODE PROCEDURES

The following is a brief overview of ultimate strength provisions for circular CFST columns given in the aforementioned codes. Only those provisions strictly related to ultimate strength analysis of axially loaded columns (unreinforced) are addressed. Detailed coverage of the relevant clauses and derivation of material properties for each code are contained in Appendix D.1 to D.3. (Note: The notation used in this text may differ from those used in the actual codes).

6.2.1 BS5400 Part 5 (1979)

The design provisions for CFST columns were based on work performed by Basu and Sommerville (1969) and Virdi and Dowling (1976) as discussed in Chapter 2. It should be noted that these design procedures were also applied in the ECCS *"Composite*

Structures" publication (1981), and form the basis of procedures adopted in the latter Eurocode 4.

6.2.1.1 Section Capacity

For short columns with slenderness ratio $L_e/D < 12$, the axial capacity of circular CFST sections is defined by:

$$N_{pl} = \eta_2 A_s f_y / \gamma_s + 0.67 A_c \left(f_{cu} + \eta_1 \frac{t}{D} f_y \right) / \gamma_c \qquad \textbf{(6.1)}$$

where η_1 , η_2 the co-efficients of confinement (given by C_1, C_2 in BS5400).

γ_c , γ_s material safety factors for concrete and steel components (1.5 and 1.1 respectively).

0.67 factor related to the design strength of concrete (ie. $f_c = 0.67 f_{cu}$).

The co-efficients η_1 and η_2 are obtained by interpolation of the values given in Table 6.1 with respect to the column L_e/D ratio.

TABLE 6.1: BS5400 Confinement Co-efficients.

L_e/D	0	5	10	15	20	25
η_1	9.47	6.40	3.81	1.80	0.48	0.00
η_2	0.75	0.80	0.85	0.90	0.95	1.00

6.2.1.2 Member Capacity

The design strength for axially loaded column given by Eqn. 6.2, is represented as a function of cross sectional capacity N_{pl} and a slenderness reduction factor K_1. The reduction factor K_1 is obtained from an appropriate column buckling curve (defined in Appendix D.1) and is related to the cross section properties in terms of a relative slenderness parameter $\bar{\lambda}$ (Eqn. 4.13).

$$N_d = K_1 N_{pl} \tag{6.2}$$

This code requires all columns to be designed for a minimum eccentricity of 0.3 by the column diameter.

6.2.2 CAN3-S16.1-M84

The Canadian Standard CAN3-S16.1-M84 is fundamentally a design code for structural steel members however includes provisions for circular CFST sections. Similar CFST design procedures were incorporated into the ISO TC 167/SCI Draft Standard for Composite Structures (1991).

6.2.2.1 Member Capacity

The CAN3 provisions, like the European codes, apply confinement factors to the effective steel and concrete strengths. However to determine the axial capacity of a CFST column, the steel tube and concrete core components are designed as separate elements each having independent slenderness reduction factors. The member capacity is given by:

$$N_d = \gamma N_s + \gamma' N_c \tag{6.3}$$

where N_c, N_s are the capacities of the concrete and steel components defined by Eqn. 6.4 and 6.6.

γ, γ' are confinement co-efficients determined by Eqn. 6.8 and 6.9.

6.2.2.2 Concrete Component

The compressive resistance of the core component is given by:

$$N_c = \phi_c 0.85 f'_c A_c \lambda_c^{-2} \left[\left(1 + 0.25 \lambda_c^{-4} \right) - 0.5 \lambda_c^{-2} \right] \tag{6.4}$$

where ϕ_c is a capacity reduction factor (taken as 0.85).

λ_c is the core slenderness factor defined by Eqn. 6.5.

$$\lambda_c = \frac{L_e}{r_c}\sqrt{\frac{f'_c}{\pi^2 E_c}} \tag{6.5}$$

r_c, E_c are the radius of gyration and elastic modulus of the concrete determined in accordance to Appendix C.2.

0.85 factor relating to the design strength of concrete.

6.2.2.3 Steel Component

The steel tube component N_s is determined as a function of the nominal steel capacity $\phi_s A_s f_y$, and a slenderness reduction factor obtained from an appropriate steel design curve as a function of λ_s. Therefore:

$$N_s \propto \lambda_s \tag{6.6}$$

where $$\lambda_s = \frac{L_e}{r_s}\sqrt{\frac{f_y}{\pi^2 E_s}} \tag{6.7}$$

Two design curves are given based on the type of tube. They are:

- Cold Formed / Non Stress Relieved
- Hot Formed / Stress Relieved

The equations defining each curve are detailed in Appendix C.2. The Cold Formed / Non Stress Relieved curve has been used for comparisons in this chapter.

6.2.2.4 Confinement Co-efficients

For columns with L_e/D ratio less than 25, the γ and γ' co-efficients are determined by:

$$\gamma = \frac{1}{\sqrt{1+\rho+\rho^2}} \tag{6.8}$$

and $$\gamma' = 1 + \left(\frac{25\rho^2\gamma}{D/t}\right)\left(\frac{f_y}{0.85f'_c}\right) \tag{6.9}$$

where $$\rho = 0.02.(25 - L/D) \tag{6.10}$$

The above derivation of co-efficients is similar to the empirical formula proposed by Virdi and Dowling (1976). For comparisons the factors η_1 and η_2 used in BS5400 and EC4 can be represented in terms of CAN3 factors where $\eta_2 = \gamma$ and $\eta_1 = 25\rho^2\gamma$.

6.2.3 Eurocode 4 (EC4) (1990)

6.2.3.1 Section Capacity

For columns having relative slenderness $\bar{\lambda} < 0.5$, the enhanced cross section capacity of a CFST column is defined by:

$$N_{pl} = A_s f_y \eta_2 / \gamma_s + A_c f'_c / \gamma_c \left[1 + \eta_1 \frac{t}{D} \frac{f_y}{f'_c}\right] \tag{6.11}$$

where η_1, η_2 are determined as functions of $\bar{\lambda}$ by Eqn's. 6.12 and 6.13.

γ_s, γ_c are material safety factors for the steel and concrete respectively.

$$\eta_1 = 4.9 - 18.5\bar{\lambda} + 17\bar{\lambda}^2 \qquad \eta_1 \geq 0.0 \tag{6.12}$$

$$\eta_2 = 0.25(3 + 2\bar{\lambda}) \qquad \eta_2 \leq 1.0 \tag{6.13}$$

Subsequently, η_1 and η_2 factors vary with respect to geometric and strength properties of the section as well as column slenderness, since $\bar{\lambda}$ is a function of both the nominal section capacity N_o and the critical buckling capacity N_{cr} (Eqn. 4.14). Due to the improved curing conditions of the concrete, hermetically sealed within the tube profile, Eurocode permits the removal of the 0.85 correction factor usually applied to the concrete strength component.

6.2.3.2 Member Capacity

Ultimate axial capacity of a member is determined in a similar manner to BS5400 where the section capacity is reduced by a design curve factor 'χ'. Eurocode 4 adopts the European Design Buckling Curve 'a' as defined in Appendix C.3 for circular filled sections. Hence:

$$N_d = \chi N_{pl} \tag{6.14}$$

Typical design curves derived from Eurocode predictions are shown in Figure 6.1. The increased magnitude of the CFST curve over that of the uniaxial buckling curve is dependent on numerous design parameters. As the η_1 curve is partially a function of $\bar{\lambda}^2$, the enhanced strength portion forms an inverted curve converging to uniaxial conditions at $\bar{\lambda}$ = 0.5. The shape of the design curves for the two previous codes are more symbolic of a continuous curve (buckling curve) than those predicted by Eurocode.

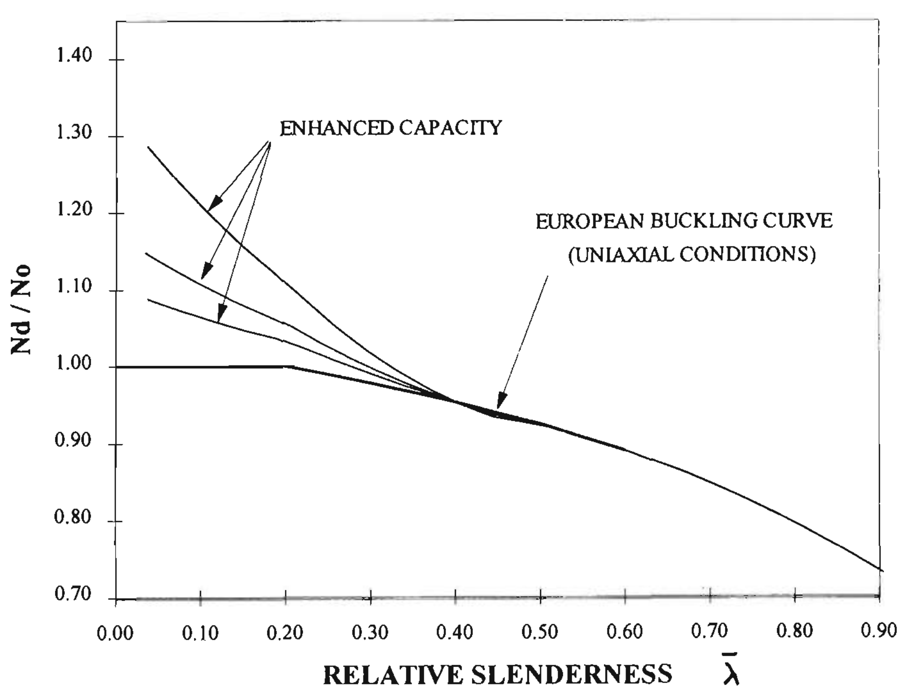

Figure 6.1: *Design load curves based on Eurocode 4 predictions.*

6.2.4 Discussion on Confinement Co-efficients

In Table 6.2 a summary of the η_1 and η_2 (γ and γ') co-efficients determined in accordance with each are presented. The values of BS5400 and CAN3 are functions of L/D while EC4 are based on relative slenderness $\bar{\lambda}$. Co-efficients are essentially the same for EC4 and CAN3 when $\bar{\lambda}$ values of 0, 0.1, 0.2 etc. are compared to L/D ratios of 0, 5, 10 etc. The η_1 co-efficients determined from BS5400 are essentially twice those predicted by CAN3. This can be explained in terms of the strength factors applied to the concrete capacity in BS5400. The effective concrete strength in BS5400 is represented by 0.67 f_{cu}/γ_c in which γ_c is taken as 1.5, hence $f_c = 0.45\ f_{cu}$. The reciprocal of 0.45 approximates to 2 which is the factor applied BS5400 η_1 values. For all intentions, each code methodology adopts design co-efficients similar to those of Virdi and Dowling (1976), although their application and derivation varies.

As discussed in Chapter 2, these simplified co-efficients are largely empirical for two principal reasons.

- The effective stresses within the steel tube are determined primarily on the L/D ratio and are independent from column strength and geometric parameters.
- No consideration is made for the reduced effectiveness of lateral confinement in HSC applications.

TABLE 6.2: Summary of Design Confinement Co-efficients.

CODE	L/D =	0	5	10	15	20	25
BS5400	η_1	9.47	6.40	3.81	1.80	0.48	0.00
	η_2	0.75	0.80	0.85	0.90	0.95	1.00
CAN3	η_1 ($25\rho^2\gamma$)	4.72	3.20	1.91	0.90	0.24	0.00
	η_2 (γ)	0.76	0.80	0.85	0.90	0.95	1.00
	λ =	0	0.1	0.2	0.3	0.4	0.5
EURO 4	η_1	4.90	3.22	1.88	0.88	0.22	0.00
	η_2	0.75	0.80	0.85	0.90	0.95	1.00

6.2.5 Discussion of Design Procedures

In summary, the characteristic differences between the codes are:

- EC4 derives η_1 and η_2 co-efficients with respect to $\bar{\lambda}$ where BS5400 and CAN3 the co-efficients are functions of L/D.
- BS5400 and EC4 member capacities are determined as functions of section capacity N_{pl} and slenderness reduction factors obtained from column buckling curves. CAN3 member capacity is based on the sum of the steel tube and concrete strength components incorporating independent slenderness factors for each material.
- The characteristic design strengths of the concrete component vary between each code. BS5400 and CAN3 apply respective design factors of 0.67 f_{cu} and 0.85 f'_c while Eurocode permits the removal of such factors.
- Numerical quantification of material properties (eg. E_c) and usage of capacity reduction factors.

6.3 COMPARISON WITH EXPERIMENTAL RESULTS

In Figure 6.2 to 6.5, the normalised failure loads from Chapter 4 are compared against the predicted capacities for each column configuration. The capacities have been plotted against the relative slenderness factor determined in accordance with EC4. For all predicted capacities the material safety factors have been taken as unity. The elastic modulus of concrete (E_c) has been determined using the equations defined in each code. For BS5400 calculations which are based on the cube strength of concrete, the correctional factor of $f_{cu} / f'_c = 1.2$ was applied. The minimum eccentricity requirement stipulated in BS5400 has been omitted. The design strength for the concrete used for concrete mixes A and B were taken as 60 and 90 MPa respectively contrary to experimental results varying between 46.3-67.4 MPa and 82.4-100.6 MPa. This enabled comparisons of columns obtained from different casting groups to be represented on the same diagram. As the design value N/N_0 is variable with respect to f'c, some figures contain minor discrepancies. In all other statistical assessment, actual experimental concrete strengths are used.

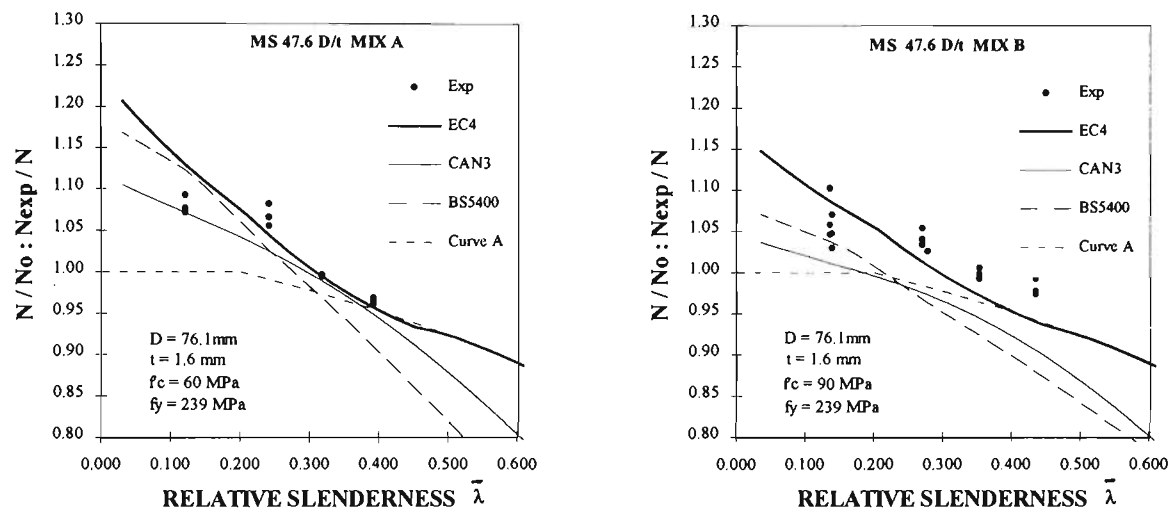

a) *MIX A (60 MPa)* b) *MIX B (90 MPa)*

Figure 6.2: *Failure load comparison with predicted curves for mild steel tube columns D/t ratio = 47.6.*

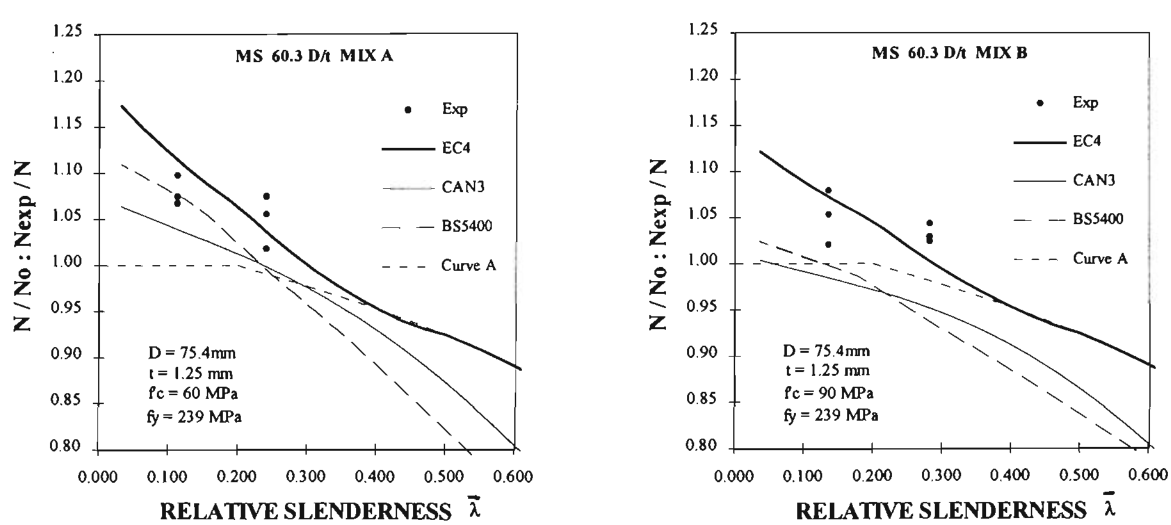

a) *MIX A (60 MPa)* b) *MIX B (90 MPa)*

Figure 6.3: *Failure load comparison with predicted curves for mild steel tube columns D/t ratio = 60.3.*

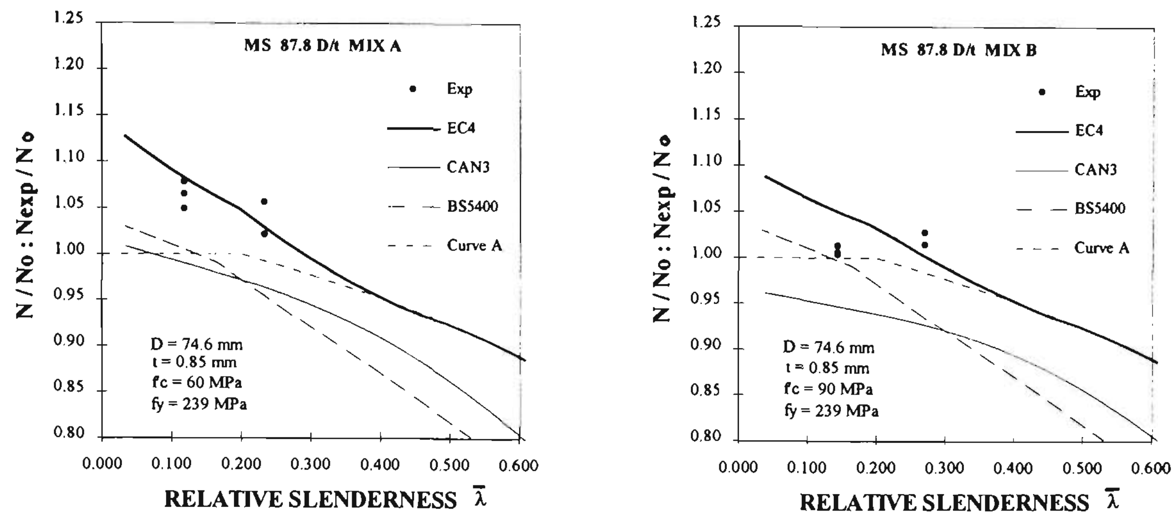

a) *MIX A (60 MPa)* b) *MIX B (90 MPa)*

Figure 6.4: *Failure load comparison with predicted curves for mild steel tube columns D/t ratio = 87.8.*

6.3.1 <u>Mild Steel CFST Columns</u>

From Figures 6.2 to 6.4 there is evidence of significant discrepancies between the predicted curves obtained from each design code. The correlation of experimental results to each code prediction has shown to be dependent on the column D/t ratio, slenderness ratio, and concrete strength. In the proceeding text the principal observations made with respect to the correlation between experimental results and each design predictions are discussed. Detailed statistical assessment of all experimental results are summarised in Section 6.3.3.

For all the experimental parameters examined, predictions based on EC4 were in excess of those obtained from BS5400 and CAN3. It was also evident that the effects of column slenderness in BS5400 and CAN3 design curves were more pronounced. Experimental results for $\bar{\lambda} > 0.2$ were shown to exhibit closest correlation with predictions based on EC4 for each D/t ratio and concrete strength. The ratio of experimental to predicted values N_{exp}/N_{calc} varied between 0.98 to 1.06. This range reduced to 1.01 to 1.04 when comparing the average results of specimens with identical column configurations. The corresponding correlation between N_{exp}/N_{calc} for BS5400 and CAN3 design curves were less favourable. In these cases the correlation varied between 1.03 - 1.15 and 1.02 - 1.13 for the respective codes. In Figure 6.4 b) (D/t 87.8 - Mix B) the column configurations examined possessed steel contribution ratio δ_s less than 0.15. As concluded from Chapter 4, no strength enhancement is expected for this limit, consequently these results have not been taken into consideration.

For stockier columns $\bar{\lambda}<0.2$, EC4 predictions consistently overestimated experimental values by up to 6 % with the ratio of N_{exp}/N_{calc} varying between 0.94 to 1.02. This excess of predicted values was observed to increase with the compressive strength of concrete. BS5400 predictions were also found to overestimate the capacities of mild steel specimens with 60 MPa concrete and D/t ratios of 47.6 and 60.3. For such configurations the N_{exp}/N_{calc} ratio for BS5400 ranged between 0.94 to 0.99, while the ratio for the remaining configurations varied between 1.00 to 1.08. CAN3 predictions were generally conservative by up to 10 %.

In summary, it was found that Eurocode 4 predictions showed the more favourable correlation with experimental failure loads for mild steel columns despite overestimating the capacities of short columns. Predictions based on this code were within 6 % of the experimental results. In practice, this maximum discrepancy would be offset by material and load reduction factors used in design.

6.3.2 High Strength Steel CFST Columns

In Figure 5.5, the comparative curves for tests specimens using HSS tube are presented. Unlike mild steel columns, the predictions based on EC4 were below the corresponding BS5400 and CAN3 capacities up to a relative slenderness of 0.6. For the limited HSS configurations examined, the most favourable correlation between experimental and predicted capacities were obtained using the BS5400 code with N_{exp}/N_{calc} between 0.98

to 1.08. Eurocode 4 predictions were observed to underestimate the experimental loads by 10 to 25 %.

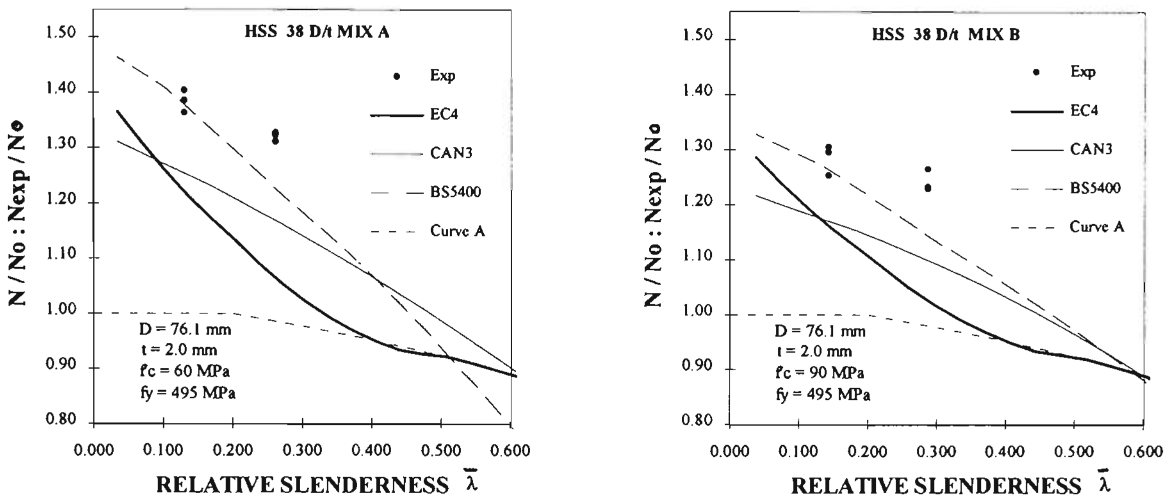

a) *MIX (60 MPa)* b) *MIX (90 MPa)*

Figure 6.5: *Failure load comparison with predicted curves for high strength steel tube columns D/t ratio = 38.05.*

Applying the confinement co-efficients derived in CAN3 to EC4 design procedures, the modified predicted capacities gave a mean value of N_{exp}/N_{calc} as 1.032 with a standard deviation of 0.014. This modified form of EC4 provided greater correlation than the other design codes considered. This suggests that the source of the discrepancy between EC4 predictions for HSS-CFST columns may originate from determining confinement co-efficients as functions of relative slenderness factor $\bar{\lambda}$. This aspect is to be discussed in further detail in Section 6.4.3. It should also be noted that the results obtained are only representative of a singular tube configuration and may be subject to further experimental studies.

6.3.3 <u>Statistical Summary of Comparisons</u>

In Figures 6.6 to 6.8, the ratios of N_{exp}/N_{calc} for all test specimens are illustrated for each design code.

6.3.3.1 BS5400

Figure 6.6 clearly illustrates the variability between BS5400 predictions and experimental failure loads for the parameters tested. For MS-CFST specimens, the scatter of data points cover a range of N_{exp}/N_{calc} between 0.944 to 1.149 (≈20%). The respective mean and standard deviation are 1.054 and 0.048. For the HSS-CFST results the comparison with predicted values was less, 0.985 to 1.104, with mean and standard deviation of 1.043 and 0.042. The ratio of N_{exp}/N_{calc} increased significantly for increases in both the compressive strength of concrete and the column slenderness.

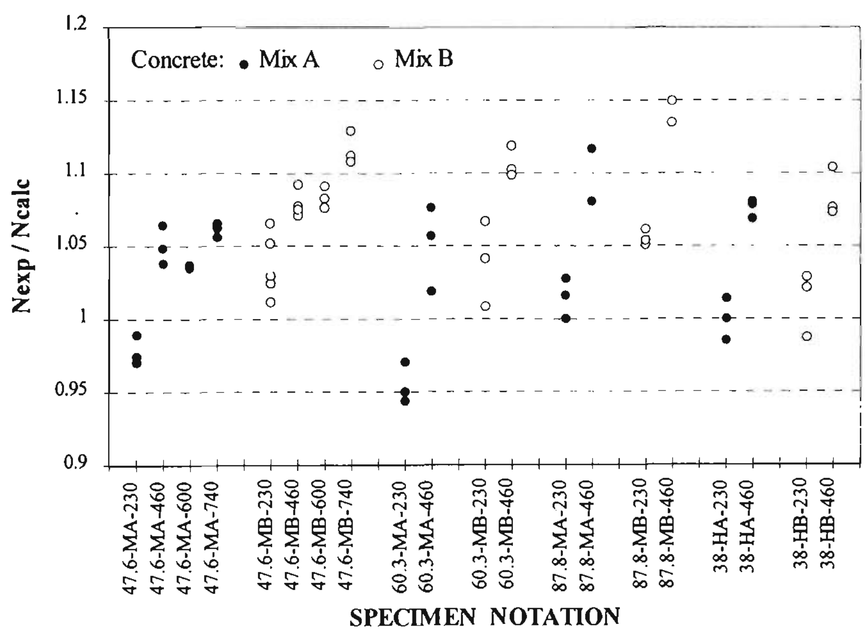

Figure 6.6: *Statistical summary of experimental comparisons with British Standard BS5400 Part 5.*

6.3.3.2 CAN3-S16.1-M84

In Figure 6.7, it is shown that with one exception, the ratio of N_{exp}/N_{calc} is in excess of unity for all test results. For MS-CFST results the range varied between 0.998 to 1.125 with mean and standard deviation of 1.064 and 0.030 respectively. This ratio was observed to increase with concrete strength and column slenderness. In the case of

HSS-CFST specimens the mean and standard deviation were 1.129 and 0.026 and were observed to decrease slightly with increases in compressive strength.

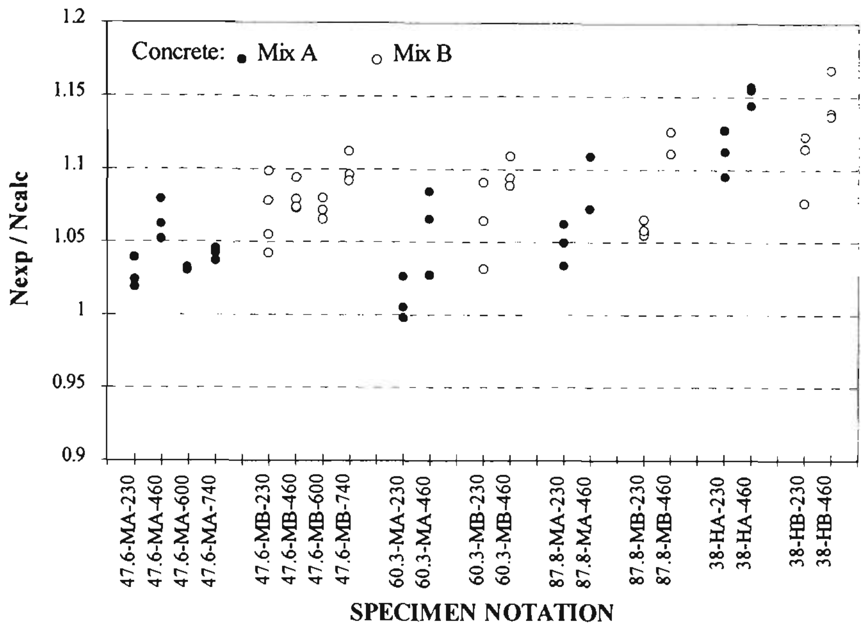

Figure 6.7: *Statistical summary of experimental comparisons with Canadian Standard CAN3-S16.1-M84.*

6.3.3.3 Eurocode 4

A summary of experimental failure loads compared with EC4 predictions is given in Figure 6.8. The difference between the correlation with results of mild steel columns to those of high strength steel columns is distinct. For MS-CFST columns with L/D less than 3, the N_{exp}/N_{calc} ratio was consistently less than unity, between 0.94 to 1.00. As the column slenderness increased the predicted capacities were shown to be greater than the experimental values. For the entire mild steel test results, the range of N_{exp}/N_{calc} varied between 0.94 to 1.055 (≈10%). This range of ± 6 % was the lowest out of the three design codes examined with mean and standard deviation of 1.000 and 0.033 respectively. The EC4 predictions were shown to exhibit deficiencies when it came to predicting the capacity of the HSS-CFST specimens. Predicted capacities were up to 25 % less than the experimental results.

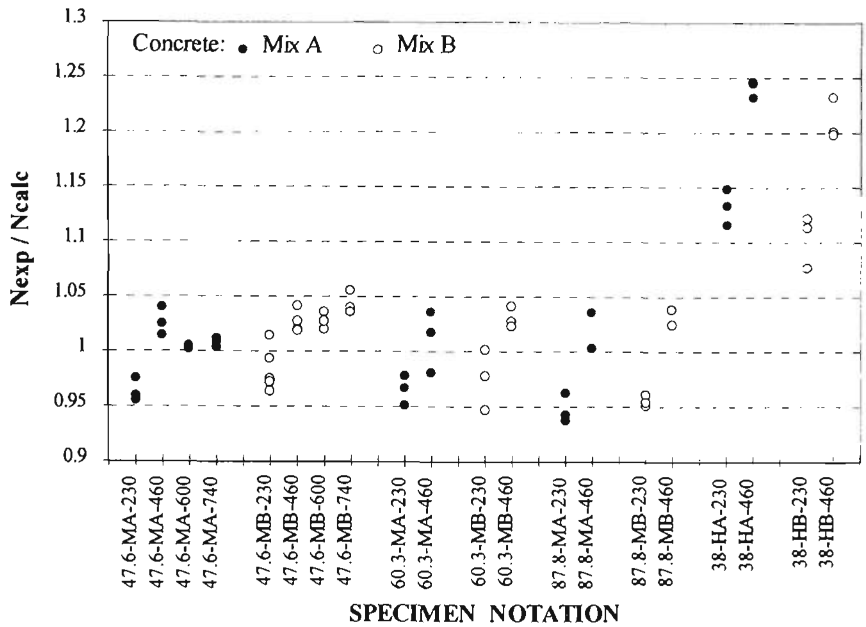

Figure 6.8: *Statistical summary of experimental comparisons with European Standard - Eurocode 4.*

6.4 PARAMETRIC STUDY

To quantitatively assess the comparative capacities of each design code with variations in design criteria, a parametric study was conducted. The parameters considered were:

- Diameter to wall thickness ratio — D/t
- Compressive strength of concrete infill — f'_c
- Yield grade of the steel tube — f_y
- Elastic modulus of the concrete — E_c

Design curves were established for each criteria allowing for column slenderness to be examined with respect to each column configuration. The input data for each case study are summarised in Table 6.3.

Note, the statistical values contained in the discussion on the comparative strengths in the following text, relate to column slenderness ratios of L/D of 3 unless specified otherwise.

TABLE 6.3: Input Data for Parametric Study.

Parameter	Case (1)	Case (2)	Case (3)	Case (4)	Case (5)
D	600	400,600,900	600	600	600
t	15,10,6.6	10	10	10	10
f'_c	50	50	30,60,90	50	90
f_y	250	250	250	250,350,450	250
E_c	As Code	As Code	As Code	As Code	±20%

Variables Case (1) & (2) : D/t Ratio Case (3) : f'_c Case (4) : f_y Case (5) : E_c

6.4.1 Effects of D/t Ratio

Two case studies were proposed to examine the effects of varying tube D/t ratio (40, 60 and 90) on the predicted capacities. Case Study 1; involved varying the wall thickness of the tube while maintaining a constant diameter, whereas for Case Study 2; the diameter was varied keeping the wall thickness constant. A yield strength of 250 MPa was adopted for the steel tube, and the concrete strength taken as 50 MPa. The limiting values of D/t ratio specified in BS5400, CAN3 and EC4 for f_y = 250 MPa are 80, 112 and 84.6 respectively. Therefore the 90 D/t ratio configuration exceeds specified limits in two of the codes examined.

Figure 6.9 summarises the normalised load (N/N_0) versus relative slenderness ($\bar{\lambda}$) curves for Case Study 1 with properties given in Table 6.3. It was found that the changes in D/t ratio had similar effects on the predicted curves for both case studies 1 and 2, hence case study 2 results have been omitted. The figures show extensive discrepancies between codes. For values corresponding to an L/D ratio of 3, the predicted capacities for CAN3 and EC4 reduced by 6 and 8 % respectively as D/t ratio increased from 40 to 90. BS5400 predictions exhibited greater sensitivity to such parametric changes with corresponding reductions of 16.5 %. With the exception of capacities determined by BS5400 for D/t = 40, the EC4 design curves gave the greatest predictions throughout the slenderness range.

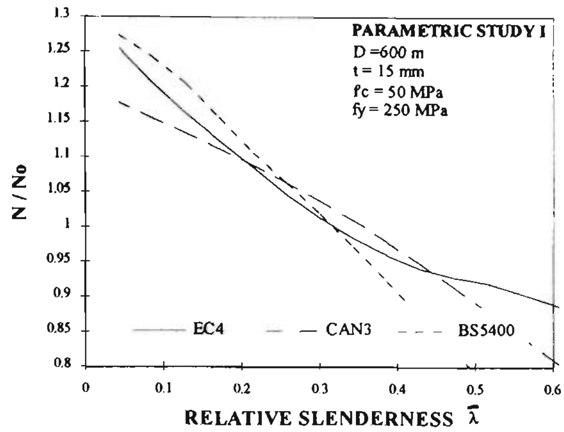

a) D/t = 40

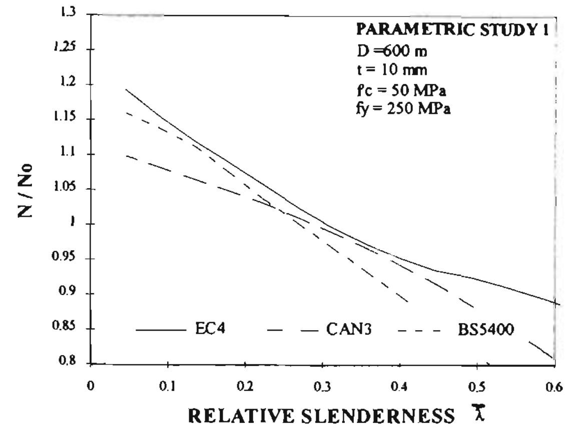

b) D/t = 60

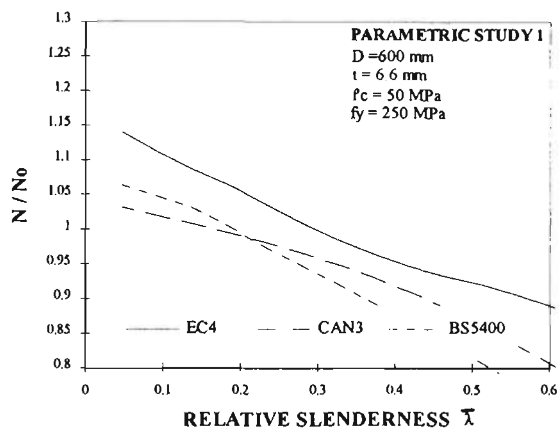

c) D/t = 90

Figure 6.9: *Effects of D/t ratio on predicted capacities.*

6.4.2 Effects of Concrete Compressive Strength

Figure 6.10 represents the effects of changes in concrete strength f'_c on the predicted design capacities. To cover the range of experimental concrete strengths examined in the scope of this research, concrete grades of 30, 60, and 90 MPa were adopted. For the 90 MPa column configuration, the steel contribution ratio (δ_s) of the section was 0.163 which exceeds the minimum requirement ($\delta_s > 0.2$) specified in both BS5400 and EC4. However, this configuration is expected to provide some strength enhancement based on the findings of experimental results in Chapter 4.

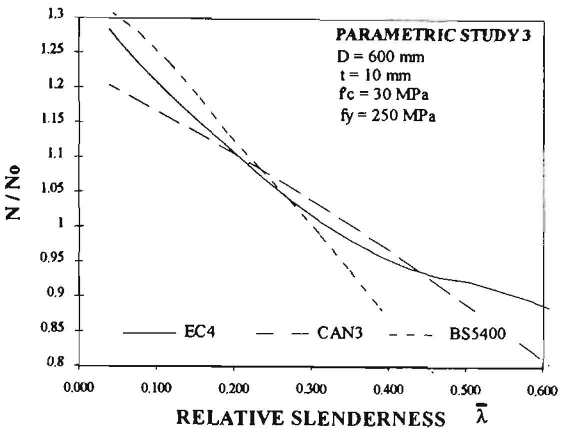

a) $f'_c = 30$ *MPa*

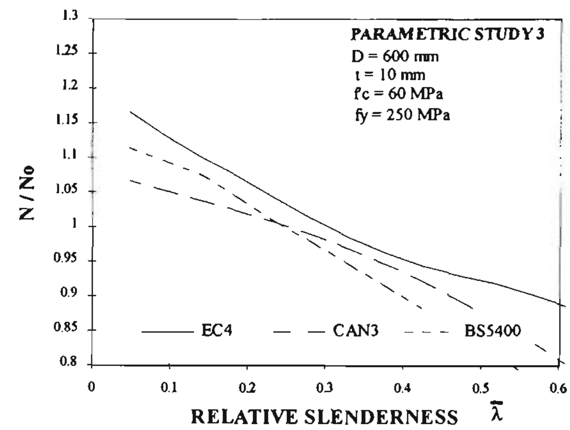

b) $f'_c = 60$ *MPa*

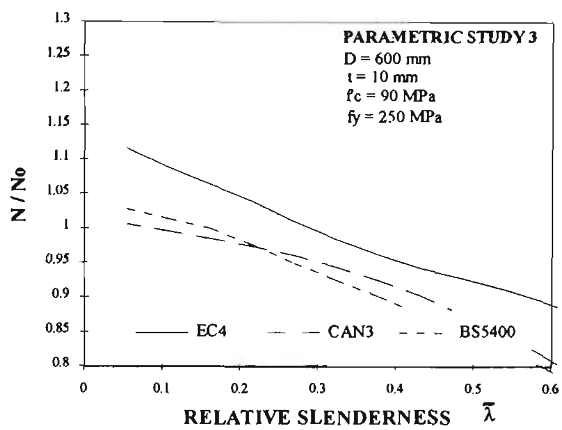

c) $f'_c = 90$ *MPa*

Figure 6.10: *Effects of* f'_c *on predicted capacities.*

For stub columns (L/D=3) with 60 and 90 MPa concrete, capacities determined by EC4 were between 5 to 8 % greater than the corresponding BS5400 and CAN3 values. The normalised load capacities for the 90 MPa columns using BS5400 and CAN3 barely exceeded unity. This indicated that for this column configuration, the two codes failed to permit any enhancement in properties of the cross section. For EC4 predictions, a 7 % increase in strength was obtained.

Once again the greatest variation for the parametric range was observed for the BS5400 code with a 24 % reduction in N/N_0 as concrete strengths increased from 30 to 90 MPa. Alternatively, values of 16 and 12 % were observed for CAN3 and EC4 respectively. The results of BS5400 may be misleading in some respect due to the application of a 1.2 correctional factor applied to relate the respective cube strengths and cylinder strengths of the concrete. In hindsight this value may require modification for HSC as discussed by Carrasquillo et al. (1982).

6.4.3 Effects of Steel Strength

The codes investigated apply limits on the grade of the steel tube in the order of 450 MPa. In practice steel tube grades range between 250 to 450 MPa. In Figure 6.11 design curves have been analysed for steel yield strengths of 250, 350 and 450 MPa. From the experimental comparisons, the enhanced properties based on EC4 for the HSS tube failure loads, were conservative with respect to both the empirical results and predictions by BS5400 and CAN3. For the increase in steel tube strength from 250 to 450 MPa, EC4 predictions only allow for a 4 % increase in N/N_o in comparison to BS5400 11 %, and CAN3 10 %.

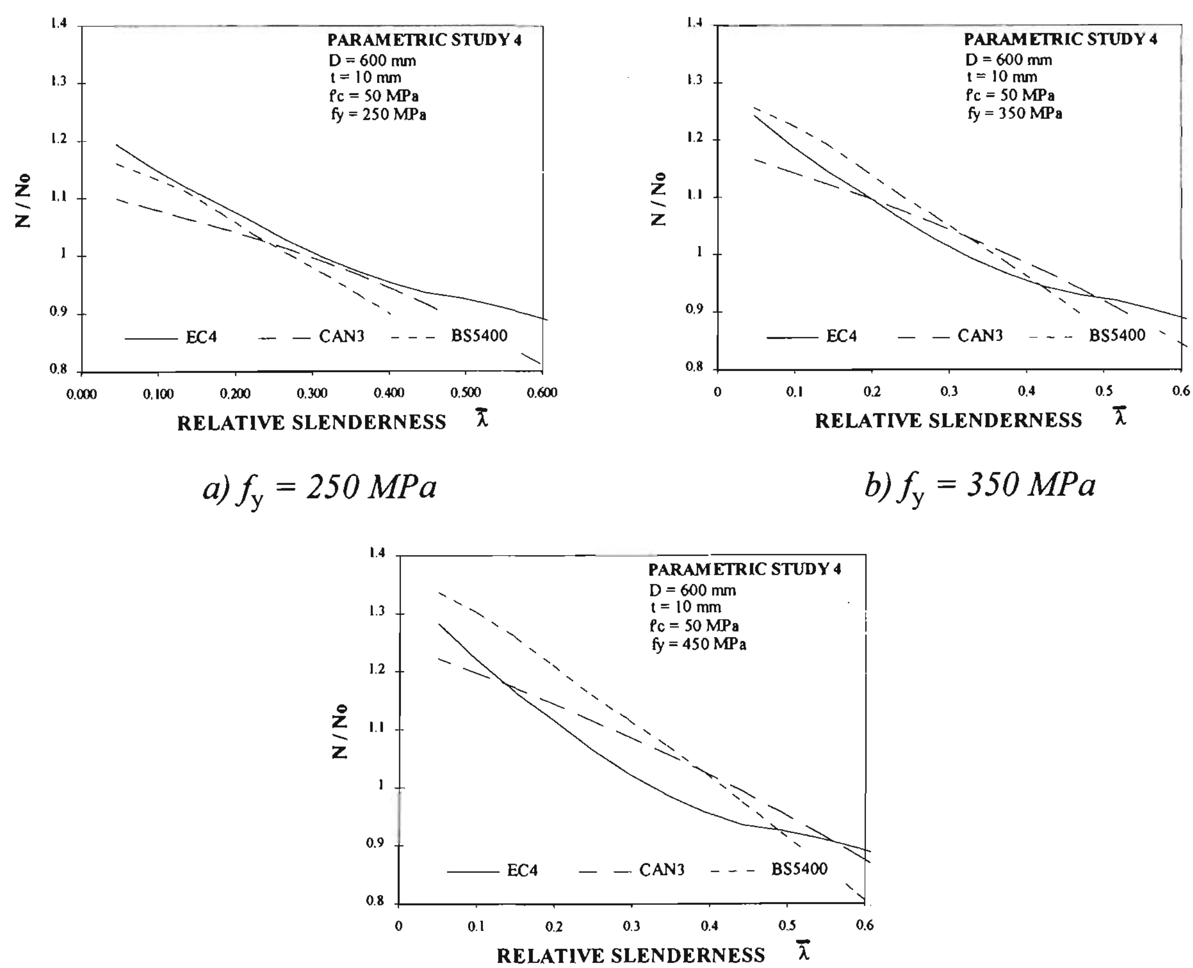

c) f_y *= 450 MPa.*

Figure 6.11: *Effects of* f_y *on predicted capacities.*

6.4.3.1 Discussion on Eurocode 4 Confinement Co-efficients

In Eurocode 4, the η_1 and η_2 design co-efficients are functions of relative slenderness $\bar{\lambda}$. Subsequently, the factors used in deriving $\bar{\lambda}$ have direct bearing on the quantities of η_1 and η_2. In Eqn. 6.15, the expanded form of $\bar{\lambda}$ demonstrates the factor is variable with a large number of geometric and strength parameters.

$$\bar{\lambda} = \sqrt{\frac{A_s f_y + A_c f'_c}{\pi^2 (0.8 E_s I_s + E_c I_c) / L_e^{\,2}}} \tag{6.15}$$

For a column of known dimensions with A_s, A_c, I_s, I_c and L_e constant, the magnitude of $\bar{\lambda}$ is increased with the application of high strength concrete and high strength steel. On the increase of $\bar{\lambda}$ there is a reduction in the η_1 co-efficient reducing the enhanced strength component of the concrete core. In the case of HSC, the increase magnitude of f'_c is accounted for to some extent in the lower denominator by the increase in elastic modulus E_c. As a consequence the magnitude of η_1 is not largely effected by increasing f'_c. In the case of high strength steel, the increase in f_y is not counteracted by any increase in E_s as this value for most steels is in the order of 200,000 MPa. This results in dramatic differences between values of relative slenderness determined for mild steel and high tensile steel columns. For the HSS-CFST columns represented in Figure 6.5, predicted $\bar{\lambda}$ values using actual yield strengths were 20 % less than those obtained assuming the properties of the mild steel tube. In turn, the values of η_1 reduced by approximately 30 %. In the case of thinwalled sections utilising HSC, a greater proportion of axial load is resisted by the concrete component. A reduction in the η_1 design factor would result in significantly lower predicted capacities.

Further test results are required to ascertain any potential modifications to Eurocode co-efficients or their derivation with particular emphasis on HSS. The limited test results reported indicate that an increase in η_1 co-efficients are necessary to fully exploit the enhanced strength of the composite section.

6.4.4 Effects of Elastic Modulus of Concrete

It has been discussed in Section 2.3.5 that existing expressions for determining the elastic modulus of concrete Ec can overestimate actual values for HSC by up to 30 %. To examine what effects this inaccuracy would have on the design strengths for the columns, Case Study 5 was undertaken. In Figure 6.12, predictions based on a given CFST cross section with 90 MPa concrete are shown. Design capacities have been plotted firstly with E_c determined in accordance with each standard, and secondly with E_c reduced by 25 %. It can be shown that variations in E_c only effect the design strengths of slender columns. In the short sections changes in capacities were infinitesimal.

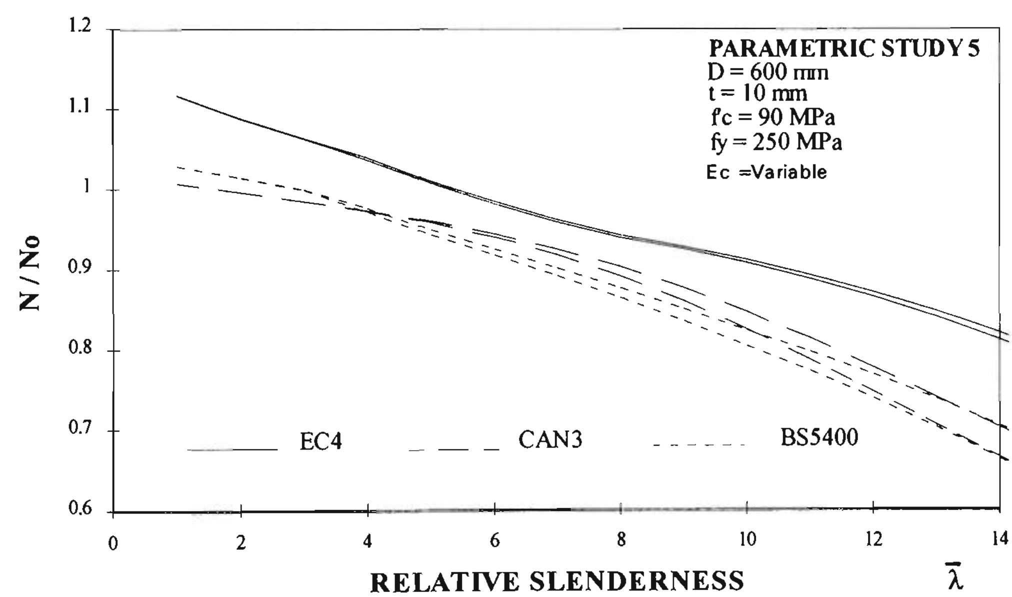

Figure 6.12: *Effects of E_c on predicted capacities.*

6.5 CONCLUSIONS AND RECOMMENDATIONS

Based on the presented comparative studies, several conclusions were drawn with respect to existing design codes and the application of high strength materials. They are:

- In comparison with experimental failure for mild steel CFST columns, predictions using Eurocode compared the most favourably despite overestimating the capacities of short columns. The ratio of N_{exp}/N_{calc} was within the range of ± 6 %. The Canadian Standard (CAN3) was conservative for all experimental parameters while the British Standard (BS5400) was sensitive to changes in D/t ratio, concrete strength and column slenderness. The experimental failure loads for increased column slenderness were observed to converge to the European Buckling Curve 'a' as specified in Eurocode 4.

- For specimens utilising high strength steel predictions by Eurocode 4 were conservative by 10 to 25 %. Improved correlation was obtained using either BS5400 or CAN3. To exploit the enhanced properties of HSS-CFST columns, a review of Eurocode 4 confinement co-efficients is necessary with respect to higher grade steels. At this stage, it was not possible to envisage any potential modifications until further empirical data is obtained.

- It was observed throughout the parametric study that for a singular column criteria, design capacities determined from each code could vary by over 25 % emphasising the need for unification of design procedures.

In concluding it is recommended that the design guidance for CFST columns given in Eurocode 4 should form the basis of design for HSC columns up to 100 MPa. However in the case of HSS, the conservative nature of Eurocode 4 suggests that it may be of further benefit to designers to apply provisions of BS5400. Furthermore, the minimum steel contribution ratio of 0.2 as specified in Eurocode 4, may be reduced to a value of $\delta_s = 0.15$ to accommodate thinwalled CFST-HSC columns.

CHAPTER 7: CONCLUSIONS AND RECOMMENDATIONS

7.1 GENERAL CONCLUSIONS EXPERIMENTAL PROGRAM

In the experimental part of this thesis, 62 scale model CFST-HSC columns were tested under concentric axial load. From this study the following conclusions were drawn:

1. The enhanced strength of CFST columns relative to the uniaxial capacity was observed to increase linearly with increases in steel contribution ratio δ_s for concrete strengths between 60 to 90 MPa. The strength enhancement ceased for limiting ranges of $\delta_s \leq 0.15$. A maximum increase of 40 % was observed for column configurations utilising the high strength tube and 60 MPa concrete.

2. The magnitude of the enhanced strength was greater in the lower strength concrete for columns having identical steel tube configurations. This is primarily due to the reduced volumetric dilatancy associated with the higher strength concretes.

3. Ductility of columns decreased with increasing compressive strength of concrete, with more brittle unloading characteristics observed. Therefore, ductility of CFST-HSC columns may be a possible consideration in the design of such columns. By using the ductility index factor (D_I) defined in Chapter 4, values for Mix A (60 MPa) concrete specimens were between 1.2 to 4.6 times greater than their Mix B (90 MPa) counterparts.

4. The primary mode of failure for short columns was the formation of an oblique shear failure within the concrete core. The inherent strength of the laterally confined concrete is therefore the principle factor in determining the ultimate capacity of CFST short columns.

5. The presence of concrete infill provided additional stability of the tube walls against the influence of local buckling mechanisms for the range of D/t ratios investigated.

6. The longitudinal strain at which volumetric expansion of the concrete infill established confinement conditions in the CFST section, was in the order of 2600 $\mu\varepsilon$ for the 90 MPa specimens. This value is generally in excess of those reported elsewhere for normal grade concretes.

7.2 DESIGN RECOMMENDATIONS

7.2.1 Semi Empirical Model

A semi empirical model was discussed for determining the ultimate capacity of CFST stub columns (L/D=3). The method incorporates a plasticity function as derived by Tomii et al. (1977) to determine the effective steel stresses σ_{sl} and σ_{st} as functions of the incremental Poisson's Ratio $d\upsilon$. From limited experimental values of $d\upsilon$, it was found that the proposed failure criteria for laterally confined HSC (without silica fume) by Setunge et al. (1992), compared favourably to the experimental Mix B concrete. Based on the aforementioned analytical procedures, expected values of $d\upsilon$ were obtained from experimental failure loads. A multi-linear empirical relationship was then obtained for the $d\upsilon$ - δ_s relationship for CFST-HSC columns with concrete strengths 60 to 90 MPa. This empirical model was proposed tentatively as only a small number of experimental results were available for comparisons, and is therefore subject to further verification.

7.2.2 Existing Design Codes

Existing design codes procedures for CFST columns given in the International Standards BS5400 Part 5, CAN3-S16.1-M84 and Eurocode 4, were reviewed in light of experimental results. In the case of mild steel CFST-HSC columns, predictions based on Eurocode 4 were agreed favourably, despite overestimating the experimental failure loads for thinwalled stub columns. It was proposed that the minimum requirement of steel contribution factor δ_s specified in Eurocode 4 be reduced to a value of 0.15 to accommodate for thinwalled HSC sections.

In the case of columns using high strength steel tube, the predictions based on Eurocode 4 were of a very conservative nature and closer correlation of results was obtained using BS5400 and CAN3 predictions. It was discussed that in order to exploit the enhanced strengths of HSS tube CFST columns, the Eurocode confinement co-efficient η_1 may require modification. Tests for HSS tube were limited to a singular tube section and conclusions should be reserved until further experimental investigations are performed.

7.3 RECOMMENDATIONS FOR FUTURE RESEARCH

The tests reported as part of this study concentrated on the ultimate load capacity and load-displacement relationships of CFST-HSC columns. In order to derive constitutive models for determining the properties of such columns, detailed examination of the longitudinal and transverse load-strain relationships for all parametric ranges are required. It is considered that in further research studies, the following aspects should be given special attention:

1. The volumetric expansion of the confined concrete and the effective stresses which develop in the steel tube for CFST columns utilising HSC and HSS.

2. The stress-strain relationship of CFST-HSC columns and the effective stiffness of the composite sections.

3. Proceeding assessment of the behaviour of the CFST-HSC column under isolated conditions, studies should be extended to account for the eccentrically loaded columns and the application of CFST columns as frame elements.

4. The effects of local buckling on column sections with D/t ratio which exceed current specified limits given in design standards.

5. There is a need for unification of International Standards to account for the enhanced characteristics of CFST columns and the development of an Australian Standard for composite columns.

REFERENCE LISTS:

1. ACI COMMITTEE 363 (1984). "State of the Art Report on High Strength Concrete." American Concrete Institute, Detroit, 48 pp.

2. AHMAD, S.H. and SHAH, S.P. (1982) "Stress-Strain Curves of Concrete Confined by Spiral Reinforcement." ACI Journal, Vol. 79, No. 6, pp 484-490.

3. AHMAD, S.H. and SHAH, S.P. (1985) "Behaviour of Hoop Confined Concrete under High Strain Rates." ACI Journal, Vol. 82, No. 5, pp 634-647.

4. AUSTRALIAN STANDARD (1988). "AS3600 Design of Concrete Structures." Standards Association of Australia, Sydney.

5. AUSTRALIAN STANDARD (1990). "AS4100 Design of Steel Structures." Standards Association of Australia, Sydney.

6. AUSTRALIAN STANDARD (1999). "AS1012 Methods of Testing Concrete." Standards Association of Australia, Sydney.

7. AUSTRALIAN STANDARD (1991). "AS1391 Methods for Tensile Testing of Metals." Standards Association of Australia, Sydney.

8. BASU, A.K. and SOMMERVILLE, W. (1969). "Derivation of Formulae for the Design of Rectangular Composite Columns." Proc. Institute of Civil Engineers, Supplementary Volume, paper 7206S, pp 233-280.

9. BRITISH STANDARDS ASSOCIATION (1979). "BS5400 Steel Concrete and Composite Bridges : Part 5 Code of Practice for the Design of Composite Bridges." British Standards Association

10. CAI, S.H. (1987). "Ultimate strength of Concrete Filled Tube Columns." Proc. of an Engineering Foundation Conference (ASCE) - New Hampshire, 7-12 June, pp 702-727.

11. CAMPBELL, I. CLARK, W. and WEBB, J. (1991) "Axial Load Capacity of Composite Steel Tube and Concrete Columns." Proc. of an International Conference on Concrete Engineering and Technology, Kuala Lumpur, Malaysia, 8-10 October.

12. CANADIAN STANDARDS ASSOCIATION (1984). "CAN3-S16.1 M84 Steel Structures for Buildings - Limit State Design." Canadian Standards Association.

13. CARRASQUILLO, R.L. NILSEN, A.H. and SLATE, F.O. (1981). "Properties of High Strength Concrete Subject to Short Term Loads." ACI Journal, Vol. 78, No. 3, May-June, pp 171-178.

14. CARRASQUILLO, R.L. SLATE, F.O. and NILSEN, A.H. (1981). "Microcracking and Behaviour of High Strength Concrete Subject to Short Term Loading." ACI Journal, Vol. 78, No. 3, May-June, pp 179-186.

15. CENTRE FOR ADVANCED STRUCTURAL ENGINEERING - UNIVERSITY OF SYDNEY (1990) "New Commonwealth Offices - Alternative Composite Column Design." November, Draft Report.

16. DESAYI, P. and KRISHNAN, S. (1964). "Equation for the Stress-Strain Curve of Concrete." ACI Journal, Vol. 61, No. 3, March, pp 345-350.

17. ELNASHI, A.J. EL-GHAZOULLI, A.Y. and DOWLING, P.J. (1991). "International Assessment of Design Guidance for Composite Columns." Journal of Constructional Steel Research, Vol. 15, pp 191-213.

18. EUROCODE EDITORIAL GROUP. (1990). "Eurocode No. 4 : Design of Composite Steel and Concrete Structures - Revised Draft October 1990."

19. EUROPEAN CONVENTION FOR CONSTRUCTIONAL STEELWORK (1981). "Composite Structures." published by the Construction Press, pp 149-173.

20. FAFITIS, A. and SHAH, S.P. (1986). "Lateral Reinforcement for High Strength Concrete Columns." High Strength Concrete, SP87, ACI, Detroit, pp 213-232.

21. GARDNER, N.J. and JACOBSON, E.R. (11967). "Structural Behaviour of Concrete Filled Steel Tubes." ACI Journal, Vol. 64, No. 7,k pp 404-413.

22. GRIMAULT, J.P. and JANSS, J. (1977). "Reduction of the Load Bearing Capacity of Concrete Filled Hollow Sections Due to Local Buckling." Stability of Steel Structures, Liege, 13-15 Apr., pp 175-179.

23. GUIAUX, P. and JANSS, J. (1970) "Buckling Behaviour of Columns made with Steel Tubes and Filled with Concrete." CIDECT Issue 70/42/E. November.

24. HWEE, Y.S and RANGAN, B.V. (1990) "Studies on Commercial High Strength Concrete." ACI Materials Journal, Vol. 87, No. 5, Sept-Oct., pp 440-445.

25. KLOPPEL, K. and GODAR, W. (1957). "Collapse Load Tests on Concrete Filled Steel Tubes and Derivation of Design Formula." Der Stahlbau, Vol. 26, No. 1, January, pp 1-10, also February, pp 44-50.

26. KNOWLES, R.B. and PARK, R. (1969). "Strength of Concrete Filled Steel Tubular Columns." Journal of Structural Division (ASCE), Vol. 95, ST12, December, pp 2565-2587.

27. KNOWLES, R.B. and PARK, R. (1970). "Axial Load Design for Concrete Filled Steel Tubes." Journal of Structural Division (ASCE), Vol.96, ST.10, Oct., pp 2125-2153.

28. LUKSHA, L.K. and NESTEROVICH, A.P. (1991). "Strength Testing of Large Diameter Concrete Filled Steel Tubular Members." Proc. of the 3rd International Conference on Steel Concrete Composite Structures, Fukuoka Japan, 26-29 September, pp 67-71.

29. MAIO, R. (1991). "The Failure Criteria for Concrete Cores in Steel Tubes." Proc. of the 3rd International Conference on Steel Concrete Composite Structures, Fukuoka Japan, 26-29 Sept., pp 37-42.

30. MAK, S.L and ATTARD, M.M. (1992). "Evaluation of Specimen End Preparation Methods on the Compressive Strength of High Strength Concrete Cylinders." Australian Civil Engineering Transactions, Vol. CE34, No. 4., December.

31. MAK, S.L. and SANJAYAN, G. (1990). "Mix Proportions of Very High Strength Concretes." I.E. Aust. Structural Engineering Conference, Adelaide, 3-5 October, pp 127-130.

32. MANDER, J.B. PRIESTLEY, M.J.N. and PARK, R. (1988). "Theoretical Stress-Strain Model for Confined Concrete." Journal of Structural Engineering (ASCE), Vol. 14, No. 8, pp 1804-1826.

33. MANDER, J.B. PRIESTLEY, M.J.N. and PARK, R. (1988). "Observed Stress-Strain Behaviour of Confined Concrete." Journal of Structural Engineering (ASCE), Vol. 114, No. 8, pp 1827-1849.

34. MATSUI, C. (1985). "Local Buckling of Concrete Filled Steel Square Tubular Columns." IABSE-ECCS Symposium, Steel in Buildings, No. 48, Luxembourg.

35. NEOGI, P.K. SEN, H.K. AND CHAPMAN, J.C. (1969). "Concrete Filled Tubular Steel Columns under Eccentric Loading." The Structural Engineer, Vol. 47, No. 5, May, pp 187-195.

36. NEVILLE, A.M. (1981). "Properties of Concrete." Published by Pitman International, London.

37. NRMCA of AUSTRALIA and CCA of AUSTRALIA (1992). "High Strength Concrete." publication, June.

38. O'BRIEN, A.D. and RANGAN, B.V. (1993). "Tests on Slender Tubular Steel Columns Filled with High Strength Concrete." to be published.

39. PAN, Y.G. and ZHONG, S.T. (1991). "Discussion on the Definition of Column Strength of Concrete Filled Steel Tubes." Proc. of the 3rd International Conference on Steel Concrete Composite Structures, Fukuoka Japan, 26-29 September, pp 7-12.

40. RANGAN, B.V. and JOYCE, M. (1992). "Strength of Eccentrically Loaded Slender Steel Tubular Columns Filled with High Strength Concrete." ACI Journal, Vol. 89, No. 6, Nov-Dec, pp 676-681.

41. RICHART, F.E. BRANDTZAEG, A. and BROWN, R.L. (1929). "The Failure of Plain and Spirally Reinforced Concrete in Compression." Bulletin 190, University of Illinois Engineering Experimental Station, Illinois.

42. SAKINO, K. and HAYASHI, H. (1991). "Behaviour of Concrete Filled Steel Tubular Stub Columns Under Concentric Loading." Proc. of the 3rd International Conference on Steel Concrete Composite Structures, Fukuoka Japan, 26-29 September, pp 25-30.

43. SALANI, H.J. and SIMS, J.R. (1964). "Behaviour of Mortar Filled Steel Tubes in Compression." ACI Journal, Vol. 61, No. 10, October, pp 1271-1283.

44. SEN, H.K. (1970). "Concrete Filled Tubular Steel Columns." Tubular Structures, No.17, November.

45. SEN, H.K. (1969). " Triaxial Effects in Concrete Filled Tubular Steel Columns." Ph.D. Thesis, University of London.

46. SETUNGE, S. ATTARD, M.M. and DARVALL, P. (1992) "Ultimate Strength Criteria for Very High Strength Concrete Subject to Triaxial Loading." Civil Engineering Report No. 1/1992, Monash University.

47. SETUNGE, S. ATTARD, M.M. and DARVALL, P. (1992). "Stress-Strain Relationship of Very High Strength Concrete." Civil Engineering Report No. 2/1992, Monash University.

48. SMADI, M.M. and SLATE, F.O. (1989). "Microcracking of High and Normal Strength Concrete under Short and Long Term Loadings." ACI Journal, Vol.86, No.2, March - April, pp 117-127.

49. TOMII, M. YOSHIMURA, K. and MORISHITA, Y. (1977). "Experimental Studies on Concrete Filled Steel Tubular Columns under Concentric Loading." Structural Stability Research Council - International Colloquium on Stability of Structures under Static and Dynamic Loads, Washington, May 17-19, pp 718-741.

50. TOMII, M. (1984). "Bond Check for Concrete Filled Steel Tubular Columns." Composite and Mixed Construction, Proc. of the US/Japan joint Seminar, 818-20 July, pp 195-205.

51. TOMII, M. (1991). "Ductile and Strong Columns Composed of Steel Tube Infilled Concrete and Longitudinal Steel Bars." Proc. of the 3rd International Conference on Steel Concrete Composite Structures, Fukuoka Japan, 26-29 September, Special Volume pp 39-66.

52. TSUJI, B. NAKASHIMA, M. and MORITA, S. (1991). "Axial Compressive Behaviour of Concrete Filled Circular Steel Tubes." Proc. of the 3rd International Conference on Steel Concrete Composite Structures, Fukuoka Japan, 26-29 September, pp 19-24.

53. URPANI, D. MAK, S.L. and ATTARD, M.M. (1991). "Curing of Very High Strength Concrete Cylinders." Civil Engineering Report No. 1/1991, Monash University.

54. VIRDI, K.S. and DOWLING, P.J. (1976). "A Unified Design Method for Composite Columns." IABSE Publication, Vol. 36-II, pp 165-183.

55. VIRDI, K.S. and DOWLING, P.J. (1975). "Bond Strength in Concrete Filled Steel Columns." CESLIC Report CCII, Imperial College, London, December.

56. WATSON, K.B. and O'BRIEN, L.J. (1990). "Tubular Composite Columns and their Development in Australia." I.E. Aust. - Structural Engineering Conference - Adelaide, 3-5 October, pp 186-190.

57. WEBB, J. and PEYTON, J.J. (1990). "Composite Concrete Filled Steel tube Columns." I.E.Aust. Structural Engineering Conference, Adelaide, 3-5 October, pp 181-185.

58. YONG, Y.K. NOUR, N.G. and NAWY, E.G. (1988) "Behaviour of Laterally Confined High Strength Concrete under Axial Loads." Journal of Structural Engineering (ASCE). Vol. 114, No. 2, February, pp 332-351.

59. ZHANG, X. JIANG, W. and WANG, D. (1991). "The Carrying Capacity of Concrete Filled Steel Tube Short Columns." Proc. of the 3rd International Conference on Steel Concrete Composite Structures, Fukuoka Japan, 26-29 September, pp 85-88.

60. ZHAO, X.L. and HANCOCK, G.J. (1991). "Tests to Determine Plate Slenderness Limits for Cold Formed Rectangular Hollow Sections of Grade C450." A.I.S.C. Journal (Australian), Vol. 25, No. 4. November.

61. ZHONG, S.T. and MAIO, R.Y. (1987). "Stress-Strain Relationship and Strength of Concrete Filled Tubes." Proc. of an Engineering Foundation Conference (ASCE) - New Hampshire, 7-12 June, pp 773-784.

62. ZHONG, S.T. YAN, S.Z. and PAN, Y.G. (1991). "Introduction to Design Regulation of CFST Structures, NDGJ 99-91 of China." Proc. of the 3rd International Conference on Steel Concrete Composite Structures, Fukuoka Japan, 26-29 September, pp 1-6.

APPENDIX A: MATERIAL PROPERTIES TEST RESULTS

TABLE A.1: Results of Steel Tensile Coupon Tests

Test No.	b (mm)	t (mm)	D (mm)	A_{coup} (mm^2)	f_y (MPa)	f_u (MPa)	e_f (%)
Mild Strength Steel (MS):							
1	15.25	1.602	76.1	24.60	237.79	300.80	20.6
2	14.34	1.602	76.1	23.11	230.16	303.70	19.6
3	16.40	1.596	76.1	26.39	248.24	287.27	17.4
4	15.48	1.594	76.1	24.85	234.18	293.73	18.0
5	14.64	1.600	76.1	23.57	240.09	288.02	24.6
6	15.80	1.592	76.1	25.34	235.97	299.11	21.2
7	15.70	1.602	76.1	25.34	237.59	300.74	15.0
8	15.66	1.594	76.1	25.15	241.79	297.46	23.8
9	15.91	1.590	76.1	25.49	245.20	299.73	23.2
				Mean	**239.0**	**297.0**	**20.4**
				SD.	**5.55**	**5.82**	**3.2**
High Strength Steel (HSS):							
1	17.12	2.000	76.10	34.54	--	496.53	3.7
2	16.45	1.998	76.10	33.14	--	494.87	4.9
3	17.08	2.000	76.10	34.46	--	494.78	4.1
4	16.51	2.002	76.10	33.33	--	493.55	2.8
5	15.61	2.000	76.10	31.46	--	497.46	3.4
6	15.20	2.000	76.10	30.61	--	495.02	4.0
				Mean	--	**495.44**	**3.8**
				SD.	--	**1.55**	**0.7**

TABLE A.2: Average Compressive Strength of Concrete Cylinder Tests and Statistical Assessment

CASTING	No. Cyl.	MIX	f'_{cm} MPa	Standard Deviation (MPa)	Standard Deviation (%)	Max. (MPa)	Min. (MPa)	Range (MPa)	Density (kg/m³)
CA3	4	A	65.4	2.0	3.0	67.3	63.6	3.7	2443
CA4	6	B	92.2	4.4	4.8	96.2	87.6	8.6	2445
CA5	4	A	67.4	1.05	1.56	68.7	66.5	2.2	2456
CA6	6	B	93.45	0.66	0.71	94.1	92.7	1.4	2447
CA7	4	A	46.3	0.55	1.19	46.7	45.5	1.2	2425
CA8	6	B	82.4	0.82	1.00	83.3	81.3	2.0	2441
CA9	6	B	94.4	1.27	1.35	95.5	92.6	2.9	2426
CA10	6	A	57.7	1.23	2.13	58.6	55.9	2.7	2417
$CA11_{(28)}$	4	B	100.2	3.05	3.05	104.0	96.7	7.3	2440
$CA11_{(test)}$	4	B	100.6	4.56	4.53	106.5	96.2	10.3	2448
CA12	6	A	58.0	1.31	2.26	59.6	56.6	3.0	2403
CA13	6	B	87.9	3.91	4.45	92.9	83.5	9.4	2417
				Max.	4.8 %			Mean	2434

TABLE A.3: Results of Concrete Core Tests - Type A

Specimen Notation	f'_c (MPa)	D (mm)	L (mm)	N_{exp} (kN)	σ_{exp} (MPa)	σ_{exp} / f'_c
CC7-1	46.3	72.9	144	196.5	47.08	1.017
CC7-2	46.3	72.9	144	208.4	49.93	1.078
CC7-3	46.3	72.9	144	200.2	47.96	1.036
				Mean.	**48.32**	**1.043**
CC8-1	82.4	72.9	144	326.0	78.10	0.948
CC8-2	82.4	72.9	144	332.4	79.64	0.967
CC8-3	82.4	72.9	144	318.9	76.40	0.927
				Mean.	**78.05**	**0.947**
CC9-1	94.4	72.9	144	382.6	91.66	0.971
CC9-2	94.4	72.9	144	378.6	90.71	0.961
CC9-3	94.4	72.9	144	389.2	93.25	0.988
				Mean.	**91.87**	**0.953**
CC10-1	57.7	72.9	144	257.0	61.57	1.067
CC10-2	57.7	72.9	144	250.1	59.92	1.038
CC10-3	57.7	72.9	144	249.3	59.73	1.035
				Mean.	**60.41**	**1.047**

TABLE A.4: Results of Concrete Core Tests - Type B

Specimen Notation	f'_c (MPa)	D (mm)	L (mm)	N_{exp} (kN)	σ_{exp} (MPa)	σ_{exp} / f'_c
C7-1	46.3	72.9	230	192.8	46.19	0.998
C7-2	46.3	72.9	230	195.2	46.77	1.010
C7-3	46.3	72.9	230	195.7	46.89	1.013
			Mean.	**194.6**	**46.6**	**1.007**
C8-1	82.4	72.9	230	327.7	78.51	0.953
C8-2	82.4	72.9	230	315.9	75.68	0.918
C8-3	82.4	72.9	230	319.8	76.62	0.930
			Mean.	**321.1**	**76.9**	**0.934**
C9-1	94.4	72.9	460	355.1	85.08	0.901
C9-2	94.4	72.9	460	350.2	83.90	0.889
C9-3	94.4	72.9	460	353.2	84.62	0.896
			Mean.	**352.8**	**84.5**	**0.895**
C10-1	57.7	72.9	460	215.8	51.70	0.896
C10-2	57.7	72.9	460	225.6	54.05	0.937
C10-3	57.7	72.9	460	216.8	51.94	0.900
			Mean.	**219.4**	**52.6**	**0.910**

APPENDIX B: LOAD - DISPLACEMENT CURVES

B.1 CFST COLUMNS

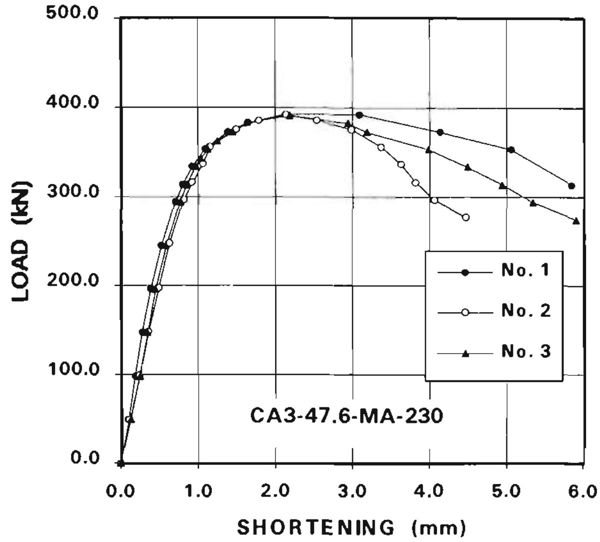

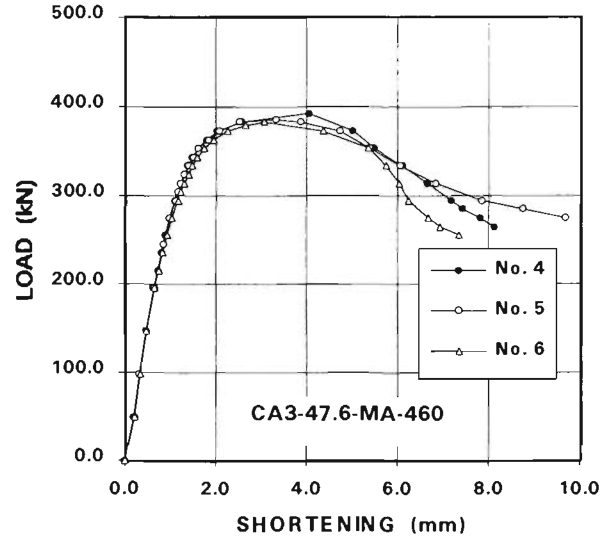

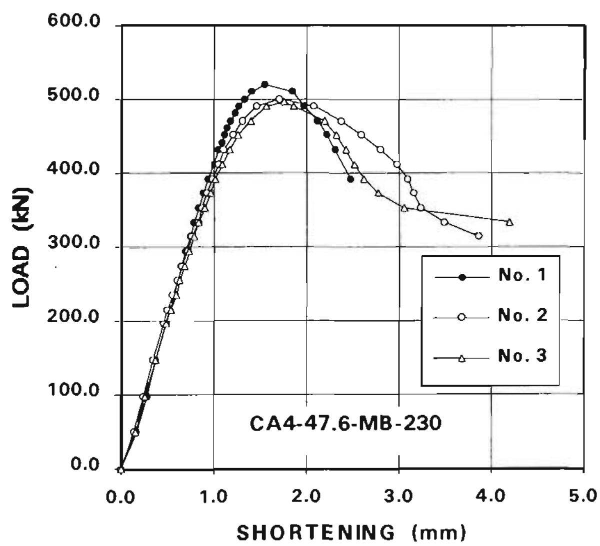

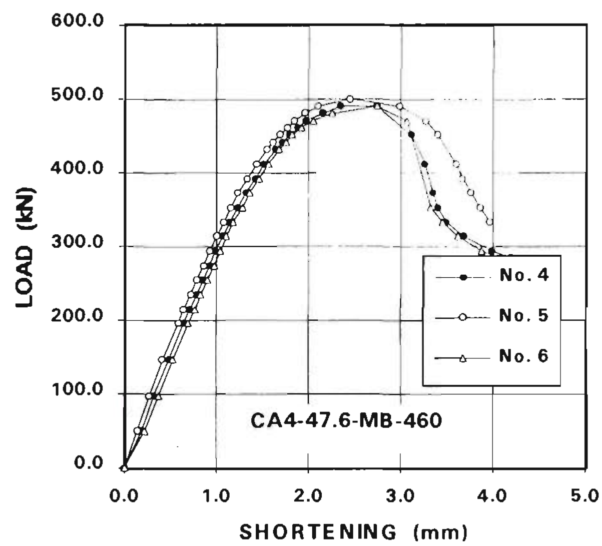

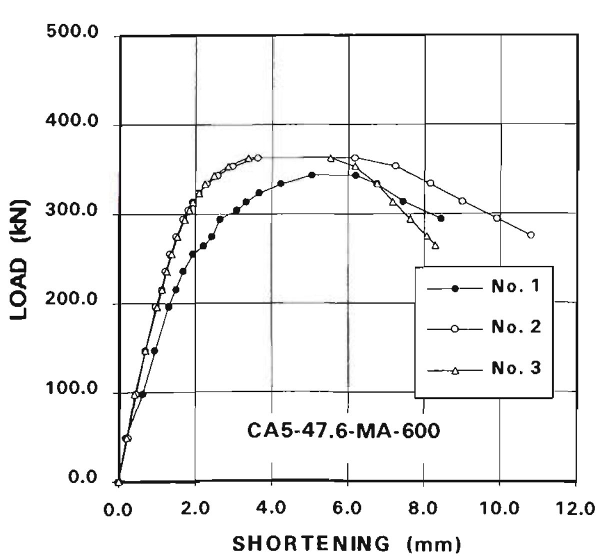

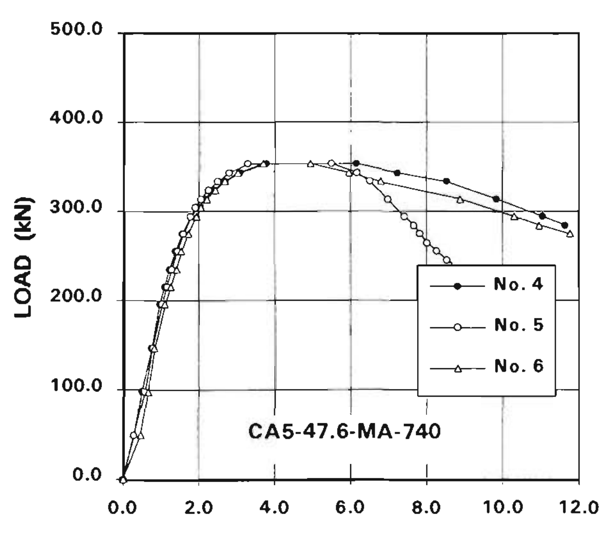

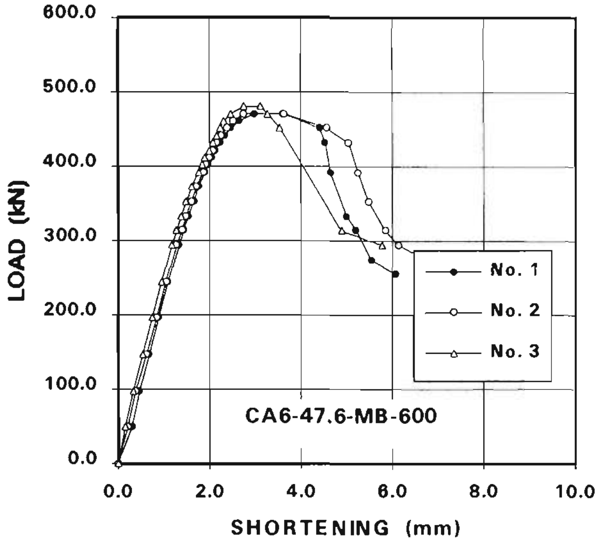
600.0
500.0
400.0
300.0
200.0
100.0
0.0
LOAD (kN)
0.0
2.0
4.0
6.0
8.0
10.0
SHORTENING (mm)
No. 1
No. 2
No. 3
CA6-47.6-MB-600

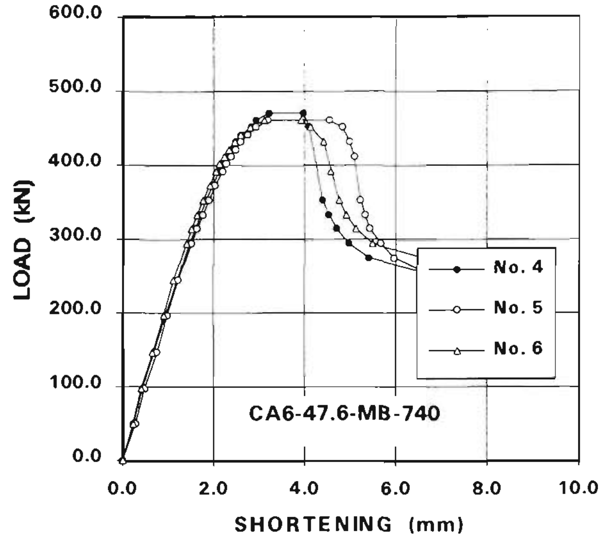
600.0
500.0
400.0
300.0
200.0
100.0
0.0
LOAD (kN)
0.0
2.0
4.0
6.0
8.0
10.0
SHORTENING (mm)
No. 4
No. 5
No. 6
CA6-47.6-MB-740

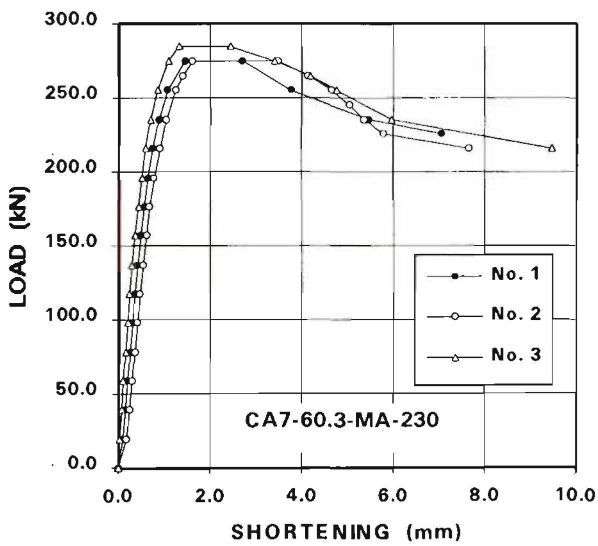
300.0
250.0
200.0
150.0
100.0
50.0
0.0
LOAD (kN)
0.0
2.0
4.0
6.0
8.0
10.0
SHORTENING (mm)
No. 1
No. 2
No. 3
CA7-60.3-MA-230

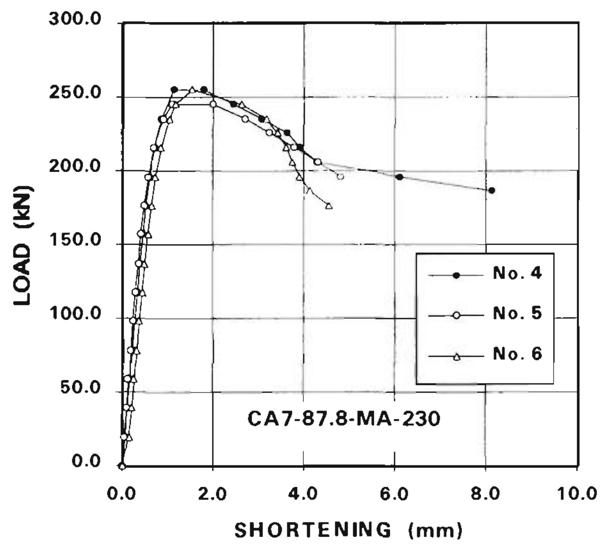
300.0
250.0
200.0
150.0
100.0
50.0
0.0
LOAD (kN)
0.0
2.0
4.0
6.0
8.0
10.0
SHORTENING (mm)
No. 4
No. 5
No. 6
CA7-87.8-MA-230

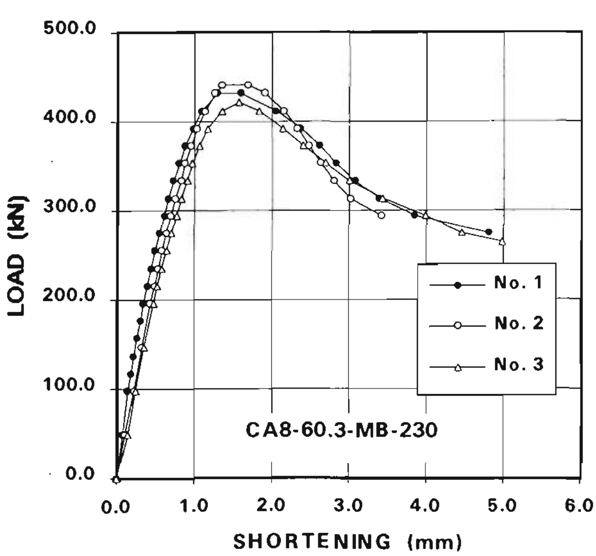
500.0
400.0
300.0
200.0
100.0
0.0
LOAD (kN)
0.0
1.0
2.0
3.0
4.0
5.0
6.0
SHORTENING (mm)
No. 1
No. 2
No. 3
CA8-60.3-MB-230

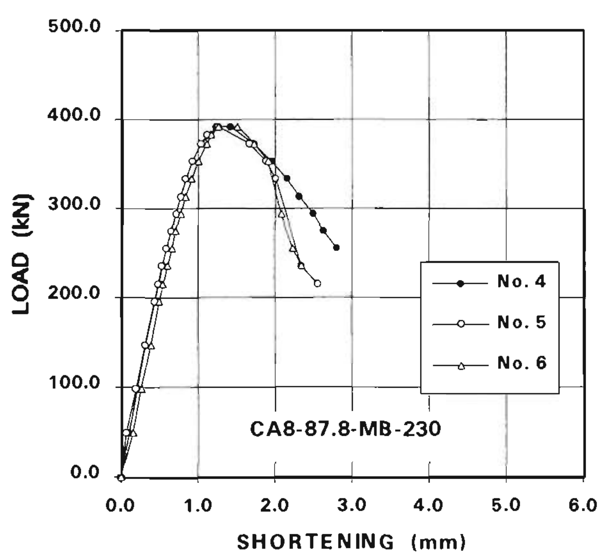
500.0
400.0
300.0
200.0
100.0
0.0
LOAD (kN)
0.0
1.0
2.0
3.0
4.0
5.0
6.0
SHORTENING (mm)
No. 4
No. 5
No. 6
CA8-87.8-MB-230

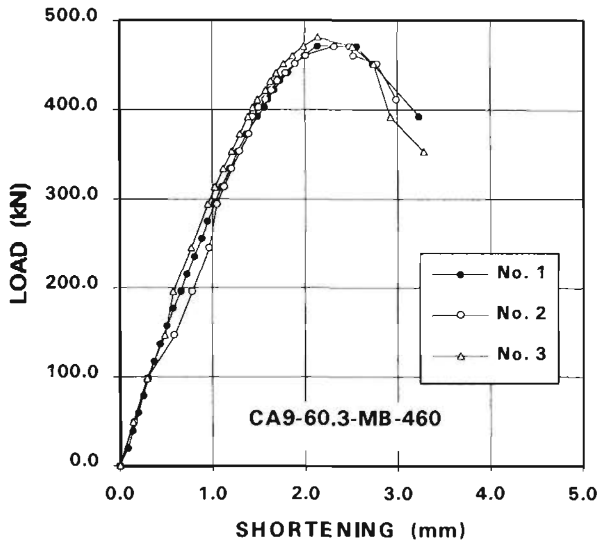
500.0
400.0
300.0
200.0
100.0
0.0
LOAD (kN)
0.0
1.0
2.0
3.0
4.0
5.0
SHORTENING (mm)
No. 1
No. 2
No. 3
CA9-60.3-MB-460

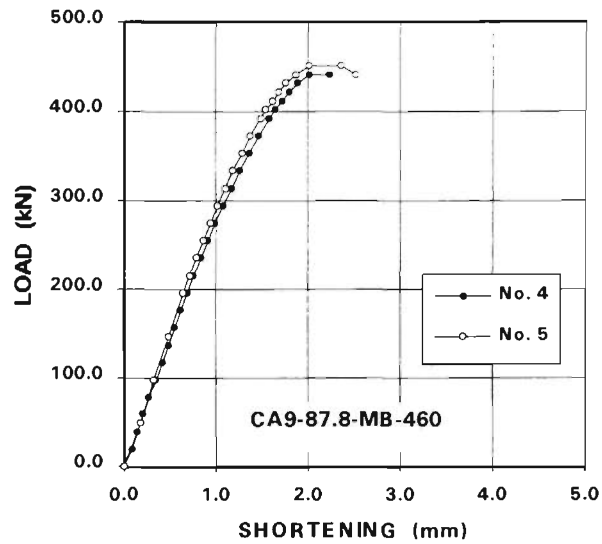
500.0
400.0
300.0
200.0
100.0
0.0
LOAD (kN)
0.0
1.0
2.0
3.0
4.0
5.0
SHORTENING (mm)
No. 4
No. 5
CA9-87.8-MB-460

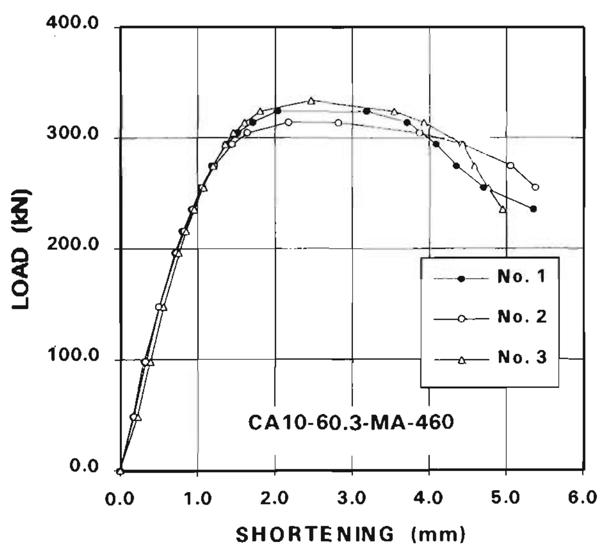
400.0
300.0
200.0
100.0
0.0
LOAD (kN)
0.0
1.0
2.0
3.0
4.0
5.0
6.0
SHORTENING (mm)
No. 1
No. 2
No. 3
CA10-60.3-MA-460

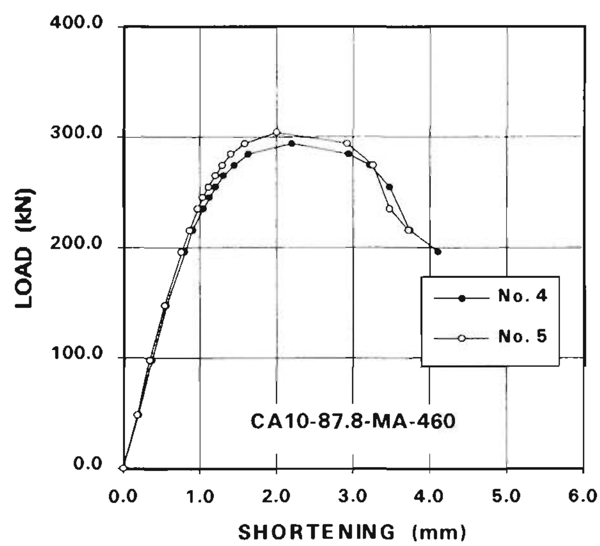
400.0
300.0
200.0
100.0
0.0
LOAD (kN)
0.0
1.0
2.0
3.0
4.0
5.0
6.0
SHORTENING (mm)
No. 4
No. 5
CA10-87.8-MA-460

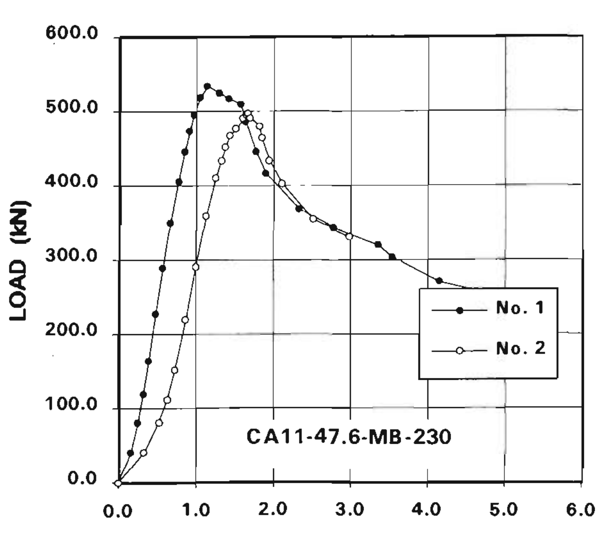
600.0
500.0
400.0
300.0
200.0
100.0
0.0
LOAD (kN)
0.0
1.0
2.0
3.0
4.0
5.0
6.0
SHORTENING (mm)
No. 1
No. 2
CA11-47.6-MB-230

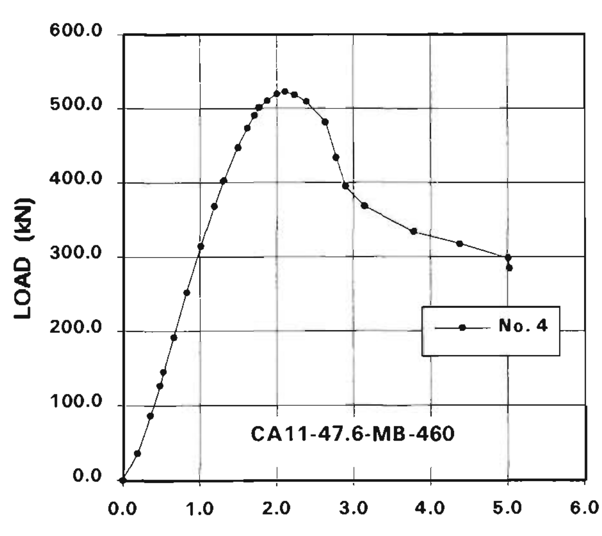
600.0
500.0
400.0
300.0
200.0
100.0
0.0
LOAD (kN)
0.0
1.0
2.0
3.0
4.0
5.0
6.0
SHORTENING (mm)
No. 4
CA11-47.6-MB-460

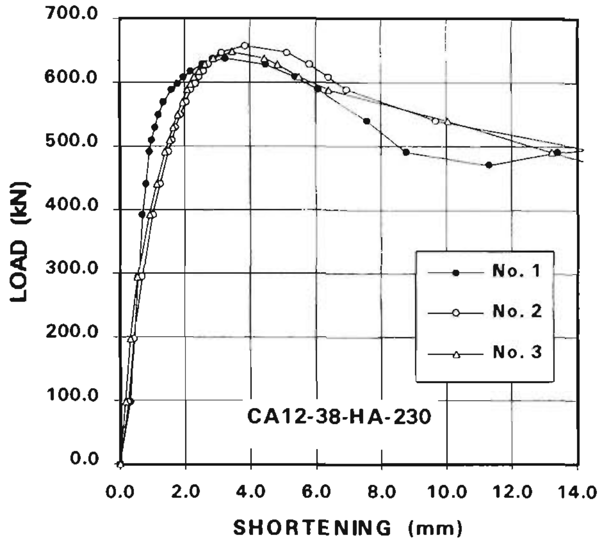

LOAD (kN)
700.0
600.0
500.0
400.0
300.0
200.0
100.0
0.0
0.0
2.0
4.0
6.0
8.0
10.0
12.0
14.0
SHORTENING (mm)
No. 1
No. 2
No. 3
CA12-38-HA-230

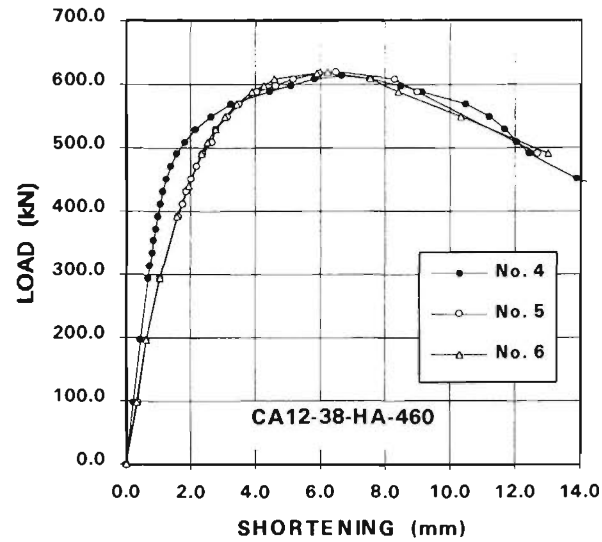

LOAD (kN)
700.0
600.0
500.0
400.0
300.0
200.0
100.0
0.0
0.0
2.0
4.0
6.0
8.0
10.0
12.0
14.0
SHORTENING (mm)
No. 4
No. 5
No. 6
CA12-38-HA-460

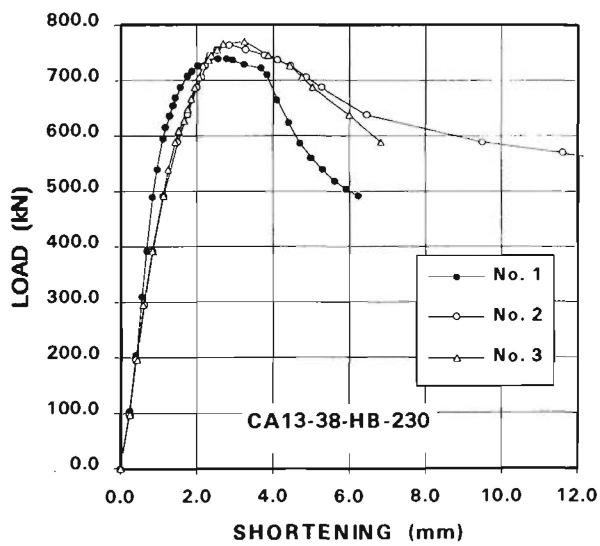

LOAD (kN)
800.0
700.0
600.0
500.0
400.0
300.0
200.0
100.0
0.0
0.0
2.0
4.0
6.0
8.0
10.0
12.0
SHORTENING (mm)
No. 1
No. 2
No. 3
CA13-38-HB-230

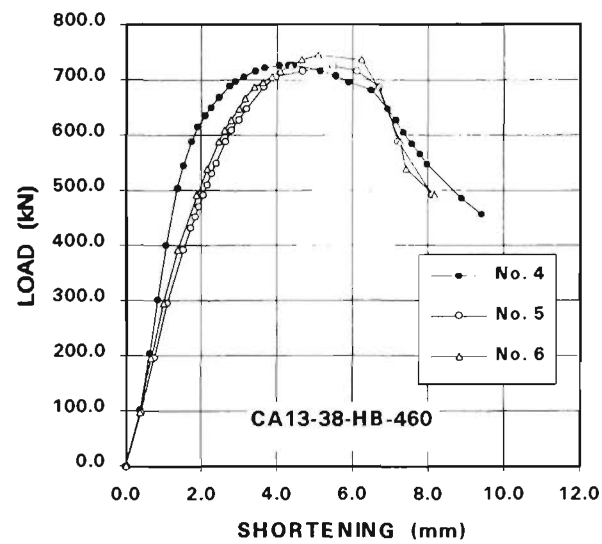

LOAD (kN)
800.0
700.0
600.0
500.0
400.0
300.0
200.0
100.0
0.0
0.0
2.0
4.0
6.0
8.0
10.0
12.0
SHORTENING (mm)
No. 4
No. 5
No. 6
CA13-38-HB-460

B.2 STEEL COLUMNS

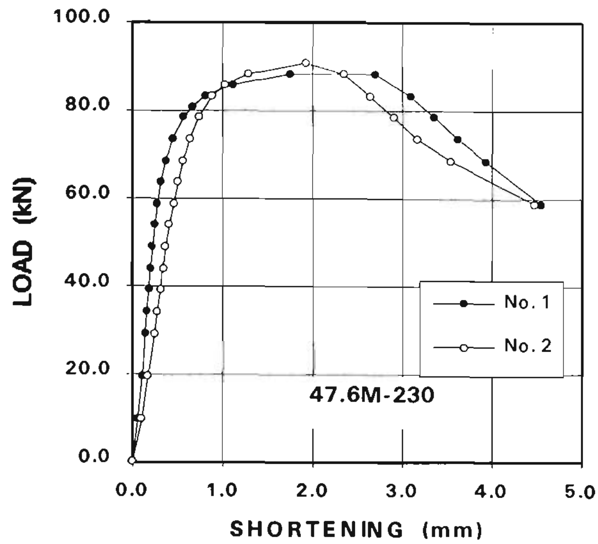

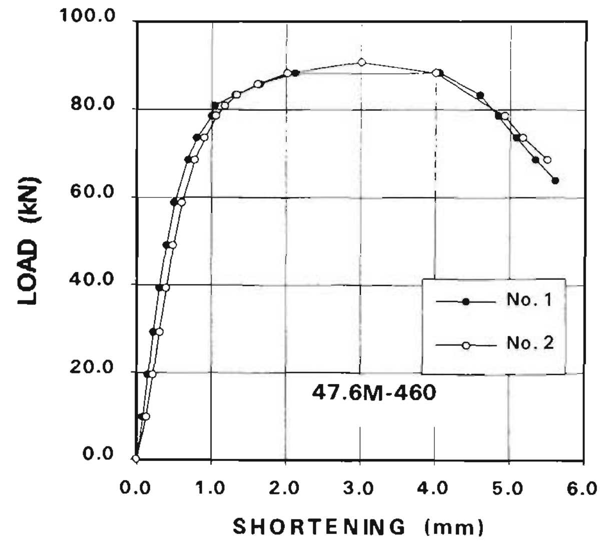

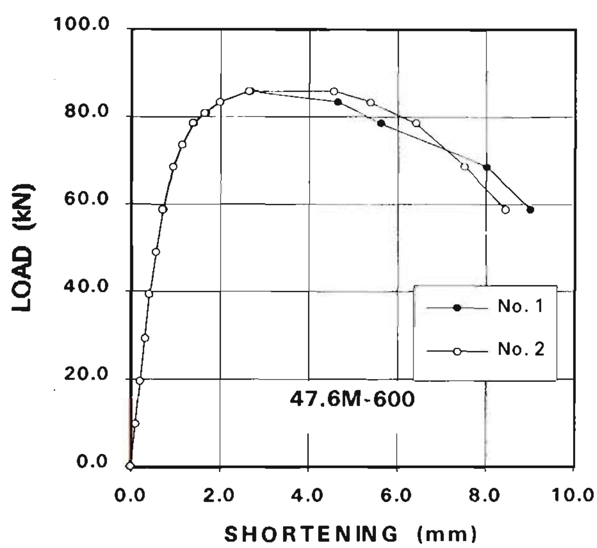

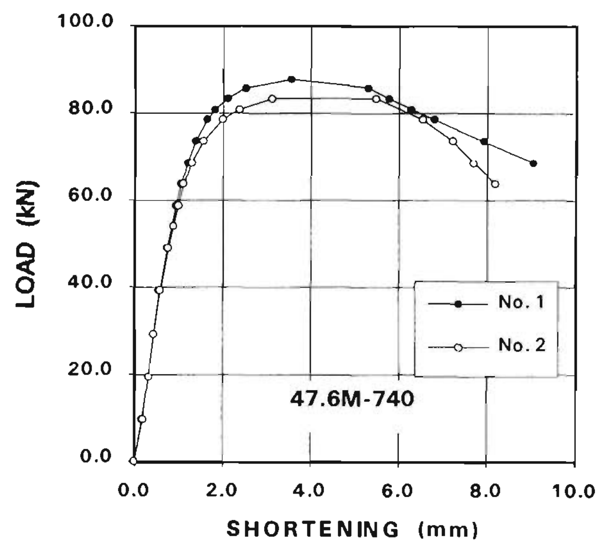

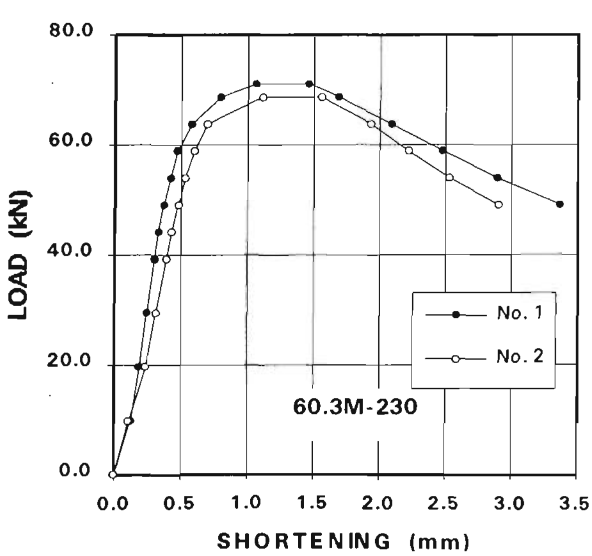

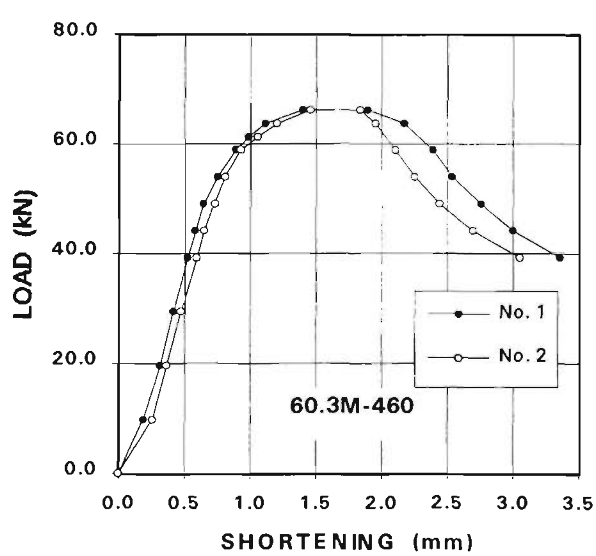

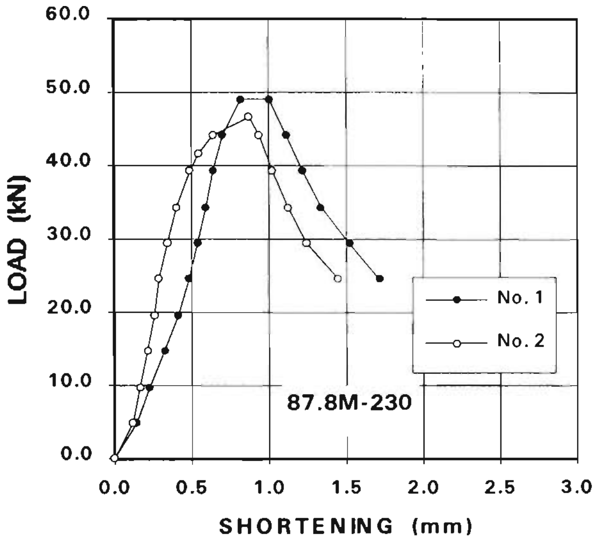

LOAD (kN)
SHORTENING (mm)
No. 1
No. 2
87.8M-230

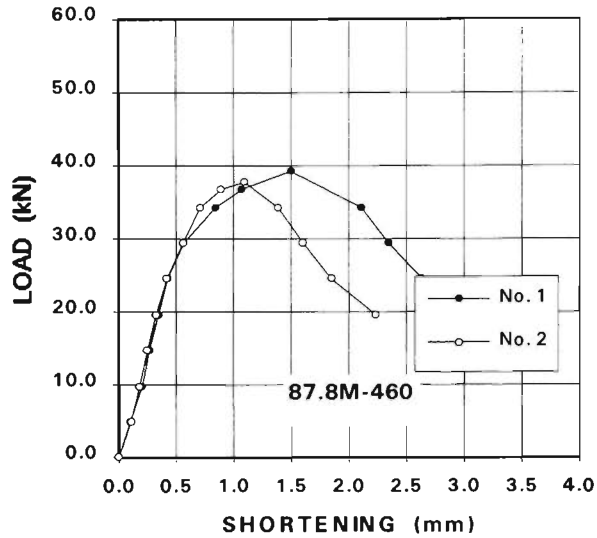

LOAD (kN)
SHORTENING (mm)
No. 1
No. 2
87.8M-460

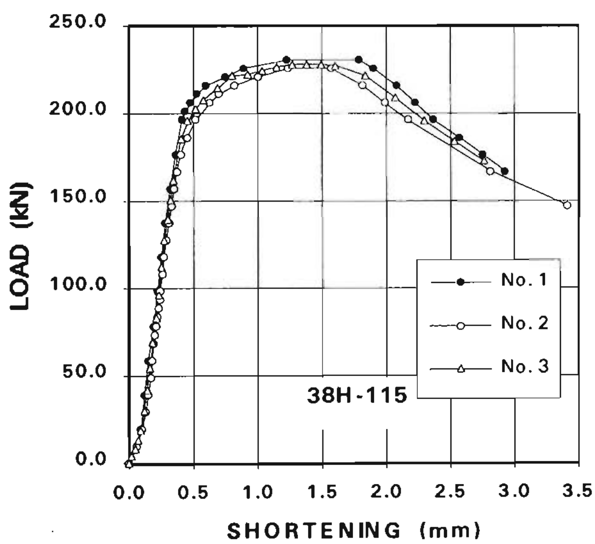

LOAD (kN)
SHORTENING (mm)
No. 1
No. 2
No. 3
38H-115

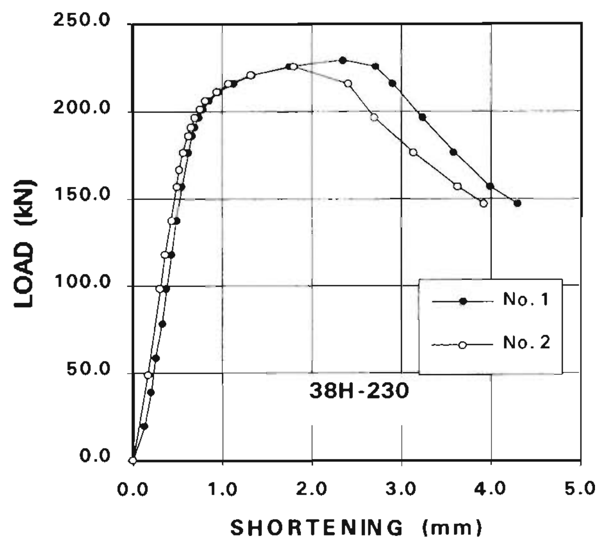

LOAD (kN)
SHORTENING (mm)
No. 1
No. 2
38H-230

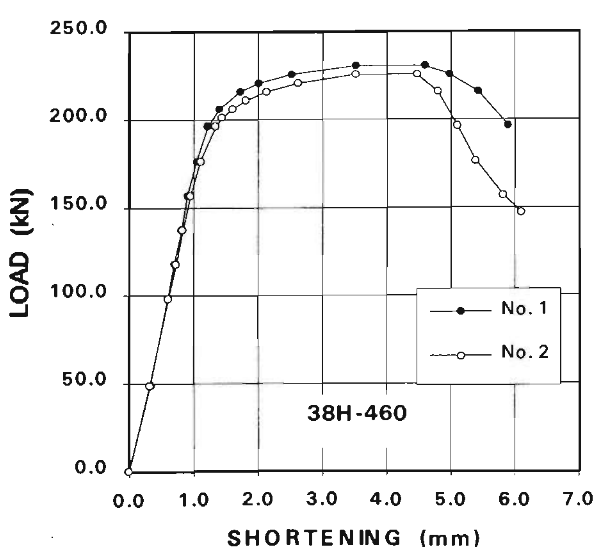

LOAD (kN)
SHORTENING (mm)
No. 1
No. 2
38H-460

APPENDIX C: ADDITIONAL CFST TEST RESULTS - VUT 1990.

The following table summarises the results of CFST column test previously performed at V.U.T, refer to Campbell et al. (1990). These results have been graphically represented in selected figures of chapter 4.

TABLE C.1: CFST Test Results 1990

Test No.	D (mm)	t (mm)	L (mm)	f'_c (MPa)	f_y (MPa)	N_{exp} (tonne)	N_{exp} (kN)
2	70.9	0.6	280	64.3	490	35.0	343.4
3	70.9	0.6	280	64.3	490	34.3	336.5
4	70.9	0.6	280	64.3	490	34.3	336.5
5	70.9	0.6	280	64.3	490	33.3	326.7
6	70.9	0.6	280	64.3	490	34.7	340.4
7	71.3	0.8	280	64.3	490	39.5	387.5
8	71.3	0.8	280	64.3	490	39.8	390.4
9	71.3	0.8	280	64.3	490	39.0	382.6
10	71.3	0.8	280	64.3	490	39.5	387.5
11	71.3	0.8	280	64.3	490	39.5	387.5
12	71.3	0.8	280	64.3	490	40.2	394.4
13	72.1	1.2	280	64.3	490	47.2	463.0
14	72.1	1.2	280	64.3	490	46.2	453.2
15	72.1	1.2	280	64.3	490	47.8	468.9
16	72.1	1.2	280	64.3	490	48.0	470.9
17	72.1	1.2	280	64.3	490	48.8	478.7
18	72.1	1.2	280	64.3	490	48.2	472.8

APPENDIX D: DESIGN CODE PROVISIONS

The following summarises provisions for CFST column design in accordance to the three International design standards discussed in Chapter 5. Only the provisions related to the ultimate strength analysis of an axially loaded circular CFST column, derivation of material properties and the limitations of each method are included.

D.1: <u>BS5400 PART 5</u>

British Standard: Code of Practice for the Design of Composite Bridges 1979.

In BS5400 the provisions for the design of composite columns are included in Chapter 11. The enhanced section capacity for circular CFST columns are defined in Clause 11.3.7.

<u>Limitations and Minimum Requirements:</u>

Concrete Strength f_{cu} :	$f_{cu} \geq 25$ MPa
Steel Tube Strength f_y :	Not Specified
Tube Thickness t :	$t \geq D(f_y / 8E_s)^{0.5}$
Slenderness L/D :	$L/D \leq 55$
Concrete Contribution Factor α_c :	$0.1 \leq \alpha_c \leq 0.8$
where:	$\alpha_c = 0.45A_cf_{cu} / N_o$

A minimum eccentricty of applied load equal to 0.3 by the tube diameter for CHS shall apply. (Min. Eccentricty = 0.3D)

<u>Section Capacity:</u>

The nominal section capacity of a composite section neglecting the influences of confining actions is defined by:

$$N_o = A_s f_y / \gamma_s + 0.67 A_c f_{cu} / \gamma_c + A_r f_{yr} / \gamma_r \qquad \textbf{(D.1)}$$

Where $\gamma_s\ \gamma_c\ \gamma_r$ are the material partial safety factors for the steel section (1.1), concrete (1.5) and reinforcement (1.15).

<u>Relative Slenderness λ:</u>

The relative slenderness λ of a composite cross section is defined as the ratio of column length to critical buckling length where:

$$\lambda = \frac{L_e}{L_E} \qquad \textbf{(D.2)}$$

L_e is the effective length of the column

L_E is the critical buckling length when Euler load $N_E = N_o$

$$L_E = \pi\sqrt{(E_s I_s + E_c I_c + E_r I_r)/N_o} \tag{D.3}$$

The elastic modulus of the concrete E_c is defined by:

$$E_c = 450 f_{cu} \tag{D.4}$$

Column Capacity CFST Short Columns:

For short circular CFST columns with effective length to diameter ratio (L_e/D) less than 12, the enhanced section and column capacities may be determined according to the following:

Column design strength N_d is a function of cross section capacity N_{pl} given by Eqn. D.6 and a slenderness reduction factor K_l obtained from an appropriate column buckling curve with respect to λ.

$$N_d = K_l N_{pl} \tag{D.5}$$

$$N_{pl} = C_2 A_s f'_y/\gamma_s + 0.67 A_c \left(f_{cu} + C_1 \frac{t}{D} f_y\right)\Big/\gamma_c + A_r f_{yr}/\gamma_r \tag{D.6}$$

The confinement co-efficients C_1 and C_2 are obtained by interpolation of the values given in the following table with respect to L_e/D ratio.

l_e/D_e	0	5	10	15	20	25
C1	9.47	6.40	3.81	1.80	0.48	0.00
C2	0.75	0.80	0.85	0.90	0.95	1.00

The column buckling curve K_l is given by Eqn. D.7 as a function of 'λ' and 'n' where n is a constant relating the cross section shape.

$$K_l = 1/2\left[1 + \frac{(1+n)}{\lambda^2}\right] - \left[\left(\frac{1}{4}\left(1 + \frac{(1+n)}{\lambda^2}\right)^2 - \frac{1}{\lambda^2}\right)^{0.5}\right] \tag{D.7}$$

where $n = \varphi \lambda_E (\lambda - 0.2) \geq 0$

$\lambda_E = \pi\sqrt{1.1 E_s / f_y}$

$\varphi = 0.002$ for circular hollow sections.

D.2: CAN3-S16.1-M84
Canadian Standard for the Design of Steel Structures for Buildings.

In the Canadian Standard, design of CFST columns is included in Clause 17.8 of the code. The design of the individual steel tube and concrete core components are determined independently with steel capacities calculated based on provisions of Clause 13.3.

Limitations:

Concrete Strength f_{cu} :	Not Specified
Steel Tube Strength f_y :	Not Specified
Diameter to Wall Thickness Ratio D/t :	$D/t \leq 28000 / f_y$
Slenderness L/D :	Confinement effective up to $L/D \leq 25$

Resistance of a CFST member:

The capacity of a CFST member C_{rc} is defined by Eqn. D.8 where separate factors account for the enhanced capacity of the concrete component γ' and the reduction of the steel tube capacity γ. Slenderness reduction effects are incorporated for each element individually.

$$C_{rc} = \gamma C_r + \gamma' C_r' \qquad \textbf{(D.8)}$$

where C_r Compressive Resistance
γ Confinement Co-efficients
(') Denotes Concrete Component

Concrete Component C_r':

The compressive resistance of the core element is defined by:

$$C_r' = \phi_c 0.85 f'_c A_c \lambda_c^{-2}\left[\left(1 + 0.25\lambda_c^{-4}\right)^{0.5} - 0.5\lambda_c^{-2}\right] \qquad \textbf{(D.9)}$$

where ϕ_c is the capacity reduction factor taken as 0.85.
λ_c is the core slenderness factor defined by Eqn. D.10

$$\lambda_c = \frac{L_e}{r_c}\sqrt{\frac{f'_c}{\pi^2 E_c}} \qquad \textbf{(D.10)}$$

where r_c is the radius of gyration of the concrete = $0.25\ d_c$.

The elastic modulus of concrete E_c is determined considering the long term effects of loading by:

$$E_c = (1+S/T).2500.(f'_c)^{0.5} \quad \textbf{(D.11)}$$

S: Short Term Load T: Total Load
(For short term load this formula may be reduced to $E_c = 5000.(f'_c)^{0.5}$)

Steel Component Cr:

The resistance of the steel tube component is determined as a function of the steel tube capacity determined by $\phi_s A_s f_y$ and a slenderness reduction factor. Two design curves are proposed first for Cold Formed or Non Stress Relieved (Eqn. D.13), the second for Hot formed or Stress Relieved Sections (Eqn. D.14). Each curve is a function of steel tube slenderness given by Eqn. D.12.

$$\lambda_s = \frac{L_e}{r_s}\sqrt{\frac{f_y}{\pi^2 E_s}} \quad \textbf{(D.12)}$$

where r_s is the radius of gyration of the steel tube

$$r_s = \frac{1}{4}\sqrt{D^2 + d_c^2} \text{ for CHS}$$

- Steel design curves for Cold Formed / Non Stress Relieved

$$\begin{cases} \phi_s A_s f_y & 0 \le \lambda_s \le 0.15 \\ \phi_s A_s f_y (1.035 - 0.202\lambda_s - 0.222\lambda_s^2) & 0.15 \le \lambda_s \le 1.0 \\ \phi_s A_s f_y (-0.111 + 0.636\lambda_s^{-1} + 0.087\lambda_s^{-2}) & 1.0 \le \lambda_s \le 2.0 \\ \phi_s A_s f_y (0.009 + 0.877\lambda_s^{-2}) & 2.0 \le \lambda_s \le 3.6 \\ \phi_s A_s f_y \lambda_s^{-2} & \lambda_s \ge 3.6 \end{cases} \quad \textbf{(D.13)}$$

- Steel design curves for Hot Formed / Stress Relieved

$$\begin{cases} \phi_s A_s f_y & 0 \le \lambda_s \le 0.15 \\ \phi_s A_s f_y (1.035 - 0.202\lambda_s - 0.222\lambda_s^{2}) & 0.15 \le \lambda_s \le 1.0 \\ \phi_s A_s f_y (-0.111 + 0.636\lambda_s^{-1} + 0.087\lambda_s^{-2}) & 1.0 \le \lambda_s \le 2.0 \\ \phi_s A_s f_y (0.009 + 0.877\lambda_s^{-2}) & 2.0 \le \lambda_s \le 3.6 \\ \phi_s A_s f_y \lambda_s^{-2} & \lambda_s \ge 3.6 \end{cases} \tag{D.14}$$

Confinement Co-efficients γ and γ':

For columns having L/D ratio less than 25 the confinement co-efficients γ and γ' are defined by Eqn's D.15 to D.17. When column slenderness exceeds 25 the values may be taken as unity.

$$\gamma = 1 \Big/ \sqrt{1 + \rho + \rho^2} \tag{D.15}$$

$$\text{and} \quad \gamma' = 1 + \left(\frac{25\rho^2\gamma}{D/t}\right)\left(\frac{f_y}{0.85f'_c}\right) \tag{D.16}$$

$$\rho = 0.02(25 - L/D) \tag{D.17}$$

D.3: EUROCODE 4

European Standard for the Design of Composite Steel and Concrete Structures (1990)

In Eurocode 4 the provisions for the design of composite columns are included in Section 4.8.

Limitations:

Concrete Strength f_{cu} :	$20 \le f'_c \le 55$ MPa
Steel Tube Strength f_y :	$f_y \le 450$ MPa
Tube Thickness t :	$D/t \le 90\,\xi^2$
where:	$\xi = \sqrt{235/f_y}$
Relative Slenderness $\bar{\lambda}$:	$\bar{\lambda} \le 2.0$
	$\bar{\lambda} \le 0.5$ for confinement considerations

Steel Contribution Ratio δ_s : $0.2 \le \delta_s \le 0.9$

where: $\delta_s = A_s f_y / N_o$

Section Capacity:

The nominal section capacity of a composite section neglecting the influences of confining actions is defined by:

$$N_o = A_s f_y / \gamma_s + \alpha A_c f'_c / \gamma_c + A_r f_{yr} / \gamma_r \qquad \textbf{(D.18)}$$

where $\gamma_s \, \gamma_c \, \gamma_r$ are the material partial safety factors for the steel section (1.1), concrete (1.5) and reinforcement (1.15).

α is the design factor for concrete strength which Eurocode permits the removal of for filled sections due to the improved curing conditions of the concrete hermetically sealed within the tube profile.

For coluumns having relative slenderness $\bar{\lambda} \le 0.5$ the enhanced cross section capacityis given by:

$$N_{pl} = A_s f_y \eta_2 / \gamma_s + A_c \left(f'_c + \eta_1 \frac{t}{D} \frac{f_y}{f'_c}\right) \Big/ \gamma_c + A_r f_{yr} / \gamma_r \qquad \textbf{(D.19)}$$

where $\eta_1 \, \eta_2$ are confinement co-efficients determined as functions of $\bar{\lambda}$ by Eqn's. D.20 and D.21.

$\gamma_s \, \gamma_c \, \gamma_r$ are the material partial safety factors for the steel section (1.1), concrete (1.5) and reinforcement (1.15).

$$\eta_1 = 4.9 - 18.5\bar{\lambda} + 17\bar{\lambda}^2 \qquad \eta_1 \ge 0.0 \qquad \textbf{(D.20)}$$

$$\eta_2 = 0.25(3 + 2\bar{\lambda}) \qquad \eta_2 \le 1.0 \qquad \textbf{(D.21)}$$

Relative Slenderness $\bar{\lambda}$ and Effective Stiffness:

The relative slenderness $\bar{\lambda}$ of a composite cross section is a function of both nominal section capacity and critical buckling capacity N_{cr} defined by:

$$\bar{\lambda} = \sqrt{\frac{N_o}{N_{cr}}} \qquad \textbf{(D.22)}$$

where N_o is determined without partial material safety factors

$$N_{cr} = \frac{(EI)_e \pi^2}{L_e^2} \quad \textbf{(D.23)}$$

where $(EI)_e$ is the effective sectional stiffness given as

$$(EI)_e = 0.8\, E_{cd}\, I_c + E_s I_s + E_r I_r \quad \textbf{(D.24)}$$

The Secant Modulus of Elasticity for the concrete core is given by Eurocode 2 :"The Design of Concrete Structures" where:

$$E_{cd} = E_{cm}/\gamma_c \quad (\gamma_c \text{ can be reduced to 1.5 to 1.35 for } E_c)$$

$$E_{cm} = 9.5(f'_c + 8)^{1/3} x 10^3 \quad \textbf{(D.25)}$$

Member Capacity:

Column design strength N_d is a function of cross section capacity N_{pl} given by Eqn. D.19 and a slenderness reduction factor χ obtained from an appropriate column buckling curve with respect to $\overline{\lambda}$.

$$N_d = \chi N_{pl} \quad \textbf{(D.26)}$$

The column buckling curve χ is given by Eqn. D.27 as a function of 'λ'.

$$X = \frac{1}{\varphi + \sqrt{\varphi^2 - \overline{\lambda}^2}} \quad \textbf{(D.27)}$$

$$\varphi = 0.5\left[1 + a\left(\overline{\lambda} - 0.2\right) + \overline{\lambda}^2\right] \quad \alpha = 0.21 \text{ for CHS}$$